OPTOKINETIC NYSTAGMUS IN FISH AND MAN

Dissertation

zur

Erlangung der naturwissenschaftlichen Doktorwürde (Dr. sc. nat.)

vorgelegt der

Mathematisch-naturwissenschaftlichen Fakultät

der

Universität Zürich

von

Chien-Cheng Chen

aus

Taiwan

Promotionskomitee

Prof. Dr. Stephan C.F. Neuhauss (Leitung der Dissertation)
Prof. Dr. Dominik Straumann
Prof. Dr. Christian Grimm
Prof. Dr. Stefan Glasauer
Dr. Melody Ying-Yu Huang

Zürich, 2014

Table of content

Summary

The optokinetic response (OKR) is an involuntary ocular motor response to a large, moving visual surround. The OKR reduces the velocity difference between the eyes and the visual surround for better vision. To generate such eye movements, a series of neural signal processing and integration steps is needed. The aims of this thesis were to study several phenomena related to the OKR for a better understanding of this reflex.

In Chapter 2, we studied how the misrouting of optic fibers changes the OKR and gaze stability. The optokinetic system is thought to be a negative feedback system, in which slow-phase eye movements (i.e. the system output) minimize retinal slip (i.e. the system error). Previous studies in zebrafish larvae found that the misrouting of optic nerves causes a positive feedback OKR, in which the slow phases amplify retinal slip. This, in turn, further induces spontaneous eye oscillations (SEOs) in the fish with the optic fibre misrouting. Whether such a mechanism also exists in humans with infantile nystagmus syndrome (INS) remained unclear so far. We tried to find the correlation of the misrouting, the OKR, and the SEOs by mimicking this misrouting in healthy subjects and analyzing the corresponding OKR and gaze stability. Computational simulations aimed to demonstrate the link between OKR performance and gaze stability was done to be a comparison.

In Chapter 3, we studied an afternystagmus occurring in human subjects after they were fixating their eyes upon a stationary visual target during optokinetic stimulation. Such an afternystagmus after suppression of optokinetic nystagmus (ASOKN) was thought to be generated by a velocity storage mechanism (VSM). However, we found that the stimulus brightness has a significant impact on the ASOKN. This finding challenges the current VSM hypotheses since a VSM effect should not be affected by stimulus brightness. In this study, we provided and examined a new hypothesis that is not related to any VSM but stimulus brightness.

In Chapter 4, we studied the VSM in zebrafish larvae. The VSM is thought to be a coupling effect of the optokinetic signals accessing the vestibular system. It has been known that horizontal angular vestibular-ocular reflex (VOR) in 5-6 days post fertilization (dpf) zebrafish larvae does not function yet, suggesting that the vestibular system might not fully develop. Thus, whether the VSM exists in these larvae is unclear. In this chapter, we found that the VSM already exists in these larvae by investigating optokinetic after-response (OKAR), which is thought to be produced by the VSM. This finding suggested that the VSM can develop prior to the horizontal angular VOR.

In Chapter 5, we discuss the potential studies brought from these reported studies.

Zusammenfassung

Als optokinetische Reaktion (Optokinetic Response, OKR) bezeichnet man eine unwillkürliche Augenbewegungsreaktion auf einer sich bewegende visuelle Umgebung, die einen grossen Teil des Blickfelds einnimmt. Um das Sehen zu ermöglichen, reduziert die OKR den Geschwindigkeitsunterschied zwischen den Augen und der visuellen Umgebung. Das Entstehen einer OKR erfordert eine bestimmte Abfolge von neuronaler Signalverarbeitung und -integration. Das Ziel der vorliegenden Arbeit besteht in der Untersuchung mehrerer OKR-relevanter Phänomene, um ein besseres Verständnis der OKR zu erhalten.

In Kapitel 2 untersuchten wir, wie die Fehlprojektion von Sehnerven OKR und Blickstabilität verändert. Bekanntermaßen handelt es sich beim optokinetischen System um ein negatives Feedback-System, in dem Augenbewegungen mit langsamer Phase, d.h. der System-Output, das Wegrutschen der Fixation der Fovea centralis, d.h. den Systemfehler, minimieren. Frühere Untersuchungen bei Zebrafisch-Eembyronen stellten fest, dass die Fehlprojektion eine OKR mit positivem Feedback verursacht, in der die langsamen Phasen das Wegrutschen der Fixation der Fovea centralis verstärken. Darüber hinaus nimmt man an, dass eine OKR mit positivem Feedback spontane Augenoszillationen auslöst, die in den Fischen mit der visuellen Fehlprojektion festgestellt wurden. Ob bei Menschen ein derartiger Mechanismus denkbar ist, war bisher unklar. Wir versuchten daher, eine Korrelation zwischen Fehlprojektion, OKR und SEOs zu finden, indem wir diese fehlgeleiteten optokinetischen Signale in gesunden Versuchspersonen simulierten und dann jeweils OKR und Blickstabilität überprüften. Zusätzlich wurde zum Vergleich eine Computersimulation angefertigt.

In Kapitel 3 untersuchten wir einen Nachnystagmus, der bei menschlichen Versuchspersonen auftritt, die mit den Augen während der optokinetischen Stimulation ein stationäres visuelles Ziel fixierten. Man nimmt an, dass ein solcher Nachnystagmus nach der Unterdrückung des optokinetischen Nystagmus (After Nystagmus after Suppression of Optokinetic Nystagmus, ASOKN) durch einen Geschwindigkeitsspeicher-Mechanismus (Velocity Storage Mechanism, VSM) erzeugt wird. Wir stellten jedoch fest, dass die Reizhelligkeit einen signifikanten Einfluss auf die Dauer des ASOKN hat. Dieses Ergebnis stellt die aktuellen VSM-Hypothesen infrage, da ein VSM-Effekt nicht von der Reizhelligkeit beeinflusst werden sollte. In dieser Studie präsentierten und untersuchten wir eine neue Hypothese, die sich nicht auf den VSM, sondern auf die Reizhelligkeit bezieht.

In Kapitel 4 untersuchten wir den VSM von Zebrafisch-Larven. Man nimmt an, dass der VSM nur bei einem funktionierenden Netzwerk zwischen vestibulärem Eingang und okulomotorischen Ausgang existiert. Man weiss, dass der horizontale schräge VOR (Vestibulo-Ocular Reflex, Vestibulookulärer Reflex) in Zebrafischembyronen in den 5-6 Tagen nach der Befruchtung noch nicht funktioniert. Man ging deshalb davon aus, dass der VSM bei diesen Larven nicht existiert. In diesem Kapitel haben wir

wir diese Frage neu gestellt, indem wir die optokinetische Nachantwort (Optokinetic After-Response, OKAR) in Zebrafisch-Larven untersuchten. Wir analysierten, ob während des vorhergehende OKR der VMS geladen wird, um die Rolle des OKR beim VSM ohne VOR zu bestimmen.

In Kapitel 5 diskutieren wir die Weiterführung dieser drei Studien.

Chapter 1

General Introduction

1.1 Optokinetic response

The optokinetic nystagmus (OKN) consists of slow-phase eye movements that follow a moving visual surround and fast-phase eye movements that reset the eyes. The optokinetic response (OKR) responsible for the OKN tries to reduce retinal slip (i.e. the velocity difference between the eyes and the moving visual surround) for better vision (Baarsma & Collewijn, 1974; Schweigart et al., 1997; Robinson, 1981). The OKR has been extensively studied in species with a fovea, such as monkeys (Takahashi & Igarashi, 1977; Igarashi et al., 1977) and humans (Honrubia et al., 1968; Abadi & Pantazidou, 1997), and without a fovea, such as rabbits (Tan et al., 1992; Tan et al., 1993), rats (Sirkin et al., 1985; Hess et al., 1985), and goldfish (Beck et al., 2004).

Conceptually, the OKR is generated by a signal processing cascade in the ocular motor system (Robinson, 1981): The image motion seen by the eyes is sent to an optokinetic system (OKS), which calculates retinal slip and generates corresponding velocity signals to move the eyes in the direction of the image motion in order to eliminate retinal slip. The eye velocity signals from the OKS are, then, converted to eye-position commands by a velocity-to-position neural integrator (VPNI). Eventually, an eye plant is controlled by these eye-position commands, generating eye movements. The VPNI also receives eye-velocity impulse signals from a fast-phase system, resulting in a quick change in eye position. The conceptual relation of the four subsystems is plotted in Fig. 1.1.

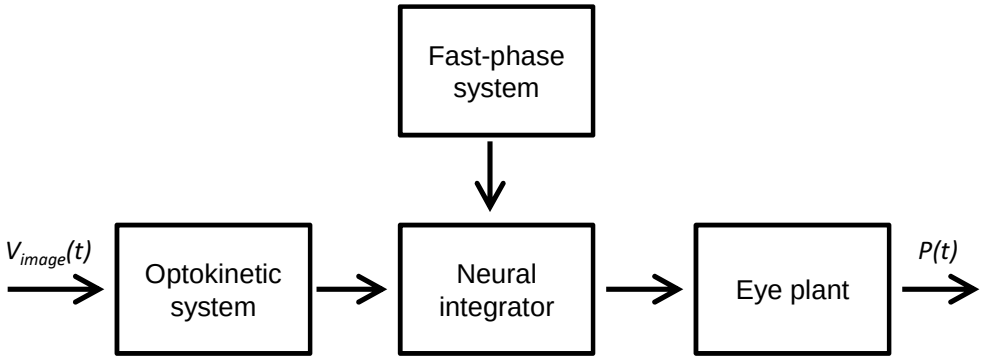

Figure 1.1 Conceptual ocular motor model for the OKN. Note that $V_{image}(t)$ represents the image velocity versus time and $P(t)$ denotes eye position versus time.

To minimize retinal slip for effective vision, the OKR often works together with the vestibular-ocular reflex (VOR) and the velocity storage mechanism (VSM). The vestibular-ocular system obtains the head-velocity signals from semicircular canals (SCC) and generates eye-velocity signals in the opposite direction of head movements to keep eye position stable in space during self-rotation. The

VSM is thought to be a coupling effect of optokinetic signals accessing the vestibular-related circuit (Cohen et al, 1977). Previous studies have suggested that the VSM can preserve low-frequency signals from the semicircular canals (Robinson, 1977; Raphan et al., 1977; Raphan et al., 1979). In addition, the VSM is thought to be responsible for the optokinetic afternystagmus (OKAN), which is characterized by nystagmus in dark subsequent to constant optokinetic stimulation (Cohen et al., 1977; Raphan et al., 1977; Raphan et al., 1979; Robinson, 1977). The conceptual relation of the OKS, the vestibular-ocular system, and the VSM is plotted in Fig. 1.2.

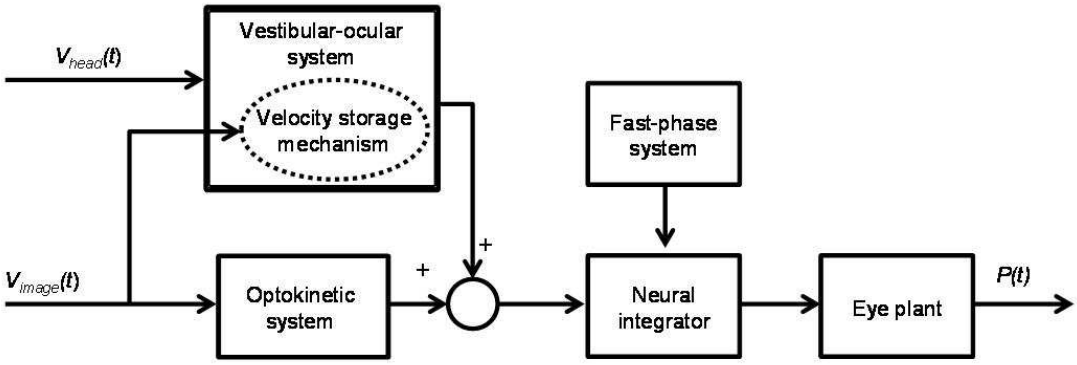

Figure 1.2 Conceptual relation between the optokinetic system, the vestibular-ocular system, and the velocity storage mechanism. The vestibular-ocular system and a pathway were added to the model shown in Fig. 1.1. The velocity storage mechanism is indicated by a dotted oval frame. Note that $V_{head}(t)$ represents head velocity versus time.

1.2 Computational model of the optokinetic response

Several computational models have been proposed to simulate OKN and OKAN (Collewijn, 1971; Raphan et al., 1977, 1979; Robinson, 1981; Maioli, 1988; Furman et al., 1989). Here we used the optokinetic and vestibular-ocular model provided by Robinson (1981) as an example to illustrate how the simulation is done. Fig. 1.3 depicts the model.

To understand how this model simulates the OKN, let us assume there is no head movement and the visual surround is moving constantly. Therefore, the head velocity ($\dot{H}$) is zero and the image velocity ($\dot{D}$) is a constant value. Initially, the eyes are stationary so that the eye velocity ($\dot{G}$) is zero. Therefore, the retinal slip ($\dot{e}$) is equal to the image velocity ($\dot{D}$). Because the fractional copy of eye-velocity commands ($k\dot{E}'$) from the vestibular nucleus (vn) is zero in the beginning, the neurally encoded velocity of the visual surround ($\dot{W}_h$) is equal to the retinal slip ($\dot{e}$). The sign-inverted neurally encoded velocity of the visual surround ($\dot{H}_v$) is sent to the OKS to generate the corresponding eye-velocity signals ($\dot{H}_{ok}$). The eye-velocity command ($\dot{E}'$) is the sign-reversed eye-velocity signals

($\dot{H}_{ok}$) because the head velocity ($\dot{H}$) is zero. The eye-velocity command ($\dot{E}'$) is sent to the VPNI and the eye plant to generate the eye velocity ($\dot{G}$) while the fractional copy of the eye-velocity command ($k\dot{E}'$) is sent back to the OKS. Since the eye velocity ($\dot{G}$) is gradually close to the image velocity ($\dot{D}$), the retinal slip ($\dot{e}$) becomes smaller and approaches zero. Because the fractional copy of the eye-velocity command ($k\dot{E}'$) is very close to the eye velocity ($\dot{G}$), the neurally encoded velocity of the visual surround ($\dot{W}_h$) and its sign-inverted signal ($\dot{H}_v$) can remain relatively unchanged. Since the sign-inverted neurally encoded velocity of the visual surround ($\dot{H}_v$) is stable, the corresponding eye-velocity signals ($\dot{H}_{ok}$) and the eye velocity ($\dot{G}$) are stable as well, meaning that the eyes can stably follow the image motion.

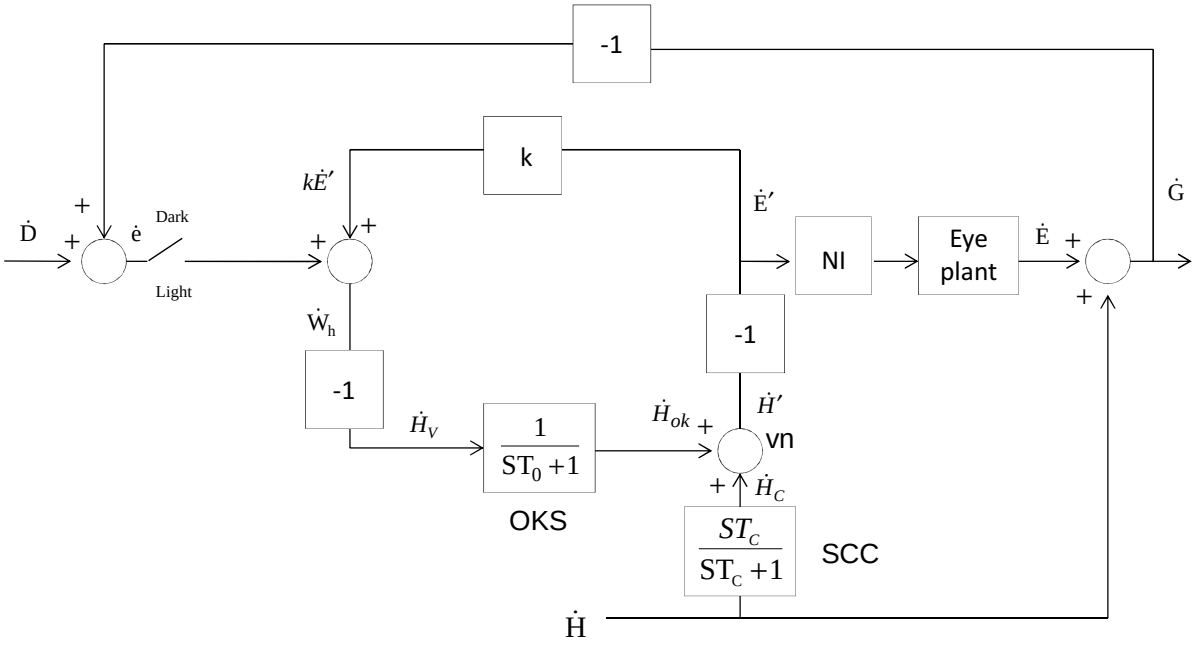

Figure 1.3 A model of the optokinetic response and the vestibular-ocular reflex adapted from Robinson (1981). SCC, OKS, vn, and NI are abbreviations for semicircular canals, optokinetic system, vestibular nucleus, and neural integrator, respectively. $\dot{e}$ denotes retinal slip, $\dot{D}$ denotes the velocity of the visual surround, $\dot{G}$ denotes eye velocity in space, T_c denotes the time constant of SCC, T_o denotes the time constant of OKS, $\dot{H}$ denotes head velocity, k denotes a gain factor close to 1. $\dot{H}_c$ denotes the neutrally encoded head velocity from the SCC, $\dot{H}_{ok}$ denotes the eye velocity signal from the OKS, $\dot{W}_h$ denotes the neurally encoded velocity of the visual surround, $\dot{H}_v$ denotes the input of OKS, $\dot{H}'$ denotes the neurally encoded velocity difference between the visual surround and the eyes, $\dot{E}'$ denotes the eye-movement command to the NI. A Dark/Light switch is applied to control the access of retinal slip to the central integration.

The system that generates the OKN is a negative feedback closed-loop system, in which the system output (i.e. eye velocity) is sent back to reduce the system error (i.e. retinal slip). The vestibular-ocular

system is an open-loop system, in which the system input (i.e. head velocity) is processed without receiving any feedback from the system output (i.e. eye velocity). The VSM is simulated by the internal positive feedback loop, where the fractional copy of the sign-inverted eye-velocity command from vn ($k\dot{E}'$ in Fig. 1.3) is sent to the OKS. The positive feedback loop can store the eye-velocity signals during optokinetic stimulation and keeps releasing eye-velocity commands in dark subsequent to the optokinetic stimulation (Robinson, 1981).

Note that, in this model, the OKR gain is always one and there is no system latency or delay to simulate the processing and transmission time. Thus, to let this model be closer to the real condition, we added a gain-control block and several delay blocks into the model. The gain-control block was placed before the OKS to determine the OKR gain. The delay blocks, representing the transmission and processing time, were placed in every path and signal processing block. Fig. 1.4A depicts the modified model.

Now, we have described how the optokinetic signals are processed in this model. After generating eye-velocity signals, these signals need to be converted to eye-position commands. Moreover, fast phases are needed for quickly resetting the eye position and maintaining the beating field. Computational simulations of the fast-phase generator, the VPNI, and the eye plant are described below.

The fast-phase generator produces eye-velocity-impulse signals to quickly reset the eye position. Previous studies described such velocity impulse signals as the gamma function shown below (van Opstal & Goossens, 2008; van der Willigen et al., 2011):

$g(t) = Gain \cdot T_0^{-\gamma} \cdot (t - t_{on})^{\gamma} \cdot exp\left(-\frac{(t-t_{on})}{\sigma_{DUR}}\right)$ with $T_0 = \sigma_{DUR}\gamma/e$ and $t \geq t_0$

Whereby t is time, t_{on} is the burst onset, σ_{DUR} is the burst duration, the exponent γ determines the gamma-burst skewness, and $Gain$ determines the amplitude of the gamma function.

The function of the VPNI is to convert eye-velocity signals to eye-position commands. Thus, gaze is stable at the new position against the elastic forces of the extra-ocular tissues that pull the eyes toward a central position (Robinson, 1964; Cohen & Komatsuzaki, 1972; Skavenski & Robinson, 1973). The VPNI can be modeled by using an integrator with a single time constant (Chen et al., 2013). Fig. 1.4B depicts the VPNI model.

The eye plant is controlled by the eye-position commands from the VPNI model. The eye plant was described as a second order system assembled by two time constants T_1 and T_2 (Keller, 1977; van Gisbergen et al., 1981). Fig. 1.4C depicts the mathematical model of the eye plant. T_1 is approximately equal to the ratio of the viscous drag and the elastic stiffness of the orbital tissues while T_2 is approximately equal to the ratio of mass of the eye ball and the viscous drag caused by the

orbital tissues. In general, T_1 is much larger than T_2 since the mass of eye ball is relatively small compared to the effect of the elastic stiffness and the viscous drag of the orbital tissues. For instance, in the model of van Gisbergen et al. (1981) for monkey, T_1 and T_2 were set to 0.15 and 0.004, respectively.

By using this model shown in Fig. 1.4, we are able to simulate the OKN as well as investigate how each subsystem affects the ocular motor behavior. Part of this model was used in Chapters 2 and 4.

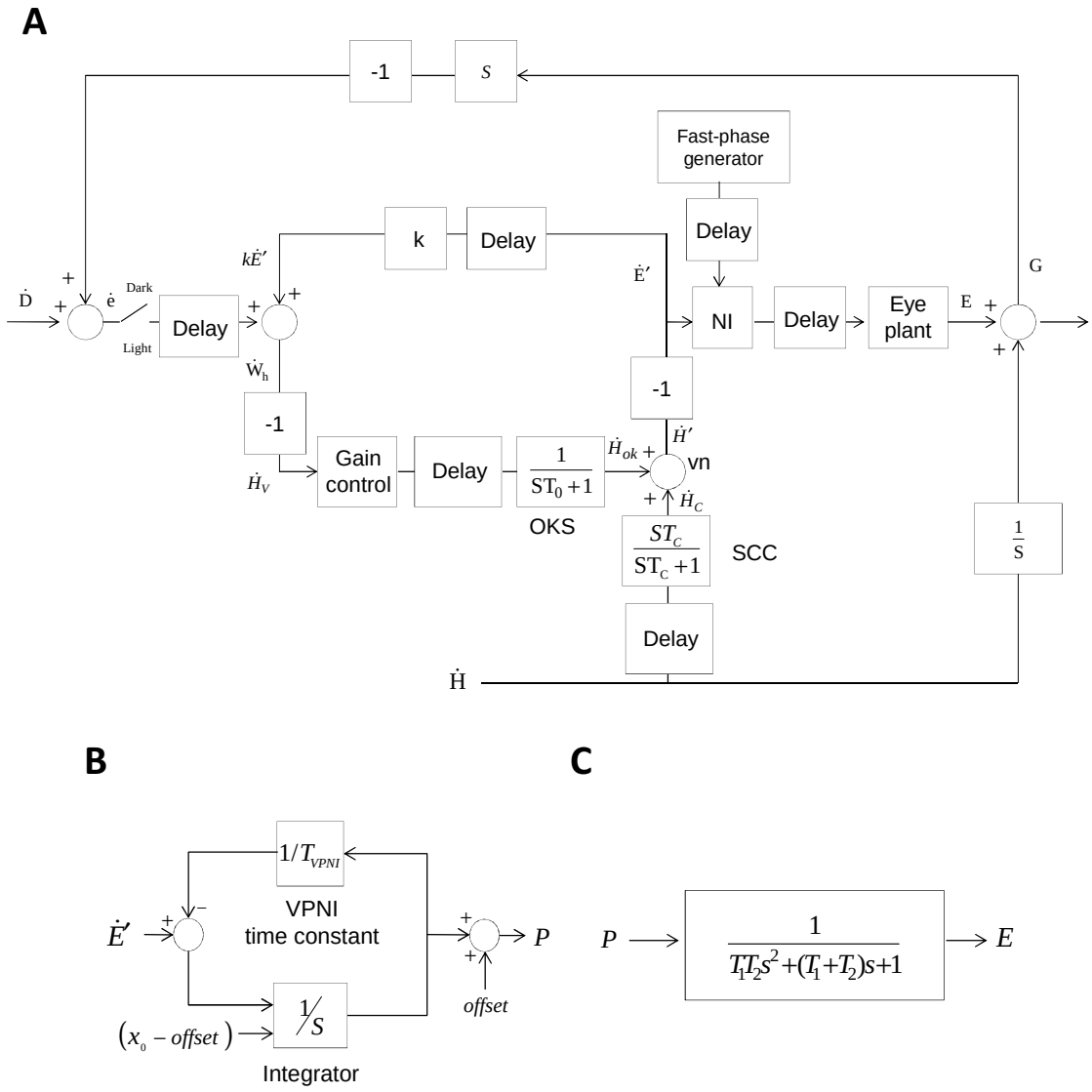

Figure 1.4 Computational model for the optokinetic nystagmus. **A** Schematic plot of the modified model. Note that G denotes eye position in space and E denotes the eye position relative to the head position. **B** The velocity-to-position neural integrator (VPNI) model. Note that $\dot{E}'$ is the eye-velocity commands, T_{VPNI} denotes the VPNI time constant, x_0 denotes the initial eye position, $offset$ denotes the null position of the eye, and P denotes the eye-position command after neural integration. **C** The mathematic model of the eye plant. The eye plant was described as a second order system assembled by two time constants, T_1 and T_2. Note that P denotes the eye-position command produced by the VPNI and E denotes the eye position.

1.3 Reversal of optokinetic nystagmus

Reversal of OKN, characterized by either slow phases moving in the opposite direction of the moving visual surround or fast phases moving in the same direction of optokinetic stimulation, has been found in some species, such as human (Halmagyi et al., 1980; Yee et al., 1980; Lueck et al., 1989; Oh et al., 2007), mice (Traber et al., 2012), zebrafish (Rick et al., 2000; Huang et al., 2006; Huber-Reggi et al., 2012), and goldfish (Easter & Schmidt, 1977). The reversal of OKN in zebrafish is thought to be caused by the misrouting of optic fibers (Rick et al., 2000; Huang et al., 2006; Huber-Reggi et al., 2012). Fig. 1.5 depicts the optic nerve projection condition in normal and achiasmatic zebrafish. In the normal condition, the visual signals from the eyes are sent to the contralateral hemisphere where the received visual signals are processed to generate eye-movement commands. These eye-movement commands, then, are sent to the contralateral and ipsilateral motor neurons to move the eyes in the direction of the moving visual surround, forming an OKN.

In the achiasma condition, the visual information seen by the left eye is sent to the ipsilateral hemisphere. But the brain still recognizes these misrouted signals as the normal ones coming from the contralateral side, meaning that the gratings are misinterpreted as moving in the temporal-to-nasal direction as if the information was originating in the right instead of the left eye. Thus, the left brain hemisphere sends eye-movement commands to contralateral motor neurons to move the right eye in the temporal-to-nasal direction. Since the eyes move conjugately, the left eye moves in the nasal-to-temporal direction, which is opposite to the moving visual surround, displaying a reversed OKN.

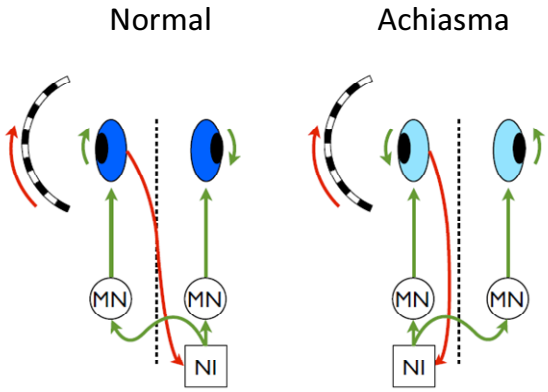

Figure 1.5 optic projection condition in the normal and achiasmatic zebrafish. This figure is adapted from Rick et al. (2000). In the normal condition, all optic fibers cross the midline to the contralateral hemisphere. In the achiasmatic condition, a large number of optic fibers do not cross the midline but project to the ipsilateral hemisphere.

Although the mechanism generating the reversal of OKN in zebrafish is clear, the mechanism in human is debated. Some have doubted the existence of a reversed OKR and suggested the reversal of OKN in human is actually gaze-modulated spontaneous nystagmus shifted by optokinetic stimulation (Halmagyi et al., 1980; Jacobs & Dell'Osso, 2004) while some thought, similar to achiasmatic zebrafish, the reversal of OKN is caused by the misrouting of optic fibers (Huang et al., 2006; Traber

et al., 2012; Huber-Reggi et al., 2012). Although there is no correlational study of the misrouting and the reversal of OKN in human, Hoffmann et al. (2003) found that, in a patient with misrouted optic nerves, the spacial organization of the misrouted optic nerves in the visual cortex presents in a way of horizontal mirror symmetry and superimposes on the normal input from the nasal retina. Fig. 1.6, adapted from Hoffmann et al. (2003), demonstrates how the misrouted visual signals are rearranged in the visual cortex. Such a mirror-symmetrical arrangement, similar to the zebrafish case, may cause a reversed OKR. However, more studies are needed to reveal the mechanism generating the reversal of OKN in human.

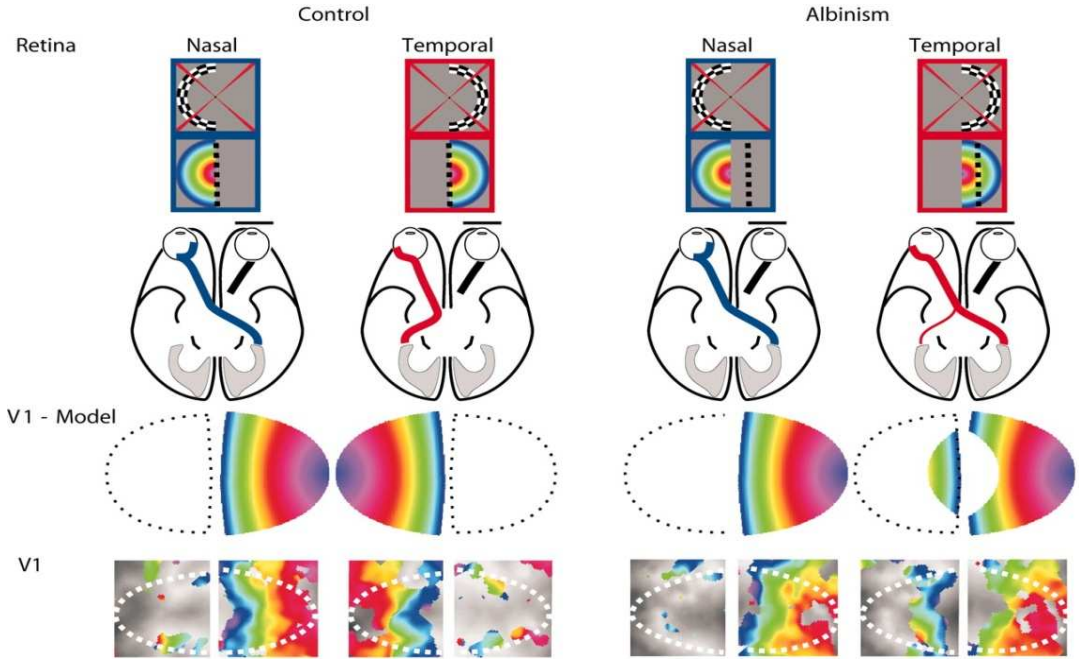

Figure 1.6 Schematic of the projection of the temporal and nasal retina of one eye in a normal control (left) and a subject with albinism (right). The figure and legend are adapted from Hoffmann et al., (2003). The first row shows the given stimuli, which is a colour map in the visual field. Dotted lines indicate the position of the line of decussation. The second row shows the projection condition of optic nerves in a healthy subject and an albino. A model of V1 and experimental results in V1 are present in the third and last rows, respectively.

1.4 Aims of this thesis

The following chapters are my main research topics on the OKN and the OKR-related phenomena in fish and human during these four years of pursuing the PhD degree. In Chapter 2, we studied how the simulated misrouting of optic fibers affects the OKR and gaze stability in healthy human. In Chapter 3, we tried to find out the mechanism responsible for afternystagmus occurring in human subjects after fixating their eyes upon a stationary visual target during optokinetic stimulation. In Chapter 4, we investigated the VSM in zebrafish larvae, in which horizontal angular VOR is absent. In Chapter 5, we discussed potential future studies based on these three reports.

1.5 Reference

Abadi R & Pantazidou M (1997) Monocular optokinetic nystagmus in humans with age-related maculopathy. Br J Ophthalmo l81, 123–129.

Baarsma E & Collewijn H (1974) Vestibulo-ocular and optokinetic reactions to rotation and their interaction in the rabbit. J Physiol 238, 603–625.

Beck JC, Gilland E, Tank DW & Baker R (2004) Quantifying the Ontogeny of Optokinetic and Vestibuloocular Behaviors in Zebrafish, Medaka, and Goldfish. J Neurophysiol 92, 3546–3561.

Chen CC, Bockisch CJ, Bertolini G, Olasagasti I, Neuhauss SC, Weber KP, Straumann D, Huang MYY (2013) Velocity storage mechanism in zebrafish larvae. J Physiol 592, 203-14.

Cohen B & Komatsuzaki A (1972) Eye movements induced by stimulation of the pontine reticular formation: evidence for integration in oculomotor pathways. Exp Neurol 36, 101–117.

Cohen B, Matsuo V & Raphan T (1977) Quantitative analysis of the velocity characteristics of optokinetic nystagmus and optokinetic after-nystagmus. J Physiol 270, 321–344.

Collewijn H (1971) An analog model of the rabbit's optokinetic system. Brain research 36, 71-88.

Easter SS & Schmidt JT (1977) Reversed visuomotor behavior mediated by induced ipsilateral retinal projections in goldfish. J neurophysiol 40, 1245-1254.

Furman, JMR, Hain TC, & Paige GD (1989) Central adaptation models of the vestibulo-ocular and optokinetic systems. Biological cybernetics 61, 255-264.

Halmagyi GM, Gresty MA, & Leech J (1980) Reversed optokinetic nystagmus (OKN): mechanism and clinical significance. Ann. Neurol 7, 429–435.

Hess BJM, Prechta W, Reber A & Cazin L (1985) Horizontal optokinetic ocular nystagmus in the pigmented rat. Neuroscience 15, 97–107.

Hoffmann MB, Tolhurst DJ, Moore AT, et al. (2003) Organization of the visual cortex in human albinism. J Neurosci 23, 8921–8930.

Honrubia V, Downey WL, Mitchell DP & Ward PH (1968) Experimental studies on optokinetic nystagmus II. Normal Humans. Acta Oto-laryngologica 65, 441-448.

Huang YY, Rinner O, Hedinger P, Liu SC, et al. (2006) Oculomotor instabilities in zebrafish mutant belladonna: a behavioral model for congenital nystagmus caused by axonal misrouting. J Neurosci 26, 9873–9880.

Huber-Reggi SP, Chen CC, Grimm L, et al. (2012) Severity of infantile nystagmus syndrome-like ocular motor phenotype is linked to the extent of the underlying optic nerve projection defect in zebrafish belladonna mutant. J Neurosci 32, 18079-86.

Igarashi M, Takahashi M & Homick JL (1977) Optokinetic nystagmus and vestibular stimulation in squirrel monkey model. Arch Otorhinolaryngol 218, 115-121.

Jacobs JB & Dell'Osso LF (2004) Congenital nystagmus: hypotheses for its genesis and complex waveforms within a behavioral ocular motor system model. J Vis 4, 604-625.

Keller EL (1977) Control of saccadic eye movements by midline brain stem neurons. In: Control of Gaze by Brain Stem Neurons, edited by R. Baker and A. Berthoz. Amsterdam: Elsevier, 327-336.

Maioli C (1988) Optokinetic nystagmus: modeling the velocity storage mechanism. The Journal of neuroscience *8*:821-832.

Lueck CJ, Tanyeri S, Mossman S, Crawford TJ, & Kennard C (1989) Unilateral reversal of smooth pursuit and optokinetic nystagmus. Revue Neurologique (Paris) 145, 656-660.
Oh SY, Shin BS, Jeong KY, Hwang JM, & Kim JS (2007) Clinical and oculographic findings of x-linked congenital nystagmus in three korean families. J Clin Neurol 3, 139-146.

Raphan T, Cohen B & Matsuo V (1977) A velocity-storage mechanism responsible for optokinetic

nystagmus (OKN), optokinetic after-nystagmus (OKAN) and vestibular nystagmus. In Control of Gaze by Brain Stem Neurons, Developments in Neuroscience, Vol. I (ed. R. Baker and A. Berthoz). Elsevier/North-Holland Biomedical Press, Amsterdam.

Raphan T, Matsuo V & Cohen B (1979) Velocity storage in the vestibuloocular reflex arc (VOR). Exp Brain Res 35, 229-248.

Rick JM, Horschke I, & Neuhauss SC (2000) Optokinetic behavior is reversed in achiasmatic mutant zebrafish larvae. Curr Biol 10, 595–598.

Robinson DA (1964) The mechanics of human saccadic eye movement. J Physiol 174, 245–264.

Robinson DA (1977) Linear addition of optokinetic and vestibular signals in the vestibular nucleus. Exp Brain Res 30, 447-450.

Robinson DA (1981) The use of control systems analysis in the neurophysiology of eye movements. Annu Rev Neurosci 4, 463–503.

Schweigart G, Mergner T, Evdokimidis I, Morand S, & Becker W (1997) Gaze stabilization by optokinetic reflex (OKR) and vestibulo-ocular reflex (VOR) during active head rotation in man. Vision Res 37, 1643–1652.

Sirkin DW, Hess BJM, & Precht W (1985) Optokinetic nystagmus in albino rats depends on stimulus pattern. Exp Brain Res 61, 218-221.

Skavenski AA & Robinson DA (1973) Role of abducens neurons in vestibuloocular reflex. J Neurophysio l36, 724–738.

Takahashi M & Igarashi M (1977) Comparison of vertical and horizontal optokinetic nystagmus in the squirrel monkey. ORL J Otorhinolaryngol Relat Spec 39, 321-329.

Tan HS, Collewijn H, & van der Steen J (1992) Optokinetic nystagmus in the rabbit and its modulation by bilateral microinjection of carbachol in the cerebellar flocculus. Exp Brain Res 90, 456-68.

Tan HS, van der Steen J, Simpson JI, & Collewijn H (1993) Three-dimensional organization of optokinetic response in the rabbit. J Neurophysiol 69, 303-317.

Traber et al. (2012) Albino mice as an animal model for infantile nystagmus syndrome. Investigative ophthalmology & visual science 53, 5737-5747.

van Gisbergen JAM, Robinson DA, & Gielen STAN (1981) A quantitative analysis of generation of saccadic eye movements by burst neurons. J Neurophysiol 45, 417-442.

van Opstal AJ & Goossens HHLM (2008) Linear ensemble-coding in midbrain superior colliculus specifies the saccade kinematics. Biological cybernetics 98, 561-577.

van der Willigen RF, Goossens HHLM & van Opstal AJ (2011) Linear visuomotor transformations in midbrain superior colliculus control saccadic eye-movements. Journal of Integrative Neuroscience 10, 277-301.

Yee RD, Baloh RW, & Honrubia V (1980) Study of congenital nystagmus: optokinetic nystagmus. Br J Ophthalmol 64, 926–932.

Chapter 2

Positive or negative feedback of optokinetic signals: Degree of the misrouted optic flow determines system dynamics of human ocular motor behavior

Chien-Cheng Chen[1,5], Christopher J. Bockisch[1,2,3], Itsaso Olasagasti[1], Konrad P. Weber[1,2], Dominik Straumann[1,4], and Melody Ying-Yu Huang[1,4]

Departments of [1]Neurology, [2]Ophthalmology, and [3]ENT, University Hospital Zurich, Zurich, Switzerland; the [4]Zurich Center for Integrative Human Physiology (ZIHP), Zurich, Switzerland. [5]PhD Program in Integrative Molecular Medicine, Life Science Graduate School, CH-8057 Zurich, Switzerland

Adaptation from an article published in IOVS 55.4 (2014): 2297-306.

Acknowledgements

The authors like to thank Marco Penner and Urs Scheifele for their excellent technical assistance. This work was supported by the Swiss National Science Foundation (SNF) grants PMPDP3_139754 (Marie Heim-Vögtlin programme) & 31003A-118069, Zurich Center for Integrative Human Physiology (ZIHP), and Betty and David Koetser Foundation for Brain Research.

Personal Contribution

Conceiving the project and designing the experiments with the other authors, performing the experiments alone, analyzing the data with CJB, and writing manuscript with MYYH, CJB, and DS.

2.1 Abstract

Purpose. The optokinetic system in healthy humans is a negative feedback system that stabilizes gaze: slow-phase eye movements (i.e. the output signal) minimize retinal slip (i.e. the error signal). A positive feedback optokinetic system may exist due to the misrouting of optic fibers. Previous studies have shown that, in a zebrafish mutant with a high degree of the misrouting, the optokinetic response (OKR) is reversed. As a result, slow-phase eye movements amplify retinal slip, forming a positive feedback optokinetic loop. The positive feedback optokinetic system cannot stabilize gaze, but leads to spontaneous eye oscillations (SEOs). Because the misrouting in human patients (e.g., with a condition of albinism or achiasmia) is partial, both positive/negative feedback loops co-exist. How this co-existence affects human ocular motor behavior remains unclear.

Methods. We presented a visual environment consisting of two stimuli in different parts of the visual field to healthy subjects. One mimicked positive feedback optokinetic signals and the other preserved negative feedback optokinetic signals. By changing the ratio and position of the two visual stimuli, various optic nerve misrouting patterns were simulated. Eye-movement responses to stationary and moving stimuli were measured and compared to computer simulations. The SEOs were correlated with the magnitude of the virtual positive feedback optokinetic effect.

Results. We found a correlation among the simulated misrouting, the corresponding OKR, and the SEOs in human. The proportion of the simulated misrouted signals needed to be > 50% to reverse the OKR and at least ≥ 70% to evoke the simulated SEOs.

Conclusion. This result provides a mechanism of how the misrouting of optic fibers in humans could lead to SEOs, offering a possible explanation for a subtype of infantile nystagmus syndrome (INS).

2.2 Introduction

The optokinetic response (OKR) is an eye movement driven by a large moving pattern. The OKR generates slow-phase eye movements following the moving pattern and fast-phase eye movements resetting the eyes to a central position. The optokinetic system is a negative feedback system that reduces the image velocity on the retina (i.e. the error signal) by keeping the slow-phase eye velocity (i.e. the output signal) close to the velocity of the visual world (Robinson, 1981). In general, a system with a high degree of negative feedback tends to be stable as it is relatively immune to internal disturbances and automatically compensates for external changes (Black, 1934). A positive feedback optokinetic system is rarely found, but may exist due to the misrouting of optic fibers (Huang et al., 2006; Huber-Reggi et al., 2012). In an achiasmatic zebrafish mutant, in which the misrouting of optic fibres sends optokinetic signals from the retina to the wrong brain hemisphere, the slow phases move in the opposite direction of the visual surround, producing a reversed OKR (Rick et al., 2000). As a result, retinal slip (i.e. the error signal) is amplified by the slow-phase eye velocity (i.e. the output signal) generating a positive feedback optokinetic loop. In general, a system with a high degree of positive feedback tends to be unstable as the error signal and the output signal drive the system out of equilibrium (Zeigler et al., 2000).

In human patients with misrouted optic fibers, either some of the temporal optic fibers erroneously cross the midline to the contralateral hemisphere, often found in albinos (Lund, 1965; Jeffery, 1977; Morland et al., 2002), or the nasal optic fibers do not cross to the contralateral hemisphere, as in achiasmia (Apkarian et al, 1995; Petros et al., 2008; Hoffmann et al., 2012). Infantile nystagmus syndrome (INS) often accompanies these conditions (Collewijn et al., 1985; St John et al., 1984; Biega et al., 2007). INS is characterized by spontaneous eye oscillations (SEOs) usually appearing within the first six months after birth (von Noorden & Campos; 2002), and sometimes co-occurs with a reversed jerk nystagmus during optokinetic stimulation (Collewijn et al., 1985; St John et al., 1984; Halmagyi et al., 1980; Yee et al., 1980; Lueck et al., 1989; Thurtell & Leigh; 2011). Recent studies have described a zebrafish mutant that has misrouted optic fibers and displays SEOs qualitatively similar to human INS patients (Huang et al., 2006; Huber-Reggi et al., 2012). However, approximately one in ten patients with the clinical features of albinism, including the misrouting of optic fibers, show no SEO (Lee et al., 2001; Gradstein et al., 2005). Moreover, the existence of reversed OKR in INS patients is debated. While reversed OKR was reported (based on a reversed nystagmus response) in INS patients (Halmagyi et al., 1980; Yee et al., 1980; Lueck et al., 1989; Oh et al., 2007) and in some albinos (Collewijn et al., 1985; St John et al., 1984), a reversed nystagmus is not consistently observed in every INS patient. Some have doubted the mechanism of the reversed nystagmus and suggested it is actually gaze-modulated spontaneous nystagmus shifted by optokinetic stimulation (Halmagyi et al., 1980; Jacobs & Dell'Osso, 2004). Since there are massive inter-individual variations of nystagmus waveforms in INS patients (Oh et al., 2007; Dell'Osso & Daroff, 1975) as well as variations of

waveforms as function of eye position (Oh et al., 2007; Halmagyi et al., 1980), it is possible that the INS results from several causes in different subpopulations of INS patients. To our knowledge, hypotheses about the origin of INS include connection faults, i.e. the misrouting of optic fibers (Huang et al., 2006; Huber-Reggi et al., 2012), motor faults (Dell'Osso, 2006), abnormal sensorimotor integration (Harris & Berry, 2006), and miscalibration of the visual system (Jacobs & Dell'Osso, 2004; Anderson, 1953). Here we are investigating whether the misrouting of optokinetic signals in humans could lead to INS-like eye-movement trajectories. Specifically, we simulated the misrouting of optic fibres and analyzed the resulting gain of OKR and the velocity of eye oscillations during attempted fixation.

In INS patients with an optic fiber misrouting, it is unlikely that the entire optic projection is aberrant. Thus, in most cases, positive and negative feedback loops co-exist (Fig. 2.1). Moreover, the range of misrouting in albinism differs considerably among individuals (Hoffmann et al., 2003). In other words, the contribution of positive and negative feedback optokinetic systems in human patients varies. In zebrafish, it has been shown that larvae with various degrees of optic nerve misprojections display different corresponding optokinetic behaviors (Huber-Reggi et al., 2012). Therefore, it is possible that the OKR in human INS patients and the presence of SEOs also differ due to various degrees of abnormal optokinetic feedback.

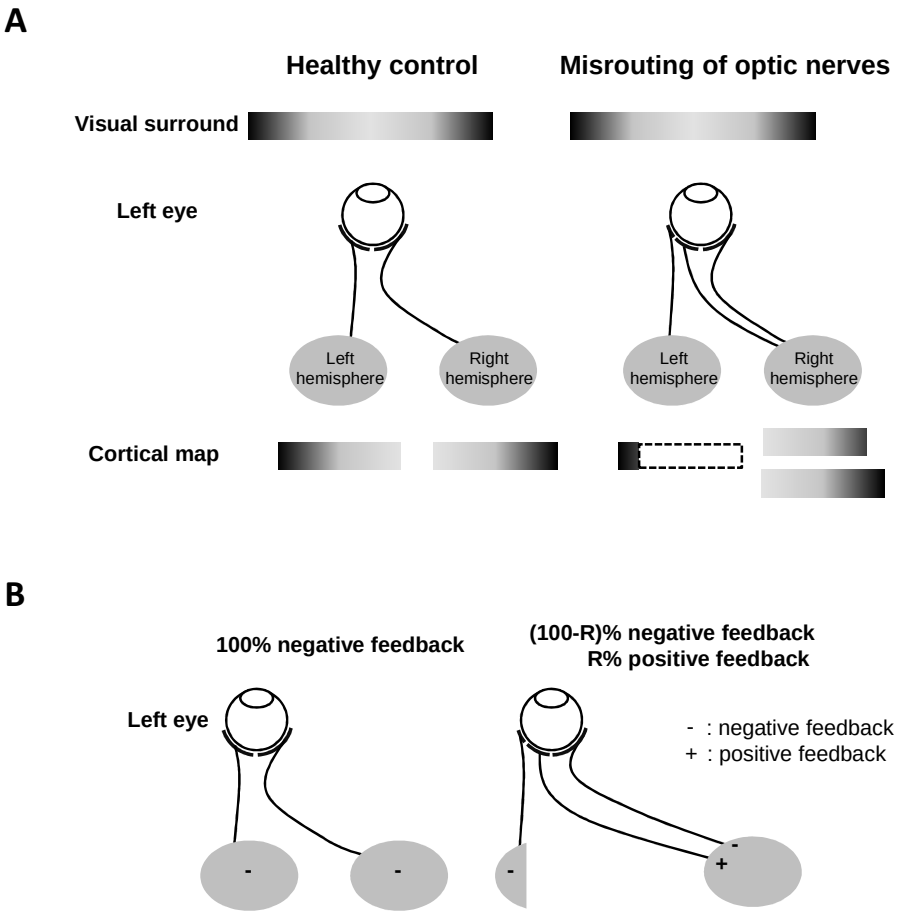

FIGURE 2.1 Schematic (**A**) and the sign of optokinetic flow (**B**) of the projection of the temporal and nasal retina of left eye in a healthy control (left) and a subject with the misrouting of optic nerves (right). (**A**) This figure is adapted from Hoffmann et al. (2003). Briefly, in the top row of Fig. 2.1A, schematics of the stimuli (the gray gradient map in the visual field is shown. In the second row, the projection of optic nerves from temporal and nasal retina is presented. In the third row, the mapping on the visual cortex is shown with the gray gradient map. In the healthy control, the gray gradient mapping represents the corresponding space organization in the visual cortex. In the patient with misrouting of optic nerves as shown in this figure, part of the cortical input from the temporal retina is misrouted onto the right hemisphere. The corresponding space organization in the visual cortex from the misrouted optic nerves, then, presents in a way of horizontal mirror symmetry (upper part) and superimposes on the normal input from the nasal retina (lower part). (**B**) In the control, all of the optic flow is channeled to the negative feedback loop. But in the patient with the misrouting of optic nerves, the horizontal mirror arrangement of the misrouting of optic nerves reverses the negative feedback loop to a positive feedback loop. R represents proportion of optic fiber misrouting.

In this study, we created a virtual visual environment to simulate the existence of two different feedback optokinetic loops in healthy subjects. The experimental environment was created by simultaneously projecting a positive feedback visual stimulus, the velocity of which was controlled based on on-line eye-movement signals to mimic a positive feedback system, and a negative feedback visual stimulus, which preserved the negative feedback system in healthy subjects, in different parts of the visual field. By varying the size and position of the positive/negative feedback stimuli in the visual

field, we measured the gaze stability and the OKR in response to various combinations of the two feedback loops. In addition, we used a mathematical optokinetic model to simulate the partial misrouting and compared our empirical data to the model results.

2.3 Materials and Methods

2.3.1 Human subjects

Experiments were performed on eight subjects, aged 23-49 years, with no abnormal neurological or ophthalmological history and normal or corrected-to-normal vision. The study was approved by the Ethics Committee of the Canton of Zürich, Switzerland, and all subjects gave their informed written consent in accordance with the declaration of Helsinki.

2.3.2 Experimental setup

A head-mounted video-oculography (VOG) device (EyeSeeCam, Munich, German) running at 220 Hz was used for the eye-movement recording. The left eye was analyzed. The subject sat in front of a screen of 178 cm in width and 130 cm in height, which was located 100 cm from the subject. Therefore, it covered 80° of the horizontal visual field and 66° of the vertical visual field. A digital projector (Panasonic PT-AE7000 Projector) operating at 60 frames per second with a spatial resolution of 1920 x 1080 pixels was used to present the visual stimuli. On-line eye-movement recording and analysis were done by commercial software (EyeSeeCam, Munich, Germany). Vertical sine-wave gratings with a spatial frequency of 0.25 cycle/degree and nearly 100% contrast (darkest luminance: 0.17 lux and lightest luminance: 330 lux) were used as the image pattern in both positive and negative feedback conditions. Thus the visual stimuli were only to test the ocular motor response in the horizontal direction. Image manipulation was done by a custom-developed script in MATLAB (Mathworks, Natick, MA) and its Psychophysics Toolbox extensions (Brainard, 1997; Pelli, 1997; Kleiner et al., 2007). The delay of the external visual feedback setup (i.e. the duration from eye-movement recording to the visual stimulus manipulation) was around 32 ms.

2.3.3 Positive and negative feedback visual stimuli for the spontaneous eye oscillation (SEO) and optokinetic response (OKR) tests

To simulate a positive feedback optokinetic system, in which retinal slip increases with eye velocity, the image velocity of the positive feedback visual stimulus was adjusted according to the current eye velocity. Since a negative feedback optokinetic system exists in healthy subjects, the negative feedback visual stimulus was stationary and did not rely on any real-time eye-movement signal. In the SEO test, we simulated how various combinations of negative and positive feedback loops react to a stationary visual surround. Fig. 2.2A illustrates how the image motions of the two feedback visual stimuli were controlled in this test. If eye movements existed, retinal slip (i.e. the error signal) would

be the negative of eye velocity because the velocity of gratings was always zero. But the error signal of the positive feedback optokinetic system would be equal to the eye velocity due to a reversed OKR. To simulate such a condition in healthy subjects, the image velocity was set to double the real-time eye velocity in the positive feedback condition. The error signal, then, became the eye velocity and a virtual positive feedback system was created.

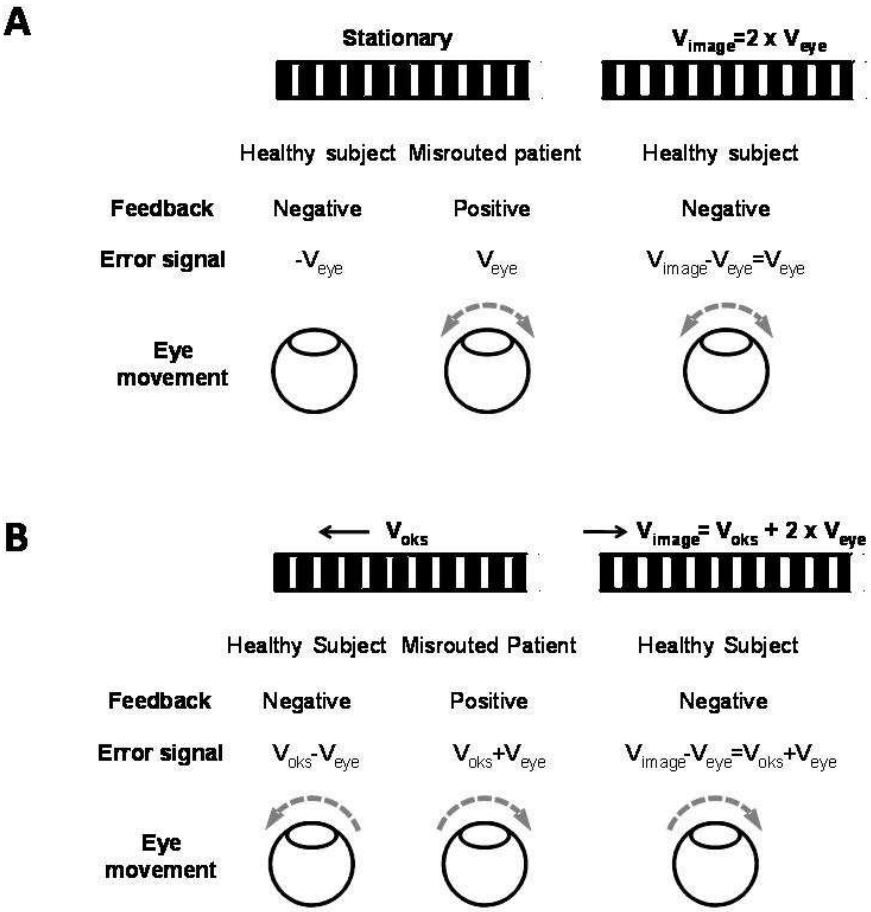

FIGURE 2.2 The image velocity of the positive feedback visual stimulus in the spontaneous eye-oscillations/optokinetic response tests. (**A**) In the spontaneous eye-oscillation test, stationary gratings were presented as the negative feedback visual stimulus. Thus, whatever the eyes moved, the stationary gratings did not move and retinal slip would be the negative of eye velocity all the time. In the healthy subject with the negative feedback optokinetic loop, the error signal is the negative of eye velocity if any eye drift occurs (first column). But in the patient with the positive feedback optokinetic loop, the error signal is the eye velocity (second column). To create this error signal in healthy subjects, the image velocity should be equal to the double eye velocity (third column). (**B**) In the optokinetic response test, constant optokinetic velocity of 20 deg/s is presented as the negative feedback visual stimulus. In the healthy subject with the negative feedback optokinetic loop, the error signal is the optokinetic velocity minus the eye velocity (first column). But in the patient with the positive feedback optokinetic loop, the error signal is the optokinetic velocity plus the eye velocity (second column) because of the reversed OKR. To create this error signal in healthy subjects, the image velocity should be equal to the optokinetic velocity with the reversed sign plus the double eye velocity (third column).

In the OKR test, we simulated how various combinations of two feedback loops react to a globally moving visual surround. Fig. 2.2B illustrates how the image motions of two feedback visual stimuli

were controlled in this test. A constantly moving image pattern (20 deg/s) was applied in the negative feedback condition. A similar calculation as described in the SEO test was applied to obtain the image velocity in the positive feedback condition. Since the positive feedback visual stimulus required the real-time eye movement information, we used the real-time horizontal left-eye movement as a feedback signal. The vertical eye movements were neglected since both of the positive/negative feedback visual stimuli were controlled to only move horizontally.

The velocity of all stimuli was not spatially adjusted when projecting on the flat screen. In other words, if the stimulus moved at constant velocity, it did move at constant pixels per second. The velocity of visual stimuli was calculated by averaging the stimulus velocity on the central 10° visual field.

2.3.4 Experimental paradigms

In each paradigm, the central visual field (ranging from 10° to 80°) received one visual stimulus while the eccentric regions (from the edge of the central stimulus to the edge of the screen at +/- 40°) received the other stimulus (Fig 2.3A and Fig. 2.4A). If the positive feedback visual stimulus was projected to the central visual field, the negative feedback visual stimulus would be shown in the peripheral visual field, and vice versa. The boundaries of the central visual field were symmetric around gaze straight ahead and moved with the left eye.

If the border of the central field stimulus crossed the edge of the screen, occurred often when the size of the central field stimulus was more than 50° (+/- 25° deviation from the center of the screen), that border would be set on the edge of the screen while the other border kept moving with the eyes. Relative positions of the two boundaries and the eyes were obtained by using the inverse tangent function taking accounts of the distance between the eyes and the flat screen. Thus, the visual stimuli were always on the same area of the retina unless the area of the visual stimuli was out of the projection range. During the tests, subjects were asked to look about straight ahead, but to let their eyes move in response to the visual stimuli. Each paradigm lasted for 30 seconds, and there was a 10-second break between paradigms. During the break, subjects were asked to stare at a fixed dot on the center of the screen and, at the same time, move his/her head to drive another moving dot, which moved with the real-time eye-in-head position to overlap with the stationary dot at the center of the screen. The dots would overlap if the head and eye-in-head positions were straight ahead, ensuring that the head position was the same at the beginning of each trial. All subjects were able to fix the moving dot to the center of the screen within the 10-second break. Also, subjects were instructed to keep their head still during each trial, and the head position was monitored by the experimenter. Thus, the head movement as well as the head position would not play an important role on the experimental outputs.

2.3.5 Computational modeling

Computer simulations done in MATLAB Simulink (Mathworks, Natick, MA) were compared to the empirical data. The model consists of a visual input generator and an optokinetic model (Fig. 2.6A). The optokinetic model is the sum of the positive and negative feedback optokinetic models, with a parameter (R) which controls the relative weighting of the two models. The negative feedback optokinetic model used here was first published by D. A. Robinson1 and has been further modified to be closer to the human OKR (see Supplemental Material). The positive feedback model was obtained by adding a gain block of the negative one after a block delay in the retina (see Supplemental Material). R (ranging from 0 to 1) indicates the proportion of the positive optokinetic systems. The motor commands from the whole model are added to obtain the final motor response. To simulate the SEO test, a small impulse (of 1 deg/s for 1 second) was given at the beginning of the simulation. To simulate the OKR test, a constant input signal (20 deg/s) was applied.

2.3.6 Data analysis

Data analysis was done with a custom-developed program written in MATLAB. Eye position was smoothened by a Gaussian low-pass filter with a cut-off frequency of 18 Hz. Eye velocity was computed by the derivative of eye position. The median, absolute eye velocity in the SEO test was calculated to represent the magnitude of the SEOs while the median eye velocity in the OKR test was calculated to represent the degree of stability of the positive and negative optokinetic systems. In the SEO and OKR test, a statistical test (t-test) was done in each subject and the whole group to examine whether an effect exists between the obtained eye velocities and the visual feedback type of central visual field while another statistical test (one-way ANOVA) was done in each subject as well as the whole group to examine whether there is a main effect between the eye velocities and the size of the central field stimulus. Moreover, regression lines of eye velocity versus central visual field area were computed in each subject and the whole group. These linear fits allow us to determine, for each subject and the whole group, if eye velocity increased with the stimulus area (that is, with the ratio of positive-to-negative feedback). In addition, the correlation (Pearson's product moment correlation) between the eye velocities in the SEO and OKR tests was calculated. These statistical tests were done in MATLAB with the Statistics Toolbox.

2.4 Results

2.4.1 Spontaneous eye oscillation (SEO)

The SEO test was applied to mimic how various combinations of positive and negative feedback loops react to a stationary stimulus. The velocity of the negative feedback stimulus in the SEO test was set to zero so that retinal slip decreased with the eye velocity. The velocity of the positive feedback stimulus in the SEO test was set to double the eye velocity so that retinal slip increased with eye velocity, i.e. the positive feedback loop (Fig. 2.2A). Fig. 2.3B shows the eye movements of one subject under all

stimulus combinations. This subject generated SEOs when the positive feedback visual stimulus was shown in the central visual field (right column), but no SEO was found when the negative feedback visual stimulus was in the central visual field (left column). Fig 2.3C shows the median absolute slow-phase eye velocity of all subjects in all conditions.

Seven of 8 subjects showed a significant eye-velocity difference between the visual feedback types of central visual field (t-test, all ps<0.05 in these 7 subjects). Overall, the average(±SD) velocity of the central visual field stimulus of positive feedback (Fig. 2.3C, right part) was 5.6±4.0 deg/s, significantly different to the one of the central visual field stimulus of negative feedback (Fig. 2.3C, left part), which was 0.6±0.5 deg/s (t-test, p<0.0001). Moreover, when the positive feedback visual stimulus was shown in the central visual field, eye velocity statistically increased with stimulus area in 6 subjects (average(±SD) slope = 0.0991(±0.0247) (deg/s)/deg; One-way ANOVA, all ps<0.05 in these 6 subjects), whereas in the negative feedback condition, none of the subjects showed a significant change in the eye velocity with the stimulus area (average(±SD) slope = 0.0004(±0.0016) (deg/s)/deg; One-way ANOVA, all ps>0.05 in all subjects). Overall, the median eye velocity increased with the size of the central visual field stimulus of positive feedback (R^2 = 0.2473; One-way ANOVA, F(1,38)=12.49, p=0.0011), but no correlation was found between the median eye velocity and the size of the central visual field stimulus of negative feedback (R^2 = 0.0337; One-way ANOVA, F(1,38)=1.33, p=0.2569). In general, the beating field of subjects during the SEO test was in the range of +/-20°, so the central projection area, which moved with left eye, did not go beyond the screen borders much when its size was less than 50°.

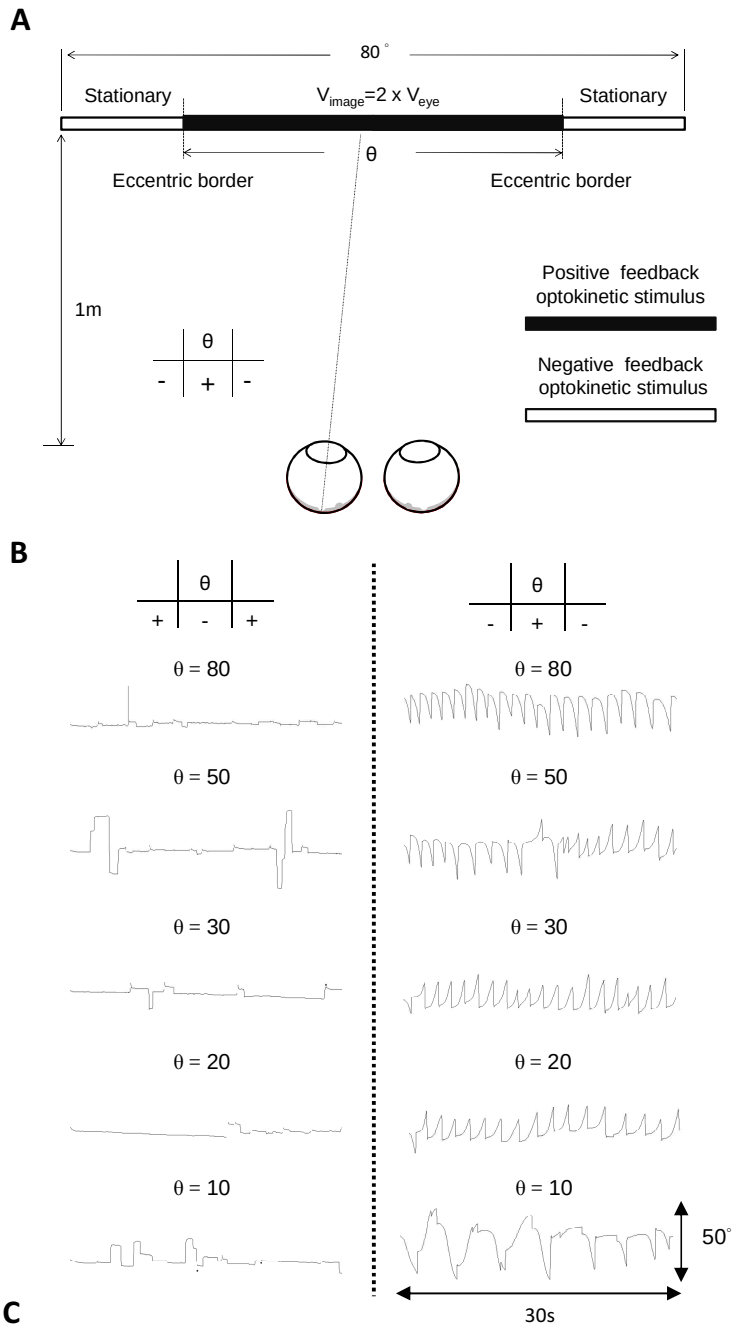

FIGURE 2.3 Visual stimulus conditions and results of the spontaneous eye-oscillations test. (**A**) Expression of the presented visual condition is shown in the 2x3 table. In the example, the positive feedback visual stimulus is projected onto the central visual field while the negative feedback visual stimulus is projected on the rest of the screen. θ is the size of the central area. (**B**) Eye movements of one subject under different stimulus combinations. The combinations of the central field stimulus of negative feedback are shown in the left column while the ones of the central field stimulus of positive feedback are shown in the right column. Different rows are different θ s. (**C**) Median absolute eye velocity of eight subjects under all stimulus combinations. The stimulus combinations, which are indicated by the tables and θ s below referred to panel A of this figure, are shown in the abscissa. The ordinate is eye velocity.

Three INS-like subtypes of SEOs (Dell'Osso & Daroff, 1975) were found during the SEO tests. Most waveforms were similar to pure unidirectional jerk nystagmus or unidirectional jerk nystagmus with extended foveation periods, in which the slow phases mainly move in one direction (see Fig. 2.3B for example, right part except the bottom). Two subjects generated bidirectional pseudo-pendular nystagmus, in which the slow phases change the direction regularly after saccades, when the positive feedback visual stimulus was only in the central 10° visual field (see Fig 2.3B for example, central area 10°). The frequency of SEOs approximately ranged between 0.3 and 0.7 Hz but varied a lot in subjects as well as the stimulus combinations (see Fig. 3B).

2.4.2 Optokinetic response (OKR)

The OKR test was applied to test how various combinations of positive and negative feedback loops react to a moving visual surround. The velocity of the negative feedback stimulus in the OKR test was set to 20 deg/s to the left. If eyes followed the negative feedback stimulus, retinal slip would decrease. The velocity of the positive feedback stimulus in the OKR test was set to 20 deg/s plus the double eye velocity (Fig. 2.2B). In this positive feedback condition, retinal slip increased even when eyes followed the positive feedback stimulus. Fig. 4B shows the eye movements of one subject under all stimulus combinations. We found that the slow phases followed the image motion presented in the central visual field, but that the magnitude of slow-phase eye velocity differed. Fig 4C shows the median eye velocity of all subjects in all conditions.

All 8 subjects showed a significant eye-velocity change regarding to the visual feedback type of central visual field (t-test, all ps<0.05 in all subjects). Overall, the average(±SD) velocity of the central visual field stimulus of positive feedback (Fig. 2.4C, right part) was -6.2±4.0 deg/s, significantly different to the one of the central visual field stimulus of negative feedback (Fig. 2.4C, left part), which was 6.9±5.0 deg/s (t-test, p<0.0001). When the positive feedback visual stimulus was in the central visual field, the eye velocity statistically changed with the stimulus area in the 6 subjects (average(±SD) slope = -0.1257(±0.0389) (deg/s)/deg, all ps<0.05 in these 6 subjects). In the negative feedback conditions, in most subjects, the eye velocities reached a maximum when the central area was small, and then did not increase further, so the eye velocity statistically increased with the size of the central visual field stimulus only in 2 subjects (average(±SD) slope = 0.1555(±0.0094) (deg/s)/deg, all ps<0.05 in these 2 subjects). Overall, however, the median eye velocity increased with the size of the central visual field stimulus of positive feedback (R^2 = 0.5297; F(1,38)=42.79, p<0.0001) and negative feedback (R^2 = 0.2005; F(1,38)=9.52, p=0.0038). In general, the beating field of subjects during the OKR test was in a range of +/-20°, so the central projection area, which moved with left eye, did not go beyond the screen borders much when its size was less than 50°.

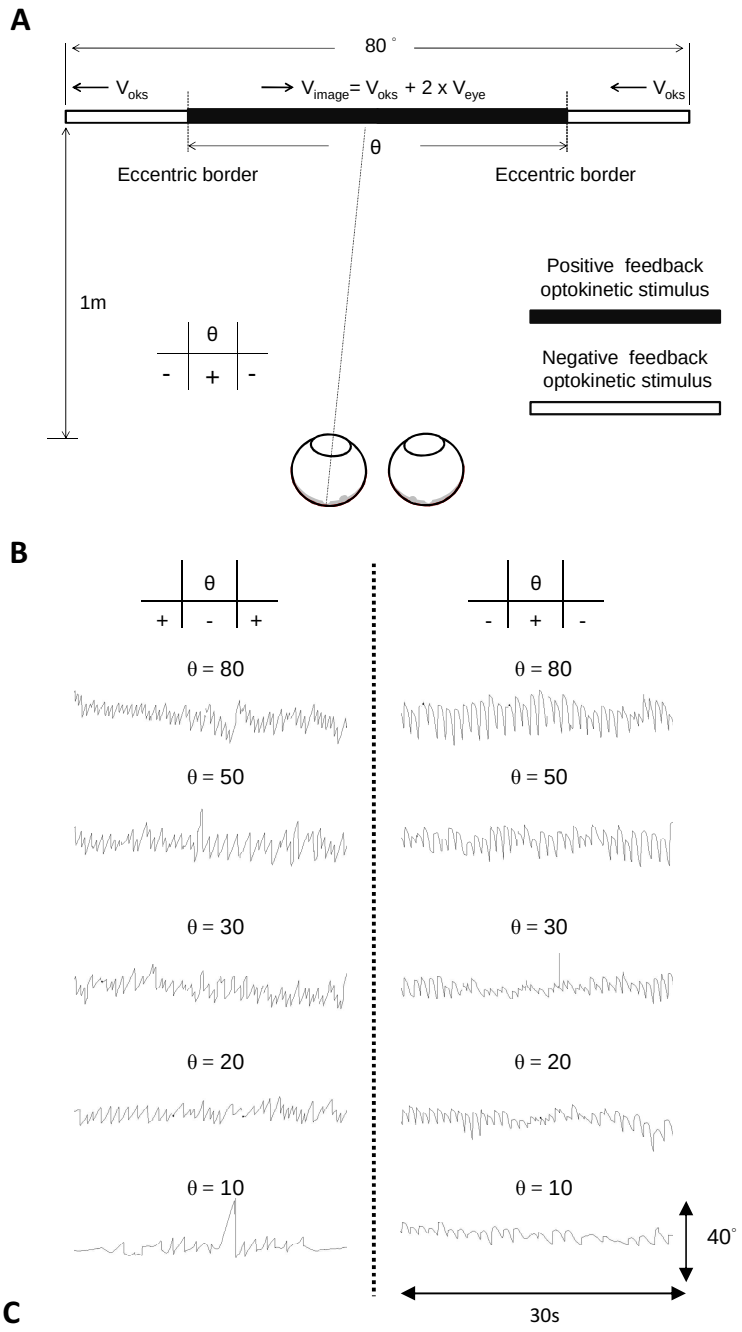

FIGURE 2.4 Visual stimulus condition and results of the optokinetic response test. (**A**) The projection conditions are the same as the ones in the spontaneous eye-oscillation test but with the visual stimuli calculated in Fig. 2B. (**B**) Eye movements of one subject under different stimulus combinations. The combinations of the central field stimulus of negative feedback are shown in the left column while the ones of the central field stimulus of positive feedback are shown in the right column. Different rows are different θ s. (**C**) Median absolute eye velocity of eight subjects under all stimulus combinations. These combinations are indicated by the tables and θ s listed below. The stimulus combinations, which are indicated by the tables and θ s below referred to panel A of this figure, are shown in the abscissa. The ordinate is eye velocity.

2.4.3 Comparison between the SEO and OKR tests

A stimulus combination represents a kind of co-existence of two feedback loops and its gaze stability and OKR were tested in the SEO and OKR tests, respectively. If the stimulus combinations in the OKR test caused slow phases to follow the negative feedback visual stimulus, gaze should be stable due to the stability of the negative feedback optokinetic loop. From the experimental results, we found that no SEO occurred (Fig 2.4C, left) when slow phases followed the negative feedback visual stimulus (Fig 2.3C, left). If the stimulus combinations caused slow phases to move in the direction of the positive feedback visual stimulus, the SEOs were expected to occur due to the instability of the positive feedback optokinetic loop. One subject (●) had no or weak SEO (Fig 2.3C, right) with the stimulus combinations where his eyes followed the positive feedback visual stimulus (Fig 2.4C, right). Moreover, three subjects generated obvious SEOs only if the size of the central visual field was ≥ 50° (Fig 2.3C, right part). Such an unexpected result, which challenges the hypothesis that the instability necessarily evokes SEOs, raises a question: how is the positive feedback optokinetic loop related to the SEOs?

To find out the relation between the SEOs and the positive feedback optokinetic loop, we then correlated the eye velocity obtained with the positive feedback stimulus in the central field in the OKR test (Fig 2.4C, right) with the corresponding data from the SEO test (Fig 2.3C, right) The correlation (Fig. 2.5) was significantly positive (Pearson linear coefficient of 0.6337, $p<0.0001$).

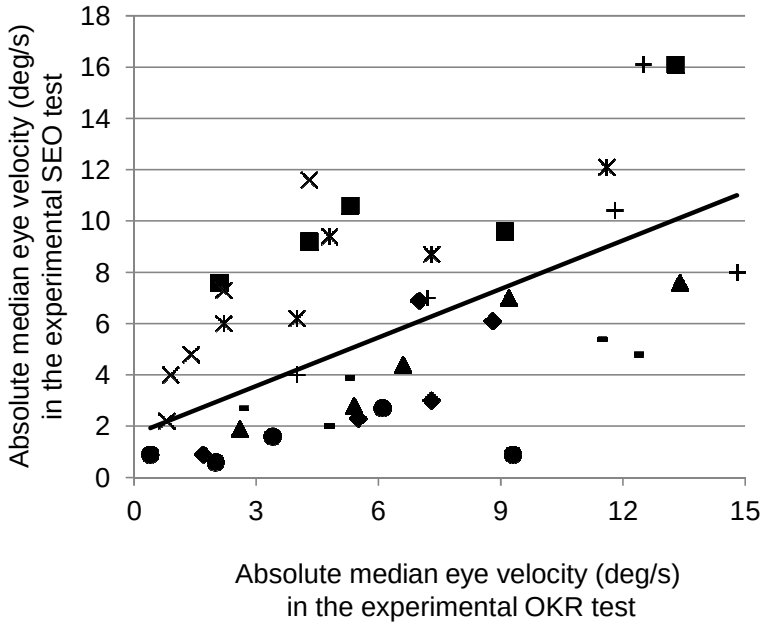

FIGURE 2.5 Correlation between the results of the SEO and OKR tests. Data points were obtained by grouping data points on the right part of Fig. 2.3C and Fig. 2.4C. For instance, if one subject showed a median eye velocity of -4.6 deg/s in the OKR test and an absolute median eye velocity of 8 deg/s in the SEO test, when the positive feedback visual stimulus was showed on the central 20° visual field, a data point (4.6, 8) was obtained. Note we only took the absolute value, which represents the degree of instability. The solid black line is a linear regression fit of the values. The degree of instability was positively correlated to the magnitude of the SEOs (Pearson's linear correlation coefficient r=0.6337, P<0.0001).

2.4.4 Computer simulation

Computer simulations were done for a comparison with the empirical data, using several different OKR gain curves (see Supplemental Material). In the simulated SEO test (Fig 6B), the eye velocity for the normal gain OKR curve starts to increase when the proportion of fiber misrouting is 0.7. For the two lower gain OKR curves, a higher proportion of simulated misrouting is needed to induce eye movements. Once the simulated SEOs are evoked, the magnitude increases with the proportion of misrouted fibers. For the two lowest OKR curves, no SEO is generated, even when the proportion of misrouted fibers is 1.0. In the simulated OKR test (Fig. 2.6C), the simulated OKR velocity is highest when there is no misrouted fiber. Then the simulated OKR velocity decreases with the proportion of the simulated optic fiber misrouting. When the proportion of the simulated optic fiber misrouting is 0.5, the simulated OKR velocity of all OKR curves becomes zero. Above 0.5, the OKR reverses for all curves.

We also tried to find out the relation between the simulated gaze stability (i.e. the data of the simulated SEO test) and the simulated OKR (i.e. the data of the simulated OKR test) in order to be a comparison with the analysis shown in Fig. 2.5. If the eye-velocity output is in the same direction of

the visual input, the negative feedback optokinetic loop dominates so that gaze should be stable. From the modeling results, we found that no simulated SEO occurs (Fig 2.6C, the data with a proportion < 0.5) when the eye-velocity output is in the same direction of the visual input (Fig 2.6B, the data with a proportion < 0.5). If the eye-velocity output is in the opposite direction of the visual input, the simulated SEOs should occur due to the instability of the positive feedback optokinetic loop. However, similar to the experimental results, no occurrence of the simulated SEO is possible (Fig 2.6B, the data with a proportion > 0.5) when the simulated output is reversed (Fig 2.6C, the data with a proportion > 0.5). We correlated the magnitude of the simulated OKR velocity of a positive-feedback-dominated system (Fig 2.6C, right part) with the corresponding data from the simulated SEO test (Fig 2.6B, right part). Similar to Fig. 2.5, the correlation (Fig. 2.7) was significantly positive (Pearson linear coefficient of 0.7855, $p < 0.0001$). However, rather than the linear relation between the two, it is more likely that the occurrence of the simulated SEOs relies on certain degree of the instability as well as the individual OKR.

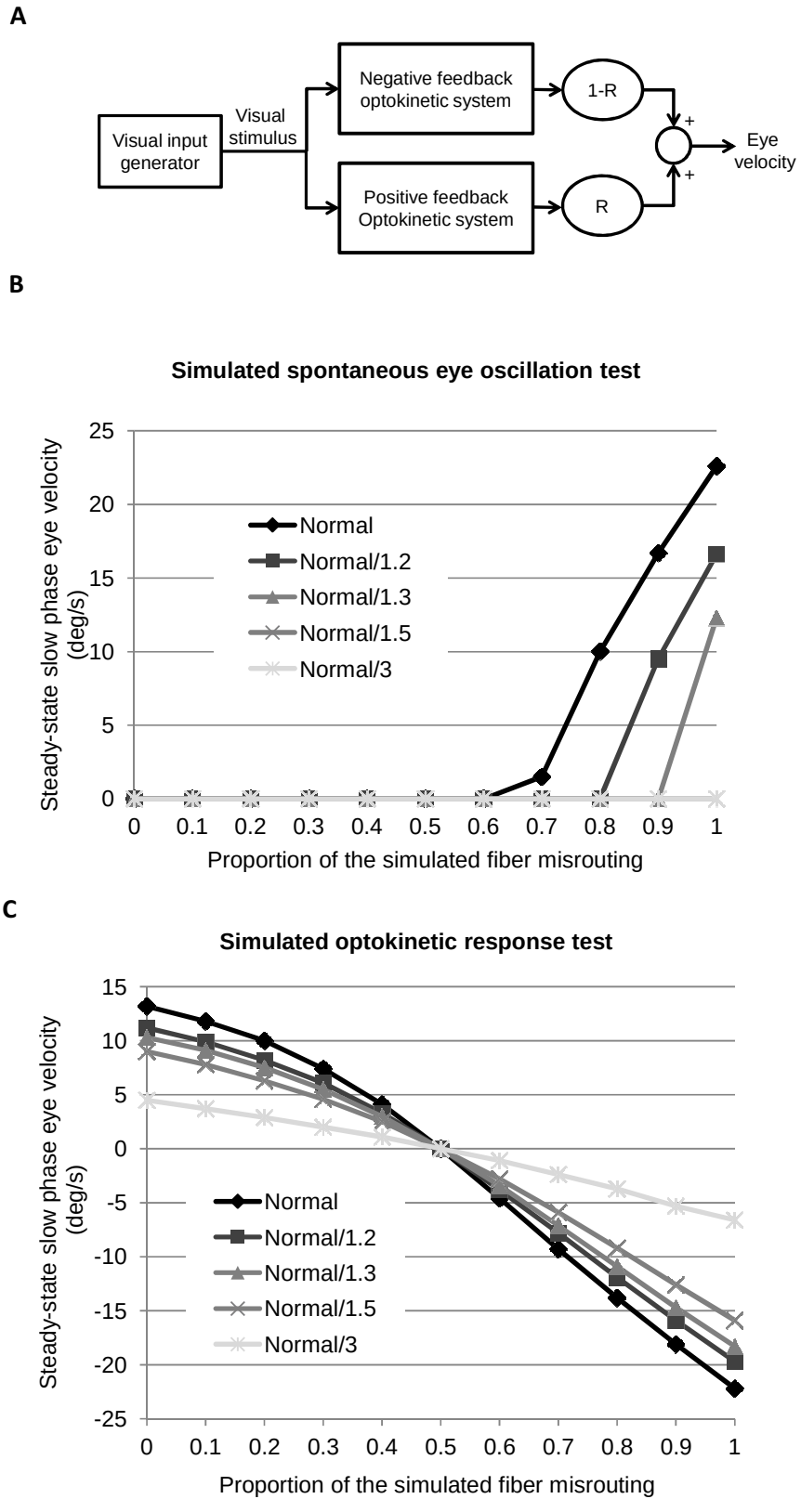

FIGURE 2.6 Computer simulation. (**A**) Schematic of the optokinetic model is shown. R represents proportion of the simulated optic fiber misrouting. (**B**) Results of the simulated SEO test. (**C**) Results of the simulated OKR test.

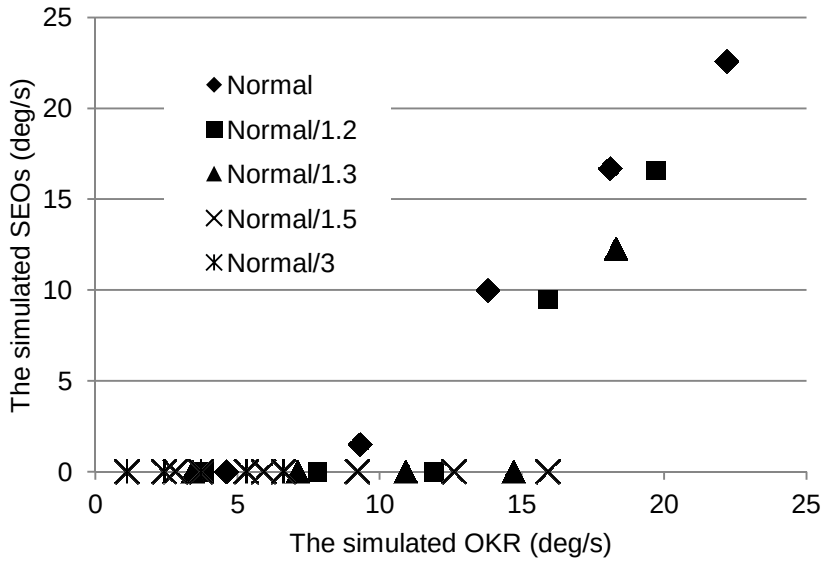

FIGURE 2.7 Correlation between the results of the simulated SEO and OKR tests with the data of a proportion > 0.5. Data points were obtained by grouping data points on the right part of Fig. 6B and Fig. 6C. The correlation was significantly positive (Pearson linear coefficient of 0.7855, $p < 0.0001$).

2.5 Discussions

2.5.1 Gaze stability and OKR of Positive/negative feedback optokinetic systems

In this study, we investigated how the simultaneous existence of positive and negative optokinetic feedback loops affects the optokinetic response (OKR) as well as fixation stability. The optokinetic system in healthy humans is a negative feedback system, in which retinal slip is reduced by keeping the slow-phase eye velocity close to the velocity of the visual world. The positive feedback system, in which retinal slip increases with the slow-phase eye movements, may be created by the misrouting of optic fibers. Our earlier studies in zebrafish larvae (Rick et al., 2000; Huang et al., 2006; Huber-Reggi et al., 2012) demonstrated that the OKR in achiasmatic mutant zebrafish larvae is reversed. In these fish, spontaneous eye oscillations (SEOs) are often observed (Huang et al., 2006; Huber-Reggi et al., 2012). Although no correlation study among the misrouting of optic fibers, the reversed OKR, and the SEOs has been done in human yet, an earlier study done by Hoffmann et al. (2003) found that the space organization in the visual cortex of the misrouting of optic fibers re-arranges in a way of horizontal mirror symmetry (Fig. 2.1A). Such a mirror-symmetrical arrangement may produce a positive feedback loop in the optokinetic system (Fig. 2.1B). Moreover, the reversal of optokinetic nystagmus during optokinetic stimulation was found to occur in some patients with infantile nystagmus syndrome (INS) (Halmagyi et al., 1980; Yee et al., 1980; Lueck et al., 1989) and albinism (Collewijn et al., 1985; St John et al., 1984) although its true mechanism was doubted as well (Jacobs & Dell'Osso, 2004). We mimicked the simultaneous existence of positive and negative feedback loops

in healthy subjects and measured the change in the OKR as well as fixation stability for a better control. The positive and negative feedback loops were experimentally achieved by performing real-time control of image motion based on on-line eye-movement recordings in each subject (Fig. 2.2). The relative amount of fiber misrouting was simulated by adjusting the stimulated retinal areas of the two feedback stimuli (Fig. 2.3A and 2.4A). Moreover, computer simulations with the different proportions of the simulated misrouting were applied as a comparison with the empirical data (Fig. 6).

From the experimental results, a significant difference of visual feedback type in the central visual field was found. the fixation stability was preserved (Fig. 2.3C, left) and slow phases followed the negative feedback visual stimulus (Fig. 2.4C, left) as long as the negative feedback visual stimulus was in the central visual field, suggesting that a negative feedback optokinetic system, irrespective of its magnitude, can effectively stabilize gaze. When the positive feedback visual stimulus was in the central visual field, the occurrence of SEOs seemed to rely on the individual response as well as the stimulus combination (Fig. 2.3C, right) but, in all subjects, slow phases followed the positive feedback visual stimulus (Fig. 2.4C, right), suggesting that a positive feedback optokinetic system has a capacity to evoke SEOs. Moreover, both the magnitude of the SEOs and the degree of the positive feedback OKR significantly increased with the size of the central field stimulus, suggesting that a higher degree of misrouted optokinetic signals can form a stronger positive feedback optokinetic system, which further induces more intense SEOs. The correlation between the degree of the positive feedback optokinetic system and the magnitude of the SEOs was significantly positive (Fig. 2.5).

In our computer simulations, if the negative feedback optokinetic system dominates (i.e. a proportion of the simulated optic fiber misrouting < 0.5), no simulated SEO occurs (Fig. 2.6B) and the simulated OKR is normal (in terms of direction) (Fig. 2.6C), similar to what we found in the experimental results. If the positive feedback optokinetic system dominates (i.e. a proportion > 0.5), the simulated OKR is reversed (Fig. 2.6C) but the simulated SEOs occur only if the proportion of the simulated optic fiber misrouting is at least 0.7 (Fig. 2.6B). Once the simulated SEOs are evoked, the magnitude increases with the proportion of the misrouting. However, with the same proportion of the misrouting, the simulated SEOs decrease, and may not occur, due to a low gain OKR curve (Fig. 2.6B). We further correlated the degree of the simulated reversed OKR with the corresponding fixation stability (Fig. 2.7). Similar to Fig. 2.5, the correlation is significantly positive. However, rather than a linear relation between these two, it is more likely that the simulated SEOs need to be triggered by certain degree of instability first and then the magnitude increases with the degree of the simulated reversed OKR.

By comparing the experimental results (Fig. 2.5) with the simulation (Fig. 2.7), we found a disagreement as to whether a low degree of the instability is able to evoke SEOs. In our simulation, the simulated SEOs need to be triggered by certain degree of instability, but the SEOs, in practice,

occurred with a weak instability. We speculate that such SEOs may result from an involvement of smooth pursuit. The stimulus combinations that caused such weak instability but obvious SEOs were that the positive feedback visual stimulus was in the central 10° or 20° visual field, which contains the fovea. The central projection area moved consistently with left eye to make sure that the central field stimuli were always in the same area of the retina. Such a condition may somehow activate the smooth pursuit system to follow the moving central visual field and induce SEOs.

The between-subject variation was large in the SEO and OKR tests (Fig. 2.3C and 2.4C). Two subjects showed relatively weak eye movements under all paradigms. Even with the stimulus combination that the negative feedback (constantly moving) optokinetic stimulus was in the central 80° visual field, their eye velocities were still low (Fig. 2.4C, left most condition), suggesting that these two subjects have a naturally low OKR. Therefore our paradigms, which mainly affected the optokinetic system, were not able to significantly change their ocular motor behavior. Moreover, from the simulation, we found that the simulated SEOs may vary considerably by just dividing the normal OKR curve by 1.2 and 1.3. With a further lower OKR curve, the simulated SEOs do not occur (Fig. 2.6B). The simulated results support that the large between-subject variation found in Fig. 3C and 4C resulted from the individual difference rather than the experimental design.

2.5.2 OKR-related visual field

From the experimental results, we found that the slow phases followed the stimulus in the central 10° visual field, even when the area of stimulation of the peripheral field was substantially larger and the stimulus of the peripheral field was conflicting to the one of the central field (Fig. 2.4C, the central two conditions), suggesting that the optokinetic signals of the central 10° visual field were weighted more than the signals from the peripheral field. This finding is consistent with numerous studies that have found that the central retina is more effective in driving the OKR (Cheng & Outerbridge, 1975; van Die & Collewijn, 1982; Howard & Ohmi, 1984; Abadi et al., 2005).

We expect that the magnitude of the median eye velocity should significantly increase with the size of the central field stimulus simply because a larger area of the central field carries more optokinetic signals than the conflicting optokinetic signals from the peripheral field. Based on the experimental results, we found that the magnitude of the median eye velocity, overall, significantly increased with the size of the central field stimulus, irrespective of the feedback type in the central field (Fig. 2.4C). However, the linear fits of the median eye velocity and the area of the central field stimulus of negative feedback were significantly positive only in two subjects (Fig. 2.4C, left part). With a careful look at the left part of Fig. 2.4C, most of subjects only showed a subtle change when the area of the central field was more than 30°, suggesting that the central 30° visual field carries most of optokinetic signals. However, such a saturation effect was not found when the positive feedback visual stimulus was in the central field (Fig. 2.4C, right part). This could be because the image velocity of the positive

feedback visual stimulus increased with the eye velocity. Therefore, in such a positive feedback condition, the visual-field effect could be affected so that the saturation effect was not found.

2.5.3 Waveform analysis

Waveforms in the SEO tests are highly reliant on the initial retinal slips as well as the interaction of the feedback stimulus and the optokinetic system. The SEOs in most subjects were unidirectional. From a system dynamics view, the unidirectional SEOs can be explained as a result of a strong positive feedback loop. The initial retinal slip, induced by either slight self-rotation or a subtle oscillation of visual surround, is random and can be in either direction. The initial retinal slip, then, is magnified and maintained by the high degree of positive feedback. Thus, the eyes keep moving in one direction and the unidirectional SEOs occur.

The bidirectional SEOs were found only in two subjects with the stimulus combinations that the positive feedback visual stimulus was in the central 10° visual field. The mechanism responsible for the bidirectional SEOs may be a weak instability of the optokinetic system and an involvement of smooth pursuit. According to the experimental results (Fig. 2.4C), the central 10° field stimulus of positive feedback can only cause the OKR to become slightly unstable. Such a slight reversed OKR might not evoke the SEOs based on the simulation readout (Fig. 2.6BC and Fig. 2.7). However, with the weak instability, eyes were no longer restrained by the optokinetic system and were free to move around. Then, the smooth pursuit might be activated by the central visual field, which moved with eyes consistently to keep the central field stimulus approximately on the same area of the retina (see experimental paradigms of Materials and Methods). When the interaction between the smooth pursuit and the central visual field happened to change the direction regularly after each saccade, the bidirectional SEOs occurs, like the lowest one of the right part in Fig. 2.3B.

2.5.4 Relation to infantile nystagmus syndrome (INS)

Human patients with the misrouting of optic fibers, such as those with albinism (Lund, 1965; Jeffery, 1977; Morland et al., 2002) and achiasmia (Apkarian et al, 1995; Petros et al., 2008; Hoffmann et al., 2012), often have infantile nystagmus syndrome (INS) (Collewijn et al., 1985; St John et al., 1984; Biega et al., 2007), in which SEOs usually appear within six months after birth (von Noorden & Campos; 2002). This study provides a possible mechanism of how the misrouting leads to SEOs. If the misrouting creates a strong positive feedback loop, SEOs are likely to occur. This study also indicates that gaze can be stable if the misrouting is not large enough to reverse the OKR or the OKR is reversed but too weak to evoke SEOs, explaining why some patients with misrouted optic fibers have stable gaze (Lee et al., 2001; Gradstein et al., 2005). Our results in normal subjects also suggest that SEOs will not occur if the OKR gain is low. Moreover, a reversed OKR can be used to test whether the INS is related to abnormal optokinetic feedback. If SEOs are linked to abnormal optokinetic feedback,

then both the OKR and the resulting nystagmus should be reversed. If INS patients do not have a reversed OKR, their nystagmus may or may not reverse and their SEOs should be due to other pathological deficits (Harris & Berry, 2006; Jacobs & Dell'Osso, 2004; Anderson, 1953; Dell'Osso, 2006).

Nystagmus in the dark, often found in the INS patient (Hertle & Dell'Osso, 2013), cannot be explained by this study. Also, frequency of SEOs in INS patients, ranged between 3 and 6 Hz (Hertle & Dell'Osso, 2013; Kumar et al., 2011) is much higher to what we presented in this study. In our study, our subjects only experience each stimulus for 30 seconds, so adaptive mechanisms were unlikely to contribute to the measured response, unlike in patients. Easter and Schmidt (1977) found that goldfish with artificially induced ipsilateral retinal projections showed SEOs and a reversed OKR. After long-lasting nystagmus in the light, the nystagmus was found to exist in the dark. In the same study, they also found that the fish began to circle after regeneration of the deflected optic nerves and the speed of circling, which is supposed to be related to the magnitude of the spontaneous nystagmus in fish, increased over weeks. If what happened in fish was also true in human, the mismatch between the INS patients and this study may be explained. However, whether this adaptation plays a role in human INS is speculative, does not explain INS in dark at birth, and requires further investigation.

2.6 Reference

Abadi RV, Howard IP, Ohmi M, Lee EE. The effect of central and peripheral field stimulation on the rise time and gain of human optokinetic nystagmus. *Perception. 2005;34:1015-1024.*

Anderson JR. Causes and treatment of congenital eccentric nystagmus. Br J Ophthalmol. 1953;37:267–281.

Apkarian P, Bour LJ, Barth PG, et al. Non-decussating retinal-fugal fibre syndrome. An inborn achiasmatic malformation associated with visuotopic misrouting, visual evoked potential ipsilateral asymmetry and nystagmus. *Brain*. 1995;118:1195–1216.

Biega TJ, Khademian ZP, Vezina G. Isolated absence of the optic chiasm: a rare cause of congenital nystagmus. *AJNR Am J Neuroradiol*. 2007;28: 392–393.

Black HS. Stabilized Feedback Amplifiers. *Bell System Tech J.* 1934;13: 1–18.

Brainard DH. The Psychophysics Toolbox. *Spat Vis*. 1997;10:433-6.

Cheng M, Outerbridge JS, Optokinetic nystagmus during selective retinal stimulation. *Exp Brain Res.* 1975;23:129-139.

Collewijn H, Apkarian P, Spekreijse H. The oculomotor behaviour of human albinos. *Brain.* 1985;108:1–28.

Dell'Osso LF, Daroff RB. Congenital nystagmus waveforms and foveation strategy. *Doc Ophthalmol*. 1975;39:155–182.

Dell'Osso LF. Biologically relevant models of infantile nystagmus syndrome: the requirement for

behavioral ocular motor system models. *Semin Ophthalmol*. 2006;21:71–77.

Easter SS, Schmidt JT. Reversed visuomotor behavior mediated by induced ipsilateral retinal projections in goldfish. *J neurophysiol.* 1977;40:1245-1254.

Gradstein L, FitzGibbon EJ, Tsilou ET, et al. Eye movement abnormalities in Hermansky-Pudlak syndrome. *J AAPOS*. 2005;9:369-378

Halmagyi GM, Gresty MA, Leech J. Reversed optokinetic nystagmus (OKN): mechanism and clinical significance. *Ann. Neurol*. 1980;7:429–435.

Hertle RW, Dell'Osso LF. Nystagmus in Infancy and Childhood: Current Concepts in Mechanisms, Diagnoses, and Management. *Oxford University Press, New York.* 2013; 1-323.

Harris C, Berry D. A developmental model of infantile nystagmus. Semin Ophthalmol. 2006;21:63–69.

Howard IP, Ohmi M. The efficiency of the central and peripheral retina in driving human optokinetic nystagmus. *Vision Res*. 1984;24:969-976.

Huang YY, Rinner O, Hedinger P, Liu SC, et al. Oculomotor instabilities in zebrafish mutant belladonna: a behavioral model for congenital nystagmus caused by axonal misrouting. *J Neurosci.* 2006;26: 9873–9880.

Huber-Reggi SP, Chen CC, Grimm L, et al. Severity of infantile nystagmus syndrome-like ocular motor phenotype is linked to the extent of the underlying optic nerve projection defect in zebrafish belladonna mutant. *J Neurosci.* 2012;32:18079-86.

Hoffmann MB, Kaule FR, Levin N, et al. Plasticity and Stability of the Visual System in Human Achiasma. *Neuron*. 2012;75:393-401.

Hoffmann MB, Tolhurst DJ, Moore AT, et al. Organization of the visual cortex in human albinism. *J Neurosci.* 2003;23:8921–8930.

Jacobs JB, Dell'Osso LF. Congenital nystagmus: hypotheses for its genesis and complex waveforms within a behavioral ocular motor system model. *J Vis*. 2004:4:604-25.

Jeffery G. The albino retina: an abnormality that provides insight into normal retinal development. *Trends Neurosci*. 1997;20:165–169.

Kleiner M, Brainard D, Pelli D, et al. What's new in Psychtoolbox-3. *Perceptio.* 2007;36:1-1.

Kumar A, Gottlob I, Mclean RJ, et al. Clinical and oculomotor characteristics of albinism compared to FRMD7 associated infantile nystagmus. *Invest Ophthalmol Vis Sci*. 2011;52:2306-13.

Lueck CJ, Tanyeri S, Mossman S, Crawford TJ, and Kennard C. Unilateral reversal of smooth pursuit and optokinetic nystagmus. *Revue Neurologique (Paris)*. 1989;145, 656-660

Lund RD. Uncrossed visual pathways of hooded and albino rats. *Science.* 1965;149:1506–1507.

Morland AB, Hoffmann MB, Neveu M,et al. Abnormal visual projection in a human albino studied with functional magnetic resonance imaging and visual evoked potentials. *J Neurol Neurosurg Psychiatry*. 2002;72:523–526.

Oh SY, Shin BS, Jeong KY, Hwang JM, Kim JS. Clinical and Oculographic Findings of X-linked

Congenital Nystagmus in Three Korean Families. J Clin Neurol. 2007;3:139-146.

Pelli DG. The VideoToolbox software for visual psychophysics: transforming numbers into movies. *Spat Vis*. 1997;10:436-442.

Petros TJ, Rebsam A, Mason CA. Retinal axon growth at the optic chiasm: to cross or not to cross. *Annu Rev Neurosci*. 2008;31:295–315.

Rick JM, Horschke I, Neuhauss SC. Optokinetic behavior is reversed in achiasmatic mutant zebrafish larvae. *Curr Biol*. 2000;10:595–598.

Robinson DA. The use of control systems analysis in the neurophysiology of eye movements. *An. Rev Neurosci*. 1981;4: 463-502.

St John R, Fisk JD, Timney B, et al. Eye movements of human albinos. *Am J Optom Physiol Opt*. 1984;61:377–385.

Thurtell MJ, Leigh RJ. Nystagmus and saccadic intrusions. *Handb Clin Neurol*, 2011;102:333-378.

Lee KA, King RA, Summers CG. Stereopsis in patients with albinism: clinical correlates. *J AAPOS*. 2001;5:98-104.

Van Die G, Collewijn H. Optokinetic nystagmus in man. Role of central and peripheral retina and occurrence of asymmetries. *Hum Neurobiol*. 1982;1:111-119.

Von Noorden GK, Campos EC. *Binocular Vision and Ocular Motility*. Mosby. St. Louis; 2002;508–533.

Yee RD, Baloh RW, Honrubia V. Study of congenital nystagmus: optokinetic nystagmus. *Br J Ophthalmol*. 1980;64: 926–932.

Zeigler BP, Praehofer H, Kim TG. Theory of Modeling and Simulation: Integrating Discrete Event and Continuous Complex Dynamic Systems. *New York: Academic Press.* 2000.

2.7 Supplemental materials

2.7.1 Modified Robinson optokinetic model

To simulate the optokinetic response (OKR), a model of optokinetic reflex and vestibulo-ocular reflex (VOR) built by Robinson (1977) was applied. Because we only focused on the OKR, part of the model related to the VOR was ignored and the rest was rearranged to obtain Robinson optokinetic model (Fig. 2.SM1). To let the optokinetic model be closer to the human OKR, we added a gain-control block and delays into the model (Fig. 2.SM2). The gain-control block was placed before the transfer function to determine the steady-state eye velocity. The relation between the steady-state eye velocity and the velocity of the visual surround is shown in Fig. 2.SM3. The data points were collected from one subject and curve fitting was done to obtain the relation (see OKR test and Data analysis in Supplemental materials for the details). The fitted curve, named Normal, was further divided by 1.2, 1.3, 1.5, and 3 to simulate various OKRs. To take the delay into account, we first measured the overall delay of the human OKR. Fig. 2.SM4 showed that the overall delay of this subject was approximately 180 ms. To distribute the overall delay to each component, we put 50 ms in delay in the retina, 30 ms in premotor delay, and 80 ms in the delay of the efference copy base on a previous study (Robinson, 1986). The central delay was then set to 100 ms to keep the overall delay 180 ms. To create a positive feedback optokinetic model caused by the misrouting of optic nerves, a gain block of the negative one, representing misleading optic signals to the wrong hemisphere, was added after the block, delay in the retina (Fig. 2.SM5). Due to this block, the perception was reversed, resulting in the eye velocity command opposite to the velocity of the visual surround. As a result, retinal slip increases with the eye velocity and a positive feedback loop was formed.

2.7.2 OKR test

One subject aged 29 years with no abnormal neurological or ophthalmological history and correct-to-normal visual acuity participated in this OKR test. Eye movements were recorded by using a head-mounted video-oculography (VOG) device (EyeSeeCam, Munich, German) with a sample rate of 220 frames/s. A screen of 178 cm in width and 130 cm in height that was placed 100 cm away from the subject. Therefore, it covered 80° of the horizontal visual field and 66° of the vertical visual field. A digital projector (Sony, VPL-PX30) operating at 60 frames per second and a spatial resolution of 1280 x 1024 pixels was used to present visual stimuli. The visual stimuli were controlled by a custom-developed script in MATLAB (Mathworks, Natick, MA) with its installation of the Psychophysics Toolbox extensions (Brainard, 1997; Pelli, 1997; Kleiner et al., 2007). Sine-wave gratings with a spatial frequency of 0.25 cycle/degree and high contrast (darkest and lightest pixels as possible) were used as the image pattern. Moving grating speeds, 10, 20, 30 … and 150 deg/s, were applied. Each condition lasted for 30 seconds and there was a 10-second break without visual stimulus between conditions.

2.7.3 Data analysis

Data analysis was done by a custom-developed program written in MATLAB. The left eye was analyzed. Eye position was smoothened by a Gaussian low-pass filter with a cut-off frequency of 18 Hz. Eye velocity was computed by the derivative of eye position. Saccades were filtered out by visual inspection. Average slow-phase eye velocity of each condition was calculated and shown in Fig. 2.SM2. The fitted curve (Normal) in Fig. 2.SM2 was done by using the nonlinear least squares method of the 'fit' function in the Curve Fitting Toolbox of MATLAB (Mathworks, Natick, MA).

2.7.4 Reference

Brainard DH. The Psychophysics Toolbox. *Spat Vis*. 1997;10:433-6.

Demer JL, Robinson DA. Different time constants for optokinetic and verstibular nystagmus with a single velocity-storage element. B*rain Res*. 1983;276:173-177.

Kleiner M, Brainard D, Pelli D, et al. What's new in Psychtoolbox-3. *Perceptio.* 2007;36:1-1.

Pelli DG. The VideoToolbox software for visual psychophysics: transforming numbers into movies. *Spat Vis*. 1997;10:436-442.

Robinson DA. Linear addition of optokinetic and vestibular signals in the vestibular nucleus. *Exp. Brain Res.* 1977;30:447-450.

Robinson DA. Is the oculomotor system a cartoon of motor control, *Prog Brain Res*. 1986;64: 411-417.

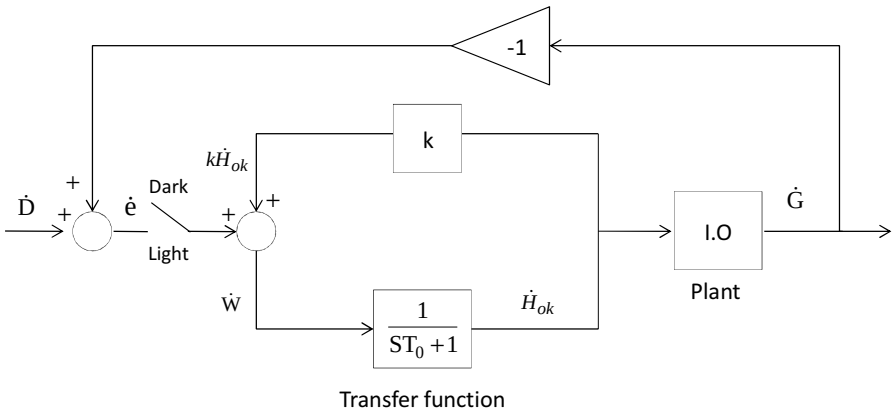

Figure 2.SM1. Robinson optokinetic model. The model was adapted from Robinson, 1977. Part of the original model related to the vestibulo-ocular reflex (VOR) was ignored or rearranged. Description of the model can be found in previous studies (Robinson, 1975; Demer & Robonson, 1983). Briefly, retinal slip ($\dot{e}$) is the difference between the velocity of the visual surround ($\dot{D}$) and the eye velocity ($\dot{G}$). The plant represents the eye and its muscles. The eye-velocity command ($\dot{H}_{ok}$) is generated by the transfer function with time constant (T_0) that provides only low-frequency signals. The eye velocity command ($\dot{H}_{ok}$) is sent to the plant to generate the eye velocity ($\dot{G}$). On other hand, a fractional copy of eye velocity ($k\dot{H}_{ok}$) is sent to calculate the neurally encoded velocity of the visual world ($\dot{W}$). The path after the eye plant indicates that the optokinetic system is a negative feedback system: retinal slip ($\dot{e}$) is an error signal and the function of the feedback system is to let the eye velocity ($\dot{G}$) to be close to the velocity of the visual surround ($\dot{D}$). Note the time constant (T_0) is set to 0.1 sec to fit the transient optokinetic response shown in Fig. 2.SM4. Since there is no retinal slip in the dark, a switch Dark/Light is applied to control the path of retinal slip.

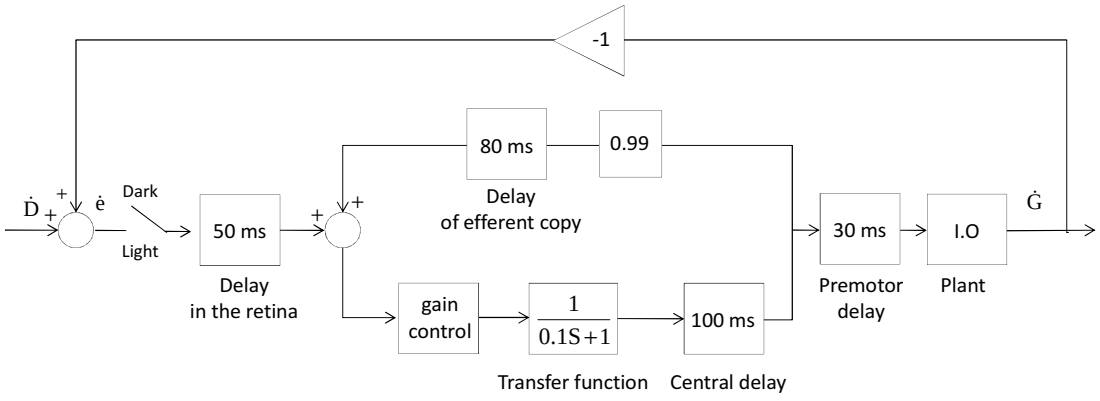

Figure 2.SM2. Modified Robinson optokinetic model. A gain control and several delays were added the original model. The optokinetic system remained a negative feedback system because the feedback loop was not influenced.

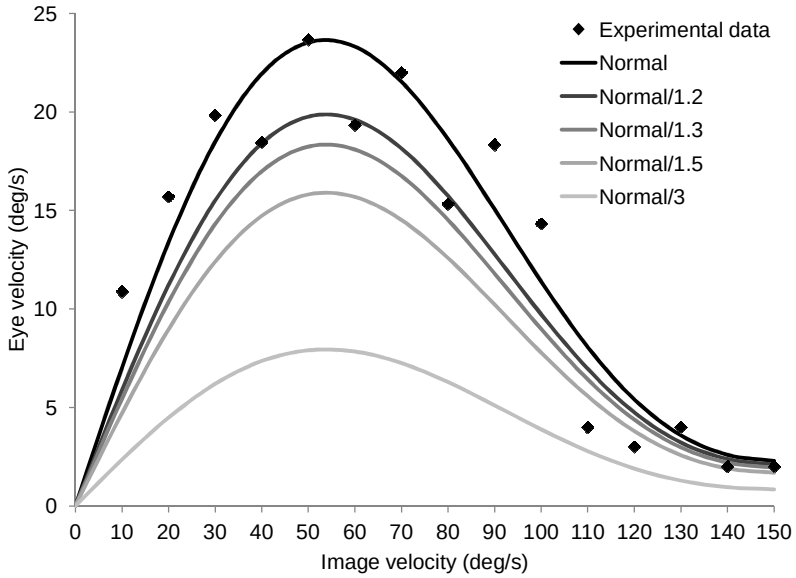

Figure 2.SM3. The average slow-phase eye velocity of one subject under different image velocities. The solid square represents the empirical data. The black line was fitted with the empirical data. The other curves were obtained by dividing the black line by 1.2, 1.3, and so on.

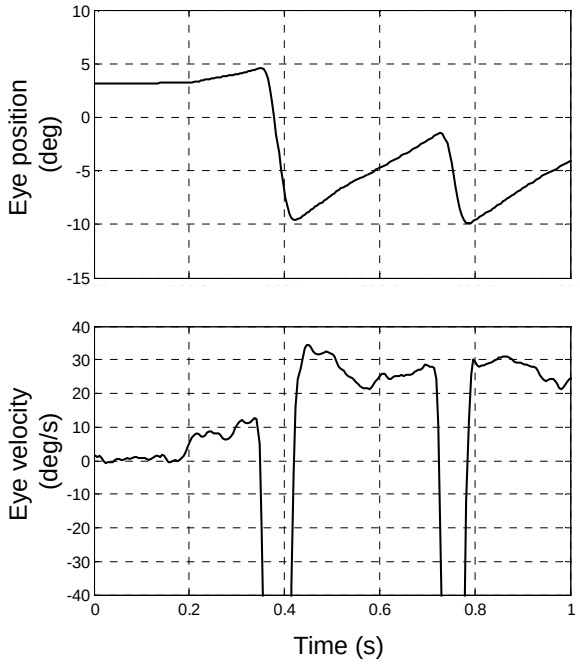

Figure 2.SM4. Latency of the human OKR. The upper part is the eye-positive curve and the lower part is the eye-velocity curve. Optokinetic stimulation started from 0 sec. The latency shown in the presenting figure was approximately 180 ms.

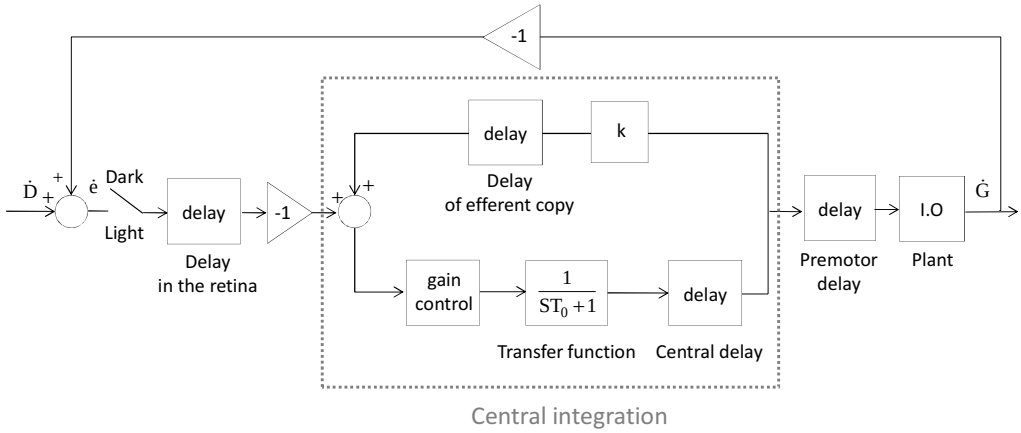

Figure 2.SM5. Positive feedback optokinetic model. By adding a gain of the negative one after the delay in the retina, the motion perception is reversed. Thus, the eye-velocity commands generated by central integration move the eyes in the opposite direction of the visual world. As a result, retinal slip increases with the eye velocity and the optokinetic system is turned into a positive feedback system.

Chapter 3

Afternystagmus in darkness after suppression of optokinetic nystagmus: an interaction of a motion aftereffect and retinal afterimages

Chien-Cheng Chen[1,5], Melody Ying-Yu Huang[1,4], Konrad P. Weber[1,2], Dominik Straumann[1,4], and Christopher J. Bockisch[1,2,3]

Departments of [1]Neurology, [2]Ophthalmology, and [3]ENT, University Hospital Zurich, Zurich, Switzerland; the [4]Zurich Center for Integrative Human Physiology (ZIHP), Zurich, Switzerland; [5]PhD Program in Integrative Molecular Medicine, Life Science Graduate School, Zurich, Switzerland

Adaptation from an article published in Experimental Brain Research (2014) doi.org/10.1007/s00221-014-3971-4.

Acknowledgements

The authors like to thank Marco Penner and Urs Scheifele for their excellent technical assistance. This work was supported by the Swiss National Science Foundation (SNF) grants PMPDP3_139754 (Marie Heim-Vögtlin programme) & 31003A-118069, Zurich Center for Integrative Human Physiology (ZIHP), and Betty and David Koetser Foundation for Brain Research.

Personal Contribution

Conceiving the project and designing the experiments with the other authors, performing the experiments and analyzing the data alone, and writing manuscript with MYYH, CJB, and DS.

3.1 Abstract

The afternystagmus that occurs in the dark after gaze fixation during optokinetic stimulation is directed in the opposite direction of the previous optokinetic stimulus. The mechanism responsible for such afternystagmus after suppression of optokinetic nystagmus (ASOKN) is unclear. Several hypotheses have been put forward to explain it, but none is conclusive. We hypothesized that ASOKN is driven by the interaction of two mechanisms: (1) motion aftereffect (MAE)-induced eye movements and (2) retinal afterimages (RAIs) produced by fixation during the suppression of optokinetic nystagmus. We examined the correlation among ASOKN, MAE-induced eye movements, and RAIs in healthy subjects. Adapting stimuli consisted of moving random dot patterns and a fixation spot and their brightness was adjusted to induce different RAI durations. Test patterns were a stationary random dot pattern (to test for the presence of a MAE), a dim homogeneous background (to test for MAE driven eye movements), and a black background (to test for ASOKN and RAIs). MAEs were reported by 16 out of 17 subjects, but only 7 out of 17 subjects demonstrated MAE-induced eye movements. Importantly, ASOKN was only found when these 7 subjects reported a RAI after suppression of optokinetic nystagmus. Moreover, the duration of ASOKN was longer for high-brightness stimuli compared to low brightness stimuli, just as RAIs persist longer with increasing brightness, even though these optokinetic stimuli induce similar optokinetic responses (OKR). We conclude that ASOKN results from the interaction of MAE-induced eye movements and RAIs.

3.2 Introduction

Optokinetic nystagmus (OKN), which is induced by a constantly moving large-field visual surround, consists of slow-phase eye movements to minimize retinal slip (i.e. the velocity difference between the eyes and the moving visual surround) and fast-phase eye movements for position reset. When the optokinetic stimulus is replaced by total darkness, nystagmus continues with a gradual decay (Ohm 1921). Optokinetic afternystagmus (OKAN) is thought to be generated by a mechanism that stores slow-phase eye velocity signals during optokinetic stimulation and keeps releasing the eye-velocity signals for a certain period after cessation of the optokinetic stimulus. This so-called velocity storage mechanism (VSM) stores velocity signals from the optokinetic and vestibular systems to preserve their low-frequency signals and hence enhance visual-vestibular cooperation during rotation in the light (Cohen et al., 1977; Raphan et al., 1977; Raphan et al., 1979; Laurens & Angelaki, 2011).

A different afternystagmus in total darkness occurs after optokinetic stimulation, during which subjects suppress OKN by fixating their eyes upon a space-fixed visual target. This afternystagmus after suppression of OKN (in the following abbreviated with ASOKN) is directed opposite of the previous optokinetic stimulus (Korenaga et al., 1996), which is in contrast to OKAN, during which the nystagmus occurs in the same direction. Kudo et al. (2002) suggested that this “reverse OKAN” results from the VSM, which is charged by retinal slip (a sensory signal) and then generates an eye velocity signal in the opposite direction of optokinetic stimulation to counteract the optokinetic signal. This keeps the fovea on a stationary target in the presence of the moving large-field visual surround. In a different interpretation, Ventre-Dominey and Luyat (2009) suggested that ASOKN is linked to the vestibular and pursuit motor systems rather than a purely sensory signal (retinal slip). Note, however, that ASOKN has not always been found; e.g. Fletcher et al. (1990) found that fixation of a small target during optokinetic stimulation almost completely prevented the development of afternystagmus and thus concluded that gaze fixation actively prevents storage of visual signals.

Gaze fixation upon a space-fixed target during optokinetic stimulation can induce a perceptual motion aftereffect (MAE). The perceptual MAE is an illusory motion perception: a stationary stimulus is perceived to move in the opposite direction of the previous optokinetic stimulus (Anstis et al., 1998; Mather et al., 1998). The perceptual MAE may drive eyes to pursue the motion illusion. Watamaniuk and Heinen (2007) demonstrated that after gaze fixation during unidirectional optokinetic stimulation eye movements were biased in the opposite direction. In the same study, these authors showed that such MAE-induced eye movements do not occur in the dark, i.e. only appear in the presence of a visual input (they used a moving random dot stimulus). This is analogous to the perceptual MAE, which also requires a visual stimulus (Wohlgemuth, 1911; Spigel, 1960; Verstraten et al., 1994; Thompson and Wright, 1994).

Prolonged ocular fixation of a visual target may induce retinal afterimages (RAIs) (Brown, 1965). RAIs, which occur on the retina due to adaptation of photoreceptors, are optical illusions that persist

after the exposure to the original image (Shimojo et al., 2001). It has been demonstrated that the duration of RAIs is positively correlated with the intensity and lasting time of the original image (Granit et al., 1930; Feinbloom, 1938; Nagamata, 1951; Lu et al., 2006). It is possible that, during optokinetic stimulation, ocular fixation of a space-fixed visual target induces a RAI as well.

We hypothesized that ASOKN is caused by an interaction of MAE-induced eye movements and RAIs and not the result of any VSM. Although MAE-induced eye movements depend on visual input and should not be activated in the dark, RAIs can be an alternative visual source to elicit these eye movements. Consequently, such eye movements would be directed opposite of the previous optokinetic stimulus. Moreover, since RAIs are eye-fixed, they would move with the MAE-induced movements of the eyes, thereby stimulating further eye movements, forming a positive feedback loop. As a result, the eyes keep moving in the direction of the MAE-induced eye movements as long as RAIs are present. Such a mechanism can maintain nystagmus independent of the VSM.

To test our hypothesis, we did a correlation study among MAE-induced eye movements, RAIs, and ASOKN in healthy human subjects. Moreover, visual stimuli of different brightness were used to evoke different RAI durations. According to our hypothesis, ASOKN would only occur in those subjects who demonstrate MAE-induced eye movements and perceive a RAI. In addition, the duration of ASOKN should be longer with a stimulus of higher brightness, just as RAIs persist longer with increasing brightness.

3.3 Materials and Methods

3.3.1 Human subjects

Experiments were performed on 10 males and 7 females, aged 23-49 years, with no abnormal neurologic or ophthalmologic history. Visual acuity was normal or corrected-to-normal., All subjects gave their informed written consent and the experiment was approved by the local ethics committee.

3.3.2 Experimental setup

A head-mounted video-oculography (VOG) device (EyeSeeCam, Munich, German) running at a frame rate of 220 Hz was used for the eye-movement recording. Subjects faced the center of a screen which was placed 100 cm away from the head of subject. The screen was 178 cm in width and 130 cm in height. Thus, it covered 80° of the horizontal visual field and 66° of the vertical visual field. A digital projector (Panasonic PT-AE7000 Projector), operating at 60 frames per second and a spatial resolution of 1920 x 1080 pixels, was used. A custom-developed script in MATLAB (Mathworks, Natick, MA, USA) and its Psychophysics Toolbox extensions (Brainard 1997; Pelli 1997; Kleiner et al., 2007) were applied to control visual stimuli. Eye position was calibrated at ± 10° of the center of the screen with a custom-developed script.

3.3.3 Visual stimulation

The optokinetic stimulus was a random pattern of 600 white dots (3 deg^2) with a dot lifetime of 150 milliseconds. The speed of each dot was 30 deg/s toward the right. In conditions with gaze fixation, a space-fixed 1.6 deg^2 yellow dot with a black ring inside was projected on the center of the screen (Fig. 1). Low and high brightness conditions were used to evoke different retinal afterimage (RAI) durations. In the high-brightness condition, the luminance of the moving dots and the yellow fixation dot were 330 lux and 314 lux, respectively. In the low brightness condition, the luminance of the moving dots and the yellow fixation dot were 68 lux and 70 lux.

3.3.4 Experimental conditions

Six conditions were applied in this study (Fig. 3.1). The sequence of conditions was randomized in each subject. Each condition was presented to subjects once.

Conditions 1 to 4 started with a 3-minute period of suppression of optokinetic nystagmus (OKN) and were followed by a 1-minute task. During the period of suppression of OKN, subjects were asked to fixate their eyes upon the yellow stationary dot in the center of the screen.

Condition 1 tested whether or not the perceptual motion aftereffect (MAE) occurred after suppression of OKN. After suppression of OKN, the speed of each random dot was set to zero during the 1-minute task. In other words, each random dot just stayed in the same position for 150 milliseconds and then reappeared in another position. The central yellow fixation dot remained unchanged. Subjects were asked to report any percept of motion in the random dot pattern while fixating the central yellow dot. The stimuli used in condition 1 were of high brightness.

With condition 2 we tested whether or not MAE-induced eye movements occurred. The period of suppression of OKN was the same as in condition 1. After suppression of OKN, no structured pattern was present on the screen. Thus, the screen luminance (0.17 lux) was uniform across the whole screen. Such a visual environment provides a visual input without fixation targets to evoke possible MAE-induced eye movements.

Conditions 3 (low brightness) and 4 (high brightness) were applied to test how afternystagmus after suppression of OKN (ASOKN), if present, changed with the RAI duration. After suppression of OKN, the visual surround was switched to dark. The dark condition was always examined before Conditions 3 and 4 by asking subjects whether they saw any light while they were covered by a lightproof cloth. Since the light from the LCD beamer we used could not be turned completely off, we found that using the cloth to completely cover the subjects head was a fast and effective way to create a dark environment for the subject. Afterwards, subjects were asked if they saw a RAI during the last minute.

Conditions 5 and 6 were applied to test whether or not low and high brightness optokinetic

stimuli could evoke the same degree of optokinetic response (OKR). No fixation was provided in these two conditions. The low brightness condition was used in Condition 5 and the high brightness condition was used in Condition 6.

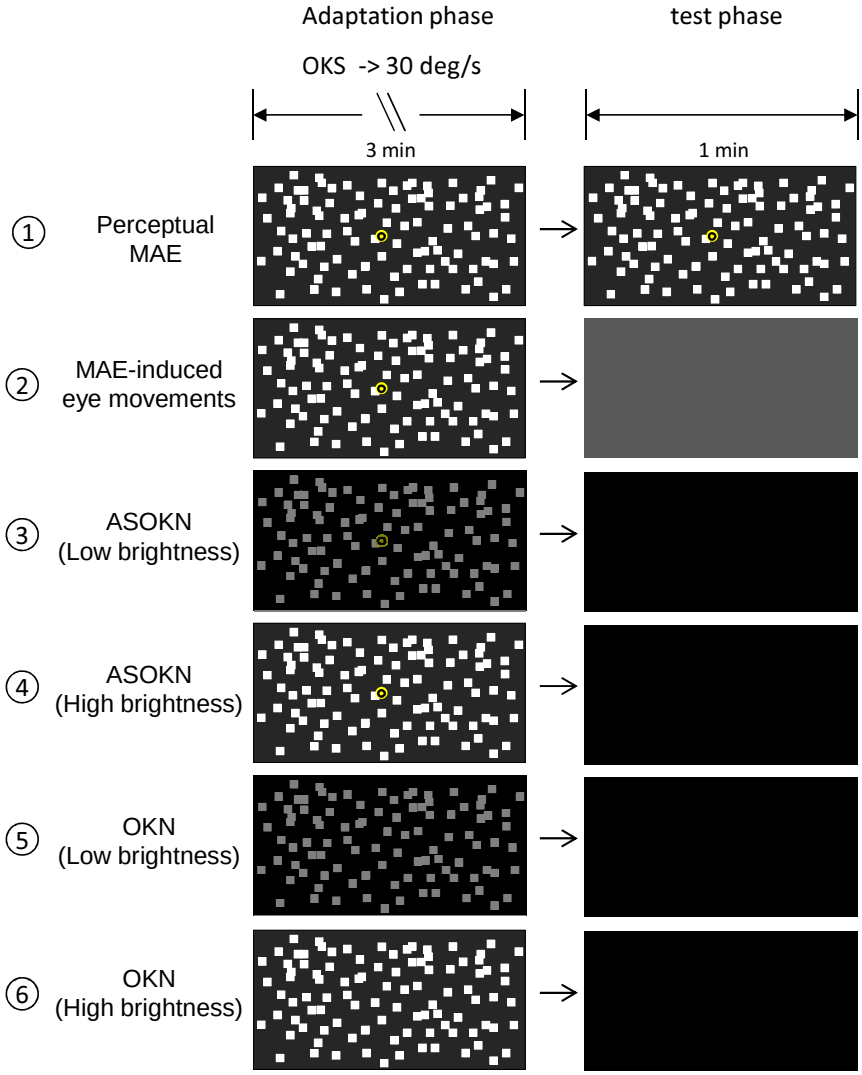

Figure 3.1 Experimental conditions. Each row represents the stimuli in a condition. The left column shows the motion stimuli (of different brightness), with or without a central fixation dot during the first phase of each condition. The right column represents the stimuli in the testing phase. Condition 1 was applied to test the perceptual MAE. The random dot pattern in the testing phase did not move. Condition 2 was applied to test the MAE-induced eye movements. Conditions 3 and 4 were designed to investigate how stimulus brightness affects ASOKN. Conditions 5 and 6, in which there was no central fixation spot, were designed to investigate how stimulus brightness affects the optokinetic response. The high brightness visual stimulus was applied on Conditions 1, 2, 4, and 6 while the low brightness one was applied on Conditions 3 and 5 (see the "visual stimulation" section of Methods for the details of the stimulus brightness).

3.3.5 Data analysis

The movement of the left eye was analyzed. Data analysis was all done by a custom-developed program written in MATLAB. Eye position was smoothened by a Gaussian low-pass filter with a cut-off frequency of 18 Hz. Eye velocity was derived from the smoothed position signal. Blink, if

occurred during the test phase, was deleted by visual inspection. Fast-phase selection was done by (1) dividing the whole eye position curve into segments based on the eye-movement direction and (2) identifying a segment as a saccade if its maximum velocity was > 30 deg/s. The other segments with a maximum velocity < 30 deg/s would be identified as part of slow phase. The duration of ASOKN and MAE-induced eye movements was determined by the number and direction of fast phases. Nystagmus was identified if the fast phases continuously move towards one direction more than 5 times. The duration was counted from the first fast phase to the last one. For instance, the eye movements shown in Fig. 3.2A, Condition 2, would be recognized as a nystagmus because the eye movements consisted of 8 fast phases moving uninterruptedly in one direction and the duration from the first fast phase to the last one was approximately 9 seconds. Maximum slow-phase eye velocities were calculated by searching for the maximum eye velocity in the opposite direction of the fast phases. Statistical tests (Paired one-tailed t-test) were done in MATLAB with the Statistics Toolbox.

3.4 Results

In Conditions 1 to 4, all subjects were able to maintain gaze fixation while a random dot pattern was moving in the background (see Fig. 3.2). In all subjects, the absolute median eye velocity was < 1 deg/s during the period of suppression of optokinetic nystagmus (OKN). Conditions 5 (low brightness) and 6 (high brightness) tested whether or not low and high brightness optokinetic stimuli would evoke similar slow-phase eye velocities during steady-state OKN. The average median eye velocity in Condition 5 (low brightness) was 17.6±8.1 deg/s while the same value in Condition 6 (high brightness) was 19.0±7.4 deg/s. The difference was not significant (paired t-test, $t = 1.61$, $p = 0.1272$).

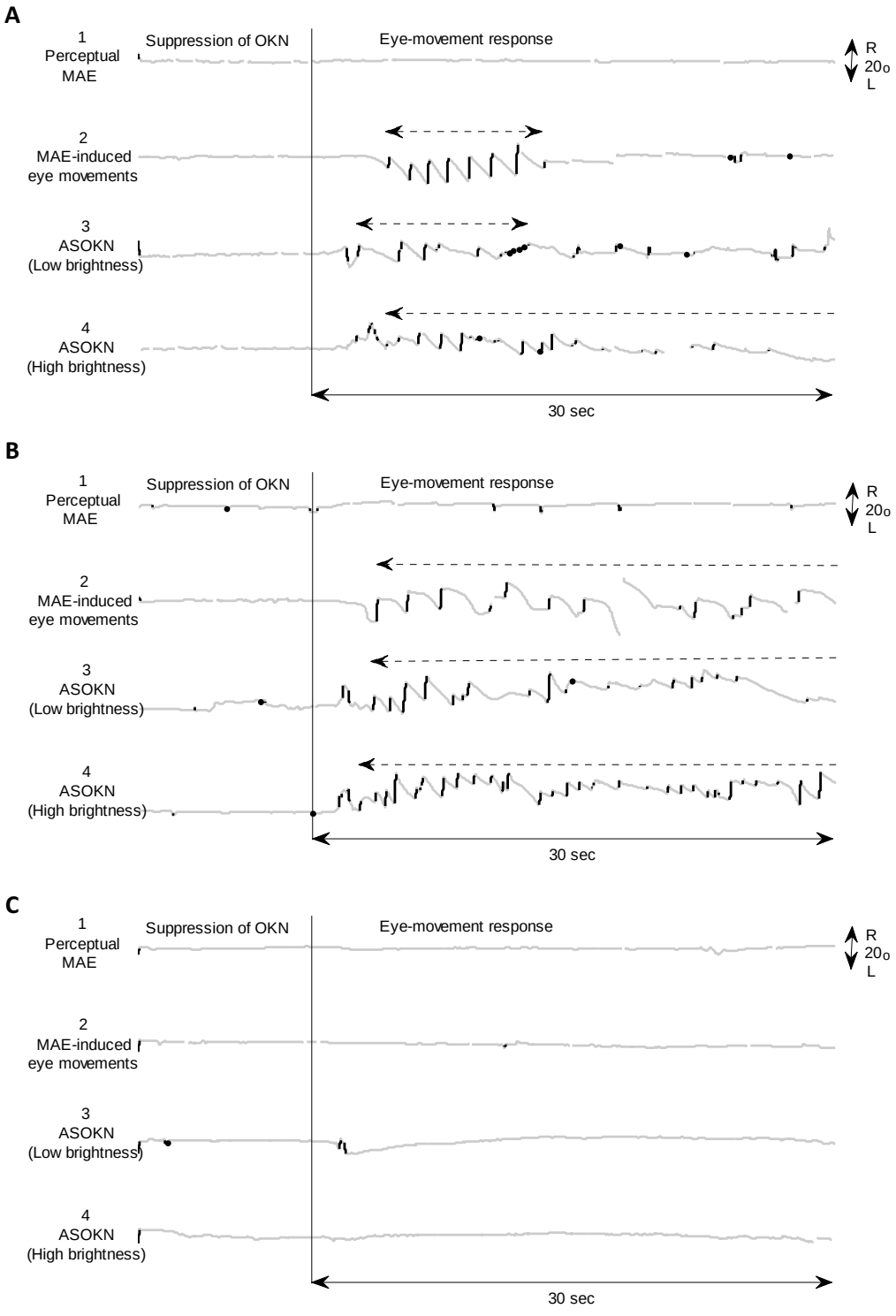

Figure 3.2 Typical examples of eye movements in (A) Subject 1, (B) Subject 2, and (C) Subject 13. Condition number is shown on the left side of each eye position trace. **A** and **B,** Two Subjects held gaze stable during the period of suppression of OKN in Conditions1 to 4. In Condition 1, gaze stayed stable in the last minute due to the strong fixation stimulus. The subjects reported a perceptual MAE. In Condition 2, the MAE-induced eye movements were found after suppression of OKN. In Conditions 3 and 4, ASOKN was found after suppression of OKN. **C,** Subject 13 also held gaze stable during the period of suppression of OKN in Conditions 1 to 4. In Condition 1, the subject reported a perceptual MAE. In Conditions 2-4, no eye movement was found after suppression of OKN. Note that grey line indicates the position with an eye velocity < 30 deg/s while black line indicates the position with an eye velocity > 30 deg/s.

Subject	1	2				3				4				5	6
	Perceptual MAE	MAE-induced eye movements				Afternystagmus after suppression of OKN								OKN	
	High brightness	High brightness				Low brightness				High brightness				Low brightness	High brightness
		Median Velocity (°/s)	Maximum SPV (°/s)	Duration (s)	Retinal Afterimage	Median Velocity (°/s)	Maximum SPV (°/s)	Duration (s)	Retinal Afterimage	Median Velocity (°/s)	Maximum SPV (°/s)	Duration (s)		Median velocity (°/s)	Median velocity (°/s)
1	√	-2.4	10	9	√	-1.9	10	10	√	-4.6	12	45		23.4	24.8
2	√	-2.5	15	60	√	-3	15	32	√	-3.5	23	42		28	29
3	√	-0.7	7	8	√	-0.6	7	4	√	-0.9	4	6		6	12.6
4	√	-2	8	50	√	-1.8	5	15	√	-2.1	9	40		24	22
5	√	-2.3	10	16	√	-3.1	8	18	√	-3.4	8	18		25.6	27.4
6	√	-1.6	10	22	X	0.3	X	X	√	-0.5	4	8		23.4	23.5
7	√	-0.8	3	11	X	-0.4	X	X	√	-0.8	2	10		12.7	10
8	√	-0.4	X	X	√	0.3	X	X	√	0	X	X		27.2	29
9	√	0.4	X	X	√	0.2	X	X	√	0.4	X	X		20.3	22.9
10	√	-0.3	X	X	X	0.3	X	X	√	-0.1	X	X		25	23
11	√	-0.4	X	X	√	-0.2	X	X	√	-0.1	X	X		19	15
12	√	-0.1	X	X	√	-0.2	X	X	√	-0.3	X	X		16	21.4
13	√	-0.1	X	X	√	-0.2	X	X	√	0	X	X		9.7	12.3
14	√	-0.1	X	X	√	-0.1	X	X	√	0.4	X	X		4.2	5.7
15	√	-0.2	X	X	X	-0.3	X	X	X	-0.2	X	X		6.5	16.3
16	√	0.1	X	X	X	-0.1	X	X	X	0	X	X		19.7	20.8
17	X	-0.3	X	X	X	-0.4	X	X	√	-0.3	X	X		8.7	7
# of presence	**16**	**7**			**11**	**5**			**15**	**7**				**17**	**17**

√=present; X=absent

Table 3.1 Summary of experimental data. Numbers at the top of the table correspond to the condition number. Subjects reporting a perceptual MAE after Condition 1 were marked with "√". In Conditions 2-4, the median eye velocity of the first 20 seconds after the period of suppressed OKN was calculated. Subjects reporting RAI in Conditions 3 and 4 were marked with a "√". Moreover, maximum slow phase velocity (SPV) and duration of the MAE-induced eye movements and ASOKN were calculated only in the subjects who had a nystagmus after suppression of OKN. In Conditions 5 and 6, median eye velocity during the 3-minute optokinetic stimulation was calculated. Number in the last row indicates the number of subjects who reported or had perceptual MAE, MAE-induced eye movements, RAIs, and ASOKN. The shaded area indicates the subjects who demonstrated the MAE-induced eye movements in Condition 2.

3.4.1 Perceptual motion aftereffect

After suppression of OKN, 16 out of 17 subjects reported that the space-fixed random dot pattern, in which each random dot stayed in the same position for 150 milliseconds and then reappeared in other positions, was perceived to move towards the left (Table 3.1). Since all subjects were asked to stare at the yellow fixed dot after suppression of OKN, gaze remained stable (see Fig. 2ABC, Condition 1 for examples).

3.4.2 Motion-aftereffect-induced eye movements

Whether or not MAE-induced eye movements appeared in subjects was evaluated in Condition 2. After suppression of OKN, 7 out of 17 subjects generated a nystagmus in the opposite direction of the previous optokinetic stimulus as they faced the stationary screen with uniformly distributed dim light (example: Fig. 3.2AB, Condition 2), while no nystagmus was recorded in the others (example: Fig. 3.2C, Condition 2). We found that the slow phases can be either linear (Fig. 3.2A, Condition 2) or exponentially increasing (Fig. 3.2B, Condition 2).

3.4.3 Retinal afterimage

Subjects were asked whether RAIs appeared after suppression of OKN in Conditions 3 (low brightness) and 4 (high brightness). Eleven subjects reported that a RAI appeared after the low brightness condition (Condition 3) while 15 subjects saw a RAI after the high brightness condition (Condition 4). Ten of 11 subjects who saw a RAI in both conditions reported that the RAI after the high brightness condition lasted longer than the one after the low brightness condition, while 1 subject reported no difference.

3.4.4 Afternystagmus after suppression of optokinetic nystagmus

Whether ASOKN requires the presence of RAI was tested in Conditions 3 (low brightness) and 4 (high brightness). Ten subjects did not generate ASOKN in either condition (see Fig. 3.2C). Two subjects had ASOKN only in Condition 4, while 5 subjects had it in both conditions (see Table 3.1). Duration and maximum slow-phase velocity of ASOKN between the two conditions were compared to determine the influence of stimulus brightness on ASOKN. The duration of ASOKN was significantly longer in the high-brightness condition (paired t-test, $t = 2.69$, $p = 0.0361$, Fig. 3.3A). However, no significant difference was found between the maximum slow-phase eye velocities of ASOKN in Conditions 3 and 4 (paired t-test, $t = 1.85$, $p = 0.1125$, Fig. 3.3B).

Interestingly, all subjects who had ASOKN in Condition 4 demonstrated MAE-induced eye movements in Condition 2. Two subjects, who showed MAE-induced eye movements in Condition 2 and reported no RAI in Condition 3, did not generate ASOKN in Condition 3 (Table 3.1).

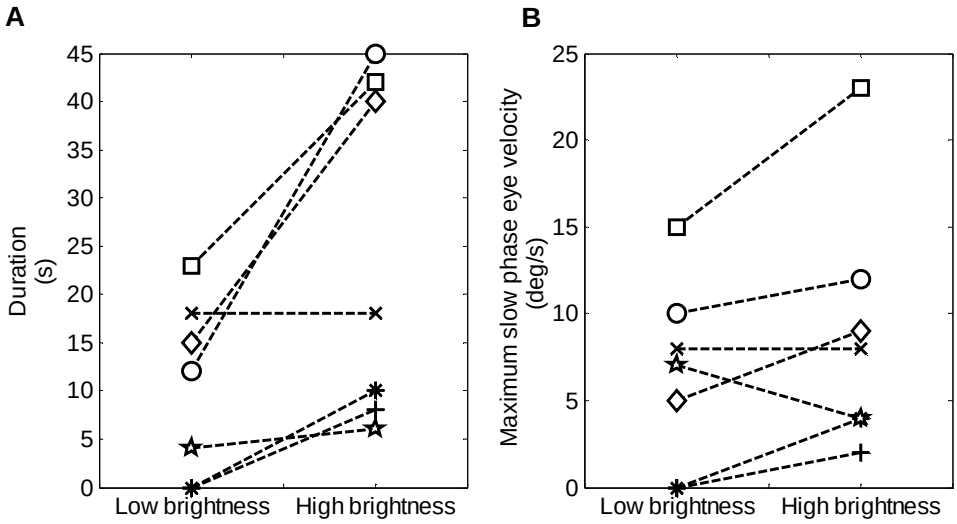

Figure 3.3 Duration (**A**) and maximum slow phase eye velocity (**B**) of ASOKN in those subjects who had ASOKN in either Conditions 3 or 4.

3.5 Discussion

3.5.1 Afternystagmus after suppression of optokinetic nystagmus

We investigated the mechanism responsible for afternystagmus after suppression of optokinetic nystagmus (ASOKN), in which slow-phase eye movements are in the opposite direction of previous optokinetic stimulation. This ASOKN was only found in a minority of healthy subjects tested. Five out of 17 subjects (29%) showed ASOKN after presenting the low-brightness stimuli, while 7 out of 17 subjects (41%) showed ASOKN after presenting the high-brightness stimuli. These percentages in this study are less than the one in a previous study that reported that ASOKN was found in 14 out of 23 subjects (61 %) (Ventre-Dominey and Luyat 2009, Table 2). In contrast, Fletcher et al., (1990) reported that none of their 4 subjects (0 %) generated ASOKN in the opposite direction of the preceding optokinetic stimulation. Hence, it seems that ASOKN highly depends on the individual subject and the parameters of the visual stimulation, such as brightness.

We found that ASOKN can be elicited if a subject shows motion-aftereffect-induced (MAE-induced) eye movements and also reports seeing retinal afterimages (RAIs). Specifically, the subjects who showed MAE-induced eye movements in Condition 2 and saw a RAI in Conditions 3 or 4 generated ASOKN (see Table 3.1). In the remaining subjects, no ASOKN was recorded. The notion that RAIs are the essential driver of ASOKN was underlined by the fact that the high-brightness stimuli induced a longer duration of ASOKN than the low-brightness stimuli (Fig. 3.3A), as RAIs persist longer with increasing brightness (Granit et al., 1930; Feinbloom 1938; Nagamata 1951).

The concurrence of RAIs, MAE-induced eye movements, and ASOKN in individual subjects suggests that ASOKN results from an interaction of the MAE-induced eye movements and RAIs. The MAE-induced eye movements are very similar to ASOKN in respect to the eye-movement direction and the precondition, i.e. gaze fixation during optokinetic stimulation. But, the MAE-induced eye movements require a visual input (Watamaniuk and Heinen 2007), different to the condition of testing ASOKN, where the visual surround is totally dark (Kudo et al.,,2002; Ventre-Dominey and Luyat, 2009). However, RAIs, if also present after suppression of optokinetic nystagmus (OKN), can be the visual input to evoke MAE-induced eye movements. Moreover, the eye-fixed RAIs may further stimulate eye movements. Such an interaction between MAE-induced eye movements and RAIs can induce an afternystagmus in the dark after suppression of OKN, (i.e. ASOKN). Only RAIs or MAE-induced eye movements alone are not sufficient to generate ASOKN.

3.5.2 Perceptual motion aftereffect (MAE) and the MAE-induced eye movements

In this study, 16 out of 17 subjects (94%) reported a perceptual MAE in Condition 1, but only 7 out of 17 subjects (41%) generated MAE-induced eye movements in Condition 2 (see Table 3.1). Why did not all subjects with a perceptual MAE show MAE-induced eye movements? We speculate that, in

these subjects, the perceptual MAE was not strong enough to drive the eyes to follow the motion illusion. However, further studies are needed to answer this question.

3.5.3 Retinal Afterimages

We controlled the brightness of the space-fixed yellow dot and the random dot pattern, to induce different strengths of RAIs. Eleven out of 17 subjects (71%) saw a RAI in Condition 3 (low brightness), while 15 out of 17 subjects (94%) reported it in Condition 4 (high brightness). Moreover, 10 out of 11 subjects who saw a RAI in Conditions 3 and 4 reported that the RAI duration was longer and stronger after the high brightness condition. Our results agree with previous studies, in which brightness of the image positively correlated to the RAI duration (Granit et al., 1930; Feinbloom 1938; Nagamata 1951; Lu et al., 2006).

3.5.4 Velocity storage mechanism

Previous studies suggested that ASOKN may be related to some sort of velocity storage mechanism (VSM), which is charged by optokinetic signals during the period of suppression of OKN and then causes afternystagmus in the subsequent dark (Kudo et al.,,2002; Ventre-Dominey and Luyat, 2009). However, Fletcher et al., (1990) suggested that gaze fixation prevents the coupling of optokinetic signals into the VSM. Our study supports the conclusion that there is no VSM being charged by retinal slip during fixation of a stationary target. In our experimental data, Conditions 5 and 6, which used the same moving random dot pattern, except for the brightness, evoked similar degrees of OKN (see Table 3.1). In other words, although the brightness was different, the two optokinetic stimuli caused a similar amount of retinal slip. In Conditions 3 and 4, however, we found that the high and low brightness conditions significantly influenced the duration of ASOKN (see Fig. 3.3A); high brightness evoked a longer ASOKN. This phenomenon cannot be explained by a hypothesis involving a VSM. Moreover, if ASOKN is really produced by a VSM, the afternystagmus in Conditions 2, 3, and 4 should be similar because a blank, low luminance screen (Condition 2) as well as the dark condition (Conditions 3 and 4) did not provide any fixation and would not affect an afternystagmus caused by the VSM. However, in practice, two subjects generated exponential increasing slow phases in Condition 2 but linear slow phases in Conditions 3 and 4 (Fig. 3.2B). The different slow-phase type between a dim homogeneous background and a dark environment may only be explained by our hypothesis that ASOKN results from an interaction of RAIs and MAE-induced eye movements, instead of a VSM.

3.5.5 Summary

In summary, we found that ASOKN occurred only if subjects had the MAE-induced eye movements and saw a RAI after suppression of OKN. Our results therefore suggest that ASOKN may be the result of an interaction between the MAE-induced eye movements and RAIs.

3.6 Reference

Anstis S, Verstraten FA, Mather G (1998) The motion aftereffect. Trends in cognitive sciences 2:111-117.

Brainard DH (1997) The Psychophysics Toolbox. Spat Vis 10:433-6.

Brown JL (1965) Afterimages. In: Graham CH (ed) Vision and visual perception. Wiley, New York London Sydney, pp 479–503.

Cohen B, Matsuo V, Raphan T (1977) Quantitative analysis of the velocity characteristics of optokinetic nystagmus and optokinetic after-nystagmus. J Physiol 270:321–344.

Feinbloom W (1938) A quantitative study of the visual after-image. Archives of Psychology (Columbia University) 233

Flechter WA, Hain TC, Zee DS (1990) Optokinetic nystagmus and afternystagmus in human being: relationship to nonlinear processing of information about retinal slip. Exp Brain Res 81:46-52.

Granit R, Hohenthal T, Uoti A (1930) On the latency of negative after-images in relation to brightness of stimulus. Acta Ophthalmologica 8:137-154.

Kleiner M, Brainard D, Pelli D (2007) What's new in Psychtoolbox-3?. Perception 36 ECVP Abstract Supplement.

Korenaga K, Makishima K, Yosida M, Kudou K, Higuchi S (1996) Experimental study on directional asymmetry of vertical OKN and OKAN. J Otolaryngol Jpn 99:1085–94.

Kudo K, Yoshida M, Makishima K (2002) Reverse optokinetic afternystagmus generated by gaze Fixation during optokinetic stimulation. Acta Otolaryngol 122:37–42.

Laurens J, Angelaki DE (2011) The functional significance of velocity storage and its dependence on gravity. Exp Brain Res 210:407-422.

Lu H, Zavagno D, Liu Z (2006) The glare effect does not give rise to a longer-lasting afterimage. Perception 35:701-707.

Mather G, Verstraten FA, Anstis S (1998) The Motion After-effect. Mit Press.

Nagamata H (1951) Contribution to the knowledge of after-images. Acta Societatis Ophthalmologicae Japonicae 55:802-806.

Raphan T, Cohen B, Matsuo V (1977) A velocity-storage mechanism responsible for optokinetic nystagmus (OKN), optokinetic after-nystagmus (OKAN) and vestibular nystagmus. In Control of Gaze by Brain Stem Neurons, Developments in Neuroscience, Vol. I (ed. R. Baker and A. Berthoz). Elsevier/North-Holland Biomedical Press, Amsterdam.

Ohm J (1921) ber optischen Drehnystagmus. Klin Mbl Augenheilk 68: 234–5.

Pelli DG (1997) The VideoToolbox software for visual psychophysics: transforming numbers into movies. Spat Vis 10:436-442.

Raphan T, Matsuo V, Cohen B (1979) Velocity storage in the vestibuloocular reflex arc (VOR). Exp Brain Res 35: 229-248.

Shimojo S, Kamitani Y, Nishida S (2001) Afterimage of perceptually filled-in surface. Science 293: 1677–80.

Spigel IM (1960) The effect of differential post-exposure illumination on the decay of the movement aftereffect. J Psychol 50:209–210.

Thompson P, Wright J (1994) The role of intervening patterns in the storage of the movement aftereffect. Perception 23:1233–1240.

Wohlgemuth A (1911) On the aftereffect of seen movement. Br J Psychol 1(Suppl):1–117.

Watamaniuk SN, Heinen SJ (2007) Storage of an oculomotor motion aftereffect. Vision research 47:466.

Ventre-Dominey J, Luyat M (2009) Asymmetry of visuo-vestibular mechanisms contributes to reversal of optokinetic after-nystagmus. 193:55-67

Verstraten FAJ, Fredericksen RE, Grusser OJ, Van de Grind WA (1994) Recovery from motion adaptation is delayed by successively presented orthogonal motion. Vision Res 34:1149–1155.

Chapter 4

Velocity storage mechanism in zebrafish larvae

Chien-Cheng Chen[1,4], Christopher J. Bockisch[1,2,3], Giovanni Bertolini[1], Itsaso Olasagasti[1], Stephan C. F. Neuhauss[5,6,7], Konrad P. Weber[1,2], Dominik Straumann[1,6,7] and Melody Ying-Yu Huang[1,6,7]

Departments of [1]Neurology [2]Ophthalmology and [3]Otorhinolaryngology, University Hospital Zurich, CH-8091, Zurich, Switzerland. [4]PhD Program in Integrative Molecular Medicine, Life Science Graduate School, CH-8057, Zurich, Switzerland. [5]Institute of Molecular Life Sciences, University of Zurich, CH-8057, Zurich, Switzerland. [6]Zurich Center for Integrative Human Physiology (ZIHP), CH-8057, Zurich, Switzerland. [7]Neuroscience Center Zurich (ZNZ), CH-8057, Zurich, Switzerland.

Adaptation from an article published in The Journal of physiology 592.1 (2014): 203-214.

Acknowledgements

The authors like to thank Kara Dannenhauer, Marco Penner, and Urs Scheifele for their excellent technical assistance. This work was supported by the Swiss National Science Foundation (SNF) grants PMPDP3_139754 (Marie Heim-Vögtlin programme) & 31003A-118069, Zurich Center for Integrative Human Physiology (ZIHP), and Betty and David Koetser Foundation for Brain Research.

Personal Contribution

Conceiving the project and designing the experiments with DS, IO, CJB, and MYYH, performing the experiments alone, analyzing the data with the other authors, and writing manuscript with MYYH and DS.

4.1 Abstract

The optokinetic reflex (OKR) and the angular vestibulo-ocular reflex (aVOR) complement each other to stabilize images on the retina despite self- or world motion, a joint mechanism that is critical for effective vision. It is currently hypothesized that signals from both systems integrate, in a mathematical sense, in a network of neurons operating as a velocity storage mechanism (VSM). When exposed to a rotating visual surround, subjects display the OKR, slow following eye movements frequently interrupted by fast resetting eye movements. Subsequent to light-off during optokinetic stimulation, eye movements do not stop abruptly, but decay slowly, a phenomenon referred to as the optokinetic after-response (OKAR). The OKAR is most likely generated by the VSM. In this study, we observed the OKAR in developing larval zebrafish before the horizontal aVOR emerged. Our results suggest that the VSM develops prior to and without the need for a functional aVOR. It may be critical to ocular motor control in early development as it increases the efficiency of the OKR.

4.2 Introduction

The optokinetic response (OKR) is a visually guided ocular motor reflex evoked by the moving surround primarily during self-motion. Via a neuronal network operating as a velocity storage mechanism (VSM), the optokinetic reflex (OKR) and the vestibulo-ocular reflex (VOR) work in concert to ensure gaze stability, being critical for effective vision (Baaarsma & Collewijn, 1974; Robinson, 1981; Paige, 1983; Schweigart et al., 1997). The OKR consists of slow-phase eye movements that stabilize images of the moving scene on the retina and oppositely directed fast phases that reset the position of the eyes. The OKR has been extensively studied in species with fovea, such as monkeys (Takahashi & Igarashi, 1977; Igarashi et al., 1977) and humans (Honrubia et al., 1968; Abadi & Pantazidou, 1997), and without fovea, such as rabbits (Tan et al., 1992, 1993), rats (Sirkin et al., 1985; Hess et al., 1985) and goldfish (Beck et al., 2004). Interestingly, after the OKR reaches a steady state during optokinetic stimulation with constant velocity, the nystagmus continues during subsequent total darkness and its slow-phase eye velocity decreases exponentially. This exponentially decaying eye velocity is called the optokinetic after-response (OKAR). The OKAR is thought to be the result of the VSM that is probably shared with the vestibular system (Cohen et al., 1977; Raphan et al., 1977, 1979; Robinson, 1977). The VSM can be charged either by the eye velocity signal of the OKR or by the angular velocity signal of the angular VOR (aVOR). The aVOR is evoked by head rotation and generates eye movements in the opposite direction of the head movement to keep the visual world stable on the retina. At present, it is suggested that the VSM exercises its effect via integration of visual information with vestibular inflow in the central vestibular pathway, which also merges different sensory input information (e.g. semicircular canals, otoliths, visual system, neck proprioception, etc.) to better estimate body motion critical for synchronizing motor output required for eye/body stabilization (Angelaki & Cullen, 2008). The existence of a VSM can explain how low-frequency signals from the semicircular canals are perseverated (Robinson, 1977; Raphan et al., 1977, 1979). In addition, it has been shown that the VSM also integrates OKR velocity signals, which can explain the phenomenon of the OKAR (Waespe & Henn, 1977; Raphan et al., 1979; Cohen et al., 1981). Since the OKAR is eliminated after bilateral labyrinthectomy (Uemura & Cohen, 1973; Zee et al., 1976; Collewijn, 1976), it is conceivable that signals from the semicircular canals are essential for the VSM. However, in small vertebrate animals such as larval teleost fish and Xenopus, it has been shown that the aVOR emerges later than the OKR, which is due to the tiny semicircular canals being too small to be functional (Beck et al., 2004; Lambert et al., 2008). Given the observation that the VSM subserves both the vestibular and optokinetic systems, and given the importance of the OKR in the visual system of afoveated animals such as teleost fish, we question whether the development of the VSM requires the behavioural onset of the aVOR. To find out whether the VSM exists before the aVOR is functional, we tested zebrafish larvae at 5–6 days post fertilization (dpf). At this stage the zebrafish OKR is fully functional, but the horizontal aVOR is not yet developed (Beck et al., 2004; Mo et al., 2010). One previous study reported that the OKAR in zebrafish larvae does not yet exist as

eye velocity elicited by optokinetic stimulation immediately dropped to zero after switching the lights off (Beck et al., 2004). However, the measured eye velocity does not represent the velocity command from the velocity storage, as the latter is integrated by the velocity-to-position neural integrator (VPNI), which in zebrafish larva is very leaky (Miri et al., 2011), before reaching the eye muscle. The leakiness of the integrator causes an almost immediate drop and a reversal of the eye velocity during OKAR, causing the eyes to rapidly return to the resting position, masking the effect of a putative VSM (Ramat & Bertolini, 2009). Therefore, using a single exponential function to analyse the velocity drop after the OKR, as Beck et al., have done, would underestimate the time constant of the velocity decay. Such a method is neither sufficient nor conclusive. We re-addressed the question of the VSM in zebrafish larvae by focusing on post-optokinetic ocular drift in the position domain, which allowed us to take into account the effect of the individual VPNI time constant of each larva.

4.3 Materials and Methods

4.3.1 Fish maintenance and breeding

Wild-type zebrafish, WIK strain, were bred and maintained as described previously (Mullins et al., 1994). Embryos were raised under a standard 10 h dark/14 h light cycle at 28°C in E3 medium (5 mm NaCl, 0.17 mm KCl, 0.33 mm CaCl2, and 0.33 mm MgSO4) (Haffter et al., 1996) and staged according to development in days post-fertilization (dpf). Ten larvae were tested.

4.3.2 Optokinetic stimulation

A schematic drawing of the setup is shown in Fig. 4.1A and B. Using four digital light projectors (Samsung SP-H03 Pico Projector), moving and stationary vertical sine-wave gratings with 100% contrast (maximum illumination 171 lux) and spatial frequency of 0.056 cycles/deg were projected onto a translucent screen wrapped around a glass cylinder at an angular velocity of 0, 10, or 20 deg/s. Moreover, four shutters were used to block the light sources of the projectors to create a totally dark environment. Data acquisition, properties of the visual stimulation, and light source switches were all controlled by custom-made programs written in LabVIEW 10.0 (National Instruments, USA) and Borland Delphi 7.0 (Borland Software Corporation, USA).

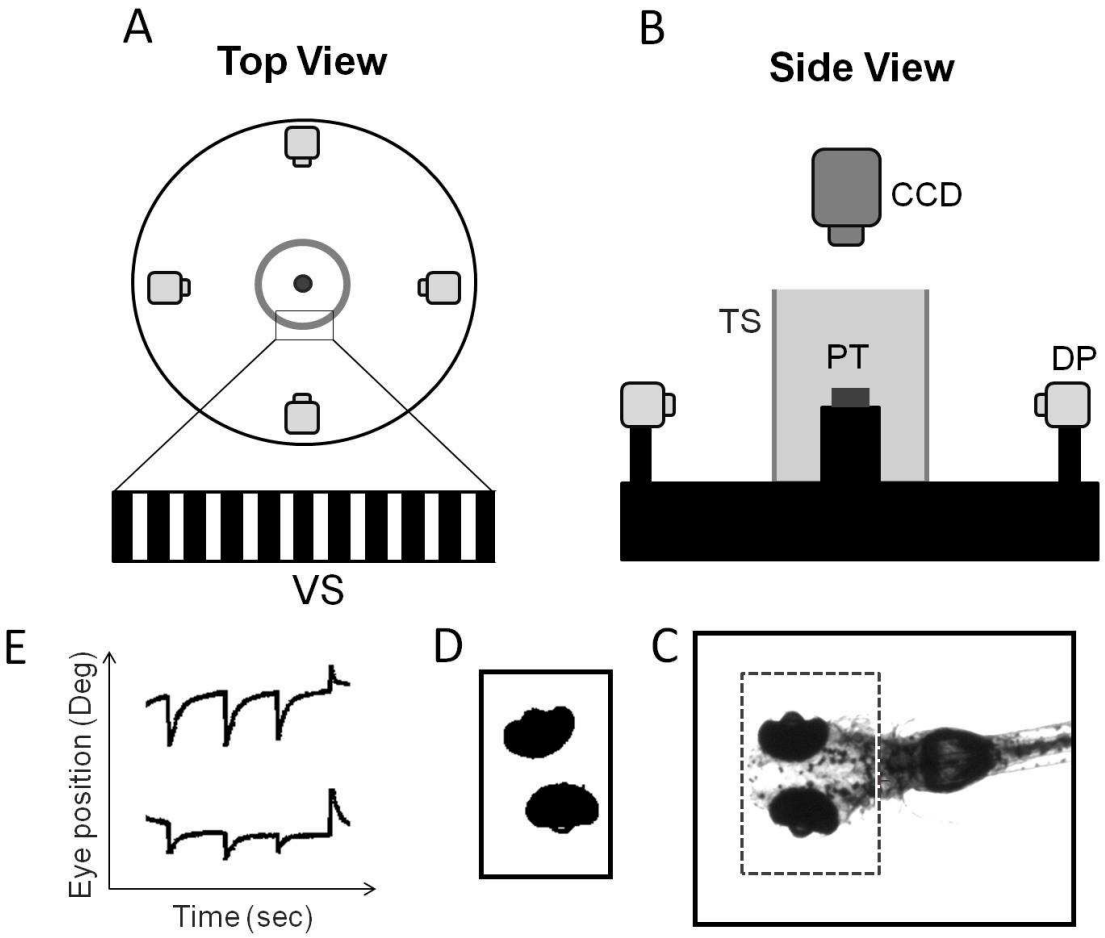

Figure 4.1 Schematic diagram of the experimental setup and the image analysis process. Top view (**A**) and side view (**B**) of the experimental setup. **C,** Recorded image of the whole body of the larval zebrafish. The dashed square indicates the ROI. **D,** The eye balls were identified and analyzed to obtain eye movements. **E,** Eye movement in space. DP, digital projector; CCD, IR-sensitive CCD camera; TS, translucent screen; VS, visual stimulus; PT, plastic tube.

4.3.3 Recording of eye/body movements

Ten larvae at 5–6 dpf were randomly chosen from a single clutch and tested individually. In order to suppress whole-body motion without constricting eye movements, single larvae were embedded dorsal side up in the centre of a 21 mm transparent plastic tube containing 3–3.5% methylcellulose. The embedded larva was placed inside the cylinder at a distance of the larva's eye to the screen of approximately 6.8 cm and was illuminated from below with infrared (IR)-emitting diodes (λ peak = 875 ± 15 nm, OIS-150 880, OSA Opto Light GmbH, Germany). During binocular stimulation, movements of both eyes were recorded by an IR-sensitive charge-couple device (CCD) camera with a sample rate of 40 frames s−1. Frames were processed by custom-developed software (LabVIEW 10.0; National Instruments, USA). Before the recording began, a region of interest (ROI) was manually selected around the eyes (Fig. 4.1C). Based on the pigmentation the software extracted the ellipse-like

shape of the eye from the ROI by applying binary threshold and a filter to delete small particles until both eyes could be clearly identified (Fig. 4.1D). Angular eye position was calculated based on the centre of mass and the axis with the lowest angular momentum of each eye and was plotted against time (Fig. 4.1E). Both image recording and analysis of eye position were achieved in real-time and were monitored during the experiment on the computer. For the subsequent off-line analysis of the eye movement relative to the body, every frame was saved during on-line recording. The larval body movement was analysed by calculating the body axis in each frame with a similar image-processing algorithm as applied in on-line eye recognition. The code for calculating the body axis was written in MATLAB (Mathworks, Natick, MA, USA).

4.3.4 Experimental procedure

Spontaneous eye movements in the dark were recorded for 10 min in each larva. Subsequently, a series of OKR/OKAR tests were performed. The angular velocity of the optokinetic stimulus was the independent variable in the OKR/OKAR test, having four levels (−10, +10, −20, +20 deg/s). A single OKR/OKAR test consisted of 30 s of stationary gratings presented to the tested larva, followed by 30 s of vertical gratings rotating at a constant angular velocity, and finally, 30 seconds of darkness. For each stimulus velocity, the OKR/OKAR test was repeated five times. Hence, a total of 20 OKR/OKAR tests (four stimulus velocities repeated five times) were applied to each larva. All larvae were recorded binocularly and data from both eyes were collected for further analysis.

4.3.5 Data analysis and iterative fitting procedure

Data analysis was done by a custom-developed program written in MATLAB (Mathworks). Eye-position traces were smoothed using a Gaussian filter with cutoff frequency of 5.5 Hz. Eye velocity was computed as the derivative of eye position. The time constants of VPNI were estimated by fitting a single exponential curve to position traces of spontaneous eye movements recorded in darkness (for details, see Results and Fig. 4.2). The VSM time constant was estimated fitting the following equation to the eye position recorded in darkness after optokinetic stimulation:

$$x(t) = (x_0 - offset) \cdot e^{\frac{-t}{T_{NI}}} + offset + Amp \cdot \left[1 \Big/ \left(\frac{1}{T_{VS}} - \frac{1}{T_{NI}}\right)\right] \cdot \left(e^{\frac{-t}{T_{NI}}} - e^{\frac{-t}{T_{VS}}}\right) \qquad (4.1)$$

where t is time, x is eye position, x0 is the initial eye position, ‘offset' is the eye position at the end of the decay, T_{NI} is the time constant of the VPNI, T_{VS} is the time constant of the VSM, and ‘Amp' is the amplitude of the VSM output. Equation (4.1) represents the combination of two terms. The first term describes the decay from an eccentric eye position in the absence of additional velocity input (i.e. a spontaneous eye drift in the dark). The second term describes the convolutional effect of the VSM and the VPNI (i.e. the VPNI receiving post-optokinetic velocity input from the VSM).

4.3.6 Statistical analysis

In order to test for directional preference in the VPNI and the VSM, we compared the following two categories using a binomial test: ‘median time constant in temporal-to-nasal (T–N) direction is greater than that in nasal-to-temporal (N–T) direction' or ‘median time constant in N–T direction is greater than that in T–N direction'. Since eye movements of both eyes are yoked, T–N movement of one eye co-occurs with N–T movement of the other eye and vice versa. Hence, we compared median time constant of T–N movement of the left eye with that of N–T movement of the right eye and vice versa across subjects.

One larva showed no movement of the left eye in T–N direction (and consequently, no movement of the right eye in N–T direction). We therefore excluded its eye movement in that direction from the tests.

4.4 Results

4.4.1 Gaze stability in the dark

Gaze was stable in the light, when the visual surround was structured (Fig. 4.2A, middle). In the dark, however, the eyes drifted centripetally after each saccade (Fig. 4.2A, left, and B). Thus, it appears that the velocity-to-position neural integrator (VPNI) in zebrafish larvae is rather leaky, which in the light is compensated by the optokinetic system, keeping gaze stable (Fig. 4.2A, middle). We characterized the VPNI by a single-exponential fit to each intersaccadic segment of eye position as a function of time (Fig. 4.2C). The mean (±SD) VPNI time constants with initial positions in the temporal and the nasal hemifields of gaze were 3.8 ± 2.1 s and 1.9 ± 0.7 s, respectively, for the left eye, and 3.7 ± 1.9 s and 2.6 ± 1.5 s, respectively, for the right eye. Values of individual zebrafish are depicted in Fig. 4.2D for visual comparison. Note there was one larva that only displayed movements of the left eye in nasal-to-temporal (N–T) direction during the 10 min dark period. Therefore, two data points were absent. There are 38 data points shown in Fig. 4.2D (9 larvae with four data points and one larva with only two data points). Using a binomial test, we found that centripetal eye drifts from temporal initial positions had longer time constants than centripetal eye drifts from nasal initial positions, $n = 19$, $Z = 3.44$, $P = 0.0003$. Whether these differences reflect mechanical properties of the eye plant or have a neural origin is still open to question.

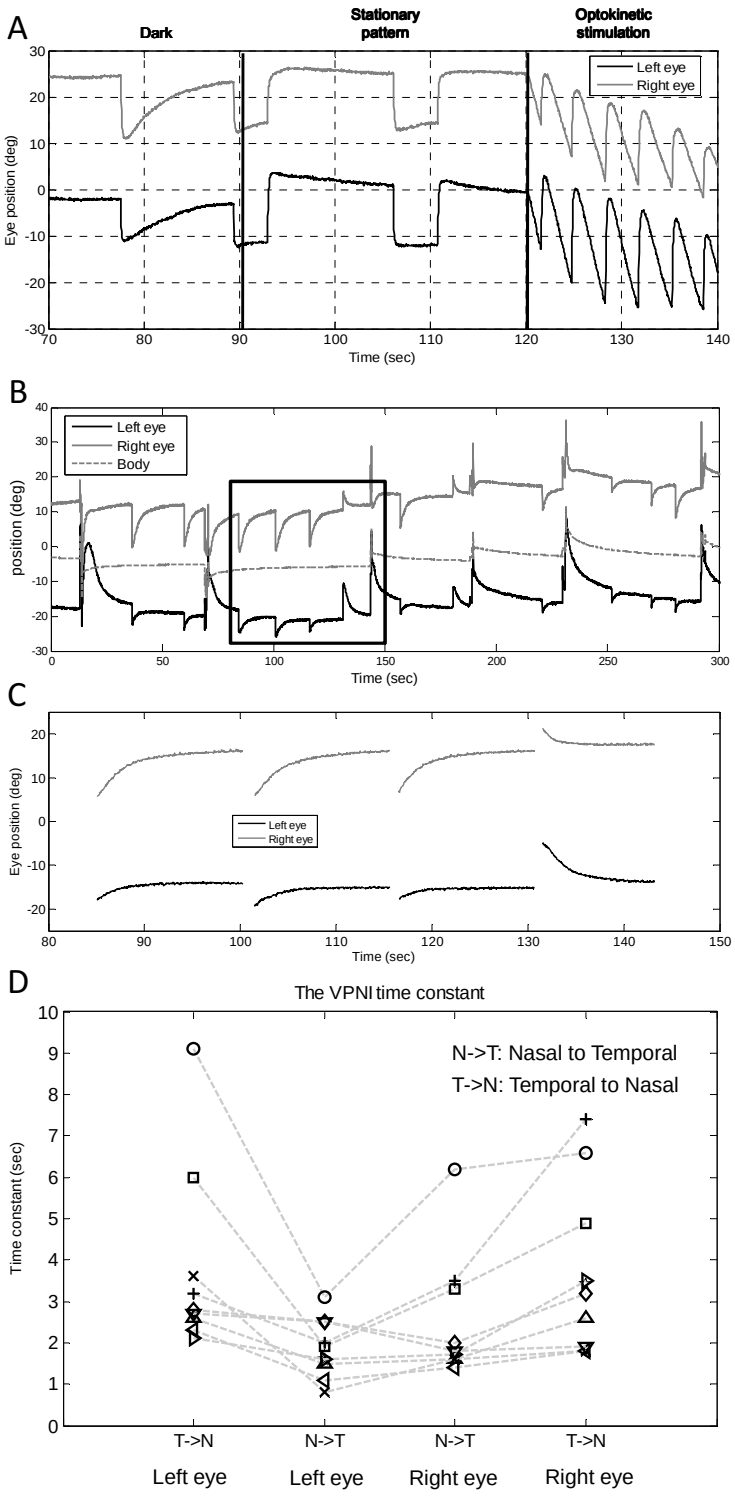

Figure 4.2 Eye movements of a zebrafish larva under various visual conditions and estimation of time constant of the VPNI. **A**, eye movements under various visual surrounds. **B**, spontaneous eye drifts in the dark. The body position trace (dotted line) was used to obtain the eye position relative to body axis. **C**, after filtering out saccades and body movements, spontaneous eye drifts were split into segments for applying a single exponential decay curve fitting to estimate the VPNI time constant. **D**, the median time constants of the VPNI of all larvae (n = 10). Note there was one larva that only showed movements of the left eye in N–T during the 10 min dark period. Therefore, nine larvae have four values indicating the median time constant of two eyes in two directions, while one larva only has two values indicating the median time constant of two eyes in one direction. The two values are not connected by any line. Values of each fish are connected by a dashed line.

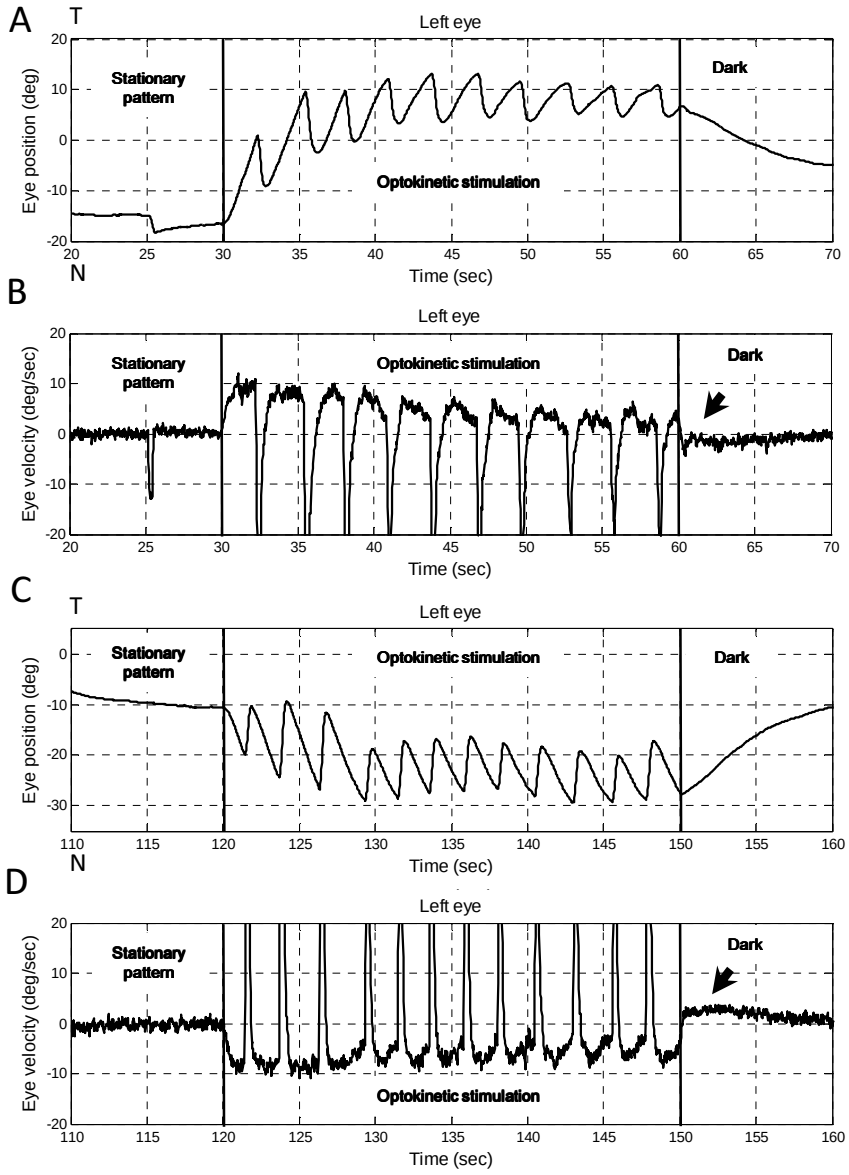

Figure 4.3 OKR of a zebrafish larva. Optokinetic stimulation was 10 deg/s in the nasal-to-temporal direction (30–60 s) and 10 deg/s s−1 in the temporal-to-nasal direction (120–150 s). **A** and **C**, left eye position versus time. **B** and **D**, left eye velocity versus time. Arrows indicate the OKAR in the velocity domain. T, temporal; N, nasal.

4.4.2 Optokinetic response (OKR)

In 5- to 6-day-old zebrafish larvae, generally, the OKR was initially efficient and the slow phase eye velocity was able to nearly reach its maximal value within 2 seconds after OKR onset. Subsequently, the slow phase eye velocity slowly decreased despite continuing optokinetic simulation with constant velocity (see typical example in Fig. 4.3). As a result, a difference between the maximum slow-phase eye velocity and the median eye velocity was observed. On average, the maximum slow phase eye velocity was 9.3 ± 0.7 deg/s at a stimulus velocity of 10 deg/s and 14.6 ± 1.6 deg/s at a stimulus velocity of 20 deg/s while the median eye velocity of the 30-second optokinetic stimulation was 5.2 ±

1.0 deg/s at a stimulus velocity of 10 deg/s and around 5.7 ± 1.5 deg/s at a stimulus velocity of 20 deg/s. Additionally, the beating field during the OKR shifted in the direction of slow phases. On average, the difference between the mean eye position during the first 10 s and the last 10 s was 9.3 ± 2.4 deg at a stimulus velocity of 10 deg/s and 7.8 ± 1.4 deg at a stimulus velocity of 20 deg/s.

4.4.3 Optokinetic after-response (OKAR)

Usually, no saccadic eye movement could be detected immediately after the lights were switched off during optokinetic stimulation (i.e. no nystagmus) was found during this time period (Fig. 4.4). The majority of eye position traces returned toward a more central eye position, which was in the opposite direction to the preceding slow phase. As a result, eye velocity quickly dropped to zero and crossed the zero line (see arrows in Fig. 4.3B and D). Specifically, when the initial position was eccentric toward the beating field at light-off, the eyes drifted directly toward the centre (Fig. 4.4B, upper three traces, and D, blue trace). However, if the initial eye position was close to the central eye position at light-off, the eyes typically continued moving in the direction of previous slow phases, before turning around to drift toward the centre (Fig. 4.4B, lowest cyan trace, and D, green and red traces).

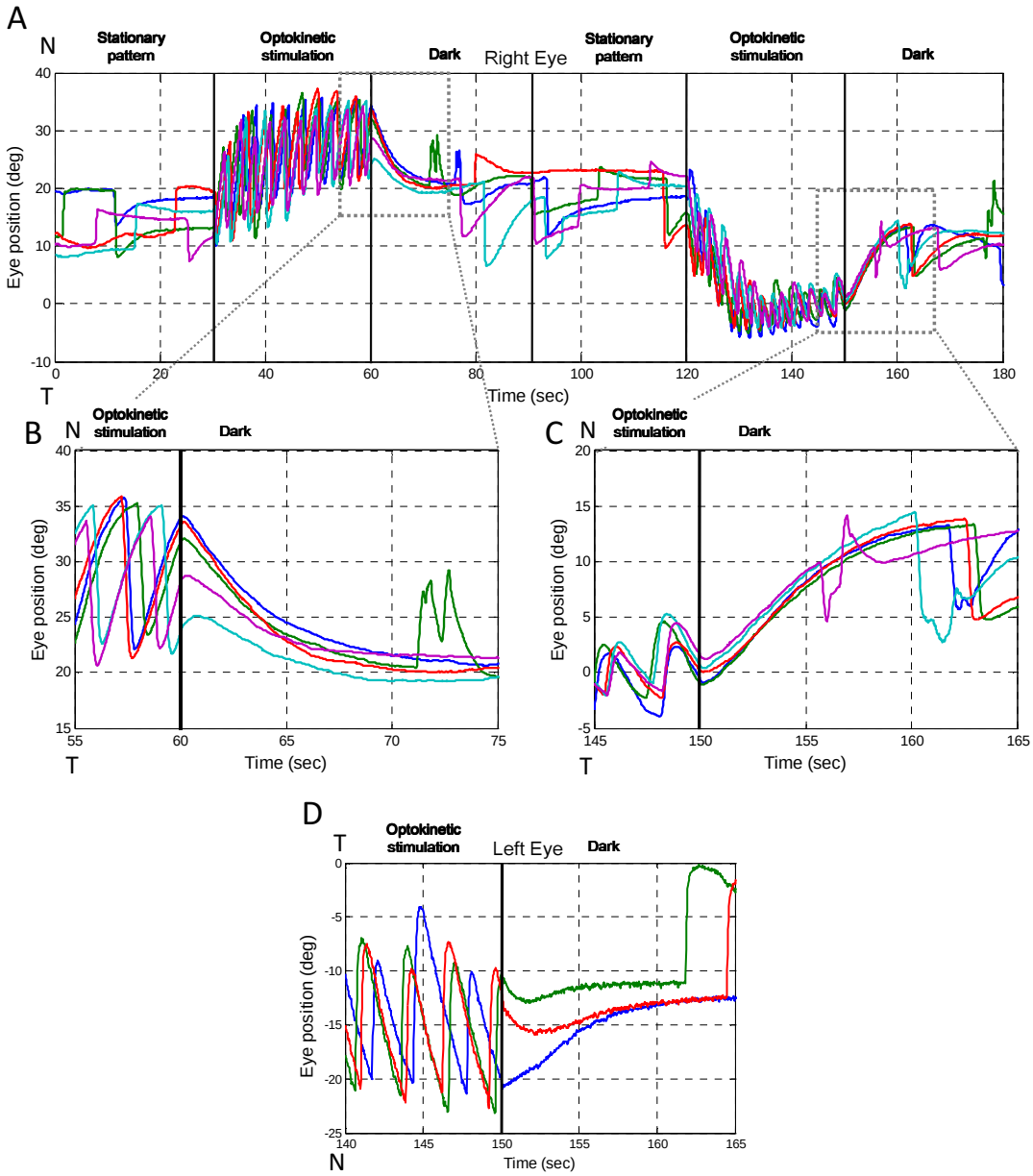

Figure 4.4 OKAR of a zebrafish larva. Visual stimuli over time: 0–30 s, stationary vertical gratings; 30–60 s, vertical gratings rotating horizontally at a constant angular velocity of 10 deg/s in one direction; 60–90 s, dark period. At 90–180 s, the same procedure was repeated with the optokinetic stimulus moving in the opposite direction (120–150 s). Different colours indicate different trials. **A**, typical eye position trace of a larval zebrafish during the OKR and OKAR tests. **B** and **C**, magnifications of Fig. 4.4A. **D**, another example of OKAR. The green and red lines indicate that OKAR continued in the direction of the OKR for 2–3 s while the blue line turned to the opposite direction immediately.

If there was no after-effect of the OKR during the subsequent period in the dark, the eyes would drift exponentially toward the centre with the time constant of the VPNI. However, we found that some post-optokinetic ocular drifts first continue in the direction of the previous OKR slow phases (see again in Fig. 4.4), suggesting the presence of an optokinetic after-effect visible at least in the position domain. To quantify this observation and verify the physiological meaning of these peculiar eye traces, we decided to compare spontaneous eye drifts in the dark with eye drifts in the dark after

optokinetic stimulation. Differences between the eye drifts in these two conditions would indicate an optokinetic after-effect, e.g. due to the velocity storage mechanism (VSM).

4.4.4 Simulation of OKAR with a leaky VPNI

To illustrate our hypothesis, namely that the difference between post-OKR and spontaneous eye drifts in the dark is due to the VSM, we first show the results of a simulation. A conceptual ocular motor model of zebrafish larvae is depicted in Fig. 4.5A. The optokinetic system receives visual input and transmits velocity signals to the VPNI, which integrates the signals to position commands. This pathway is represented with continuous lines. If the VSM exists, it will be charged by the velocity signals from the optokinetic system and then releases the velocity signals to the VPNI as shown with dashed lines. We then modelled spontaneous eye drifts in the dark with a single time constant representing a leaky integrator (Fig. 4.5B). With zero velocity input (e.g. when the OKR is inactive such as in darkness), eye position traces decay exponentially from eccentric positions reached by a saccade (Fig. 4.5C). However, if the input to the leaky VPNI is an exponentially decaying velocity signal, representing the perseverated optokinetic signal in the dark, i.e. stored velocity by leaky integration, we obtain curves resembling the post-OKR eye drifts recorded in zebrafish larvae (compare Fig. 4.5D to Fig. 4.4B). Specifically, eye drifts from initial positions close to the centre position continued their path in the direction of the velocity signal before drifting toward the centre (Fig. 5D, lower traces). In contrast, eye drifts from initial positions eccentrically displaced in the direction of the velocity signal decay immediately toward the centre position (Fig. 4.5D, upper traces).

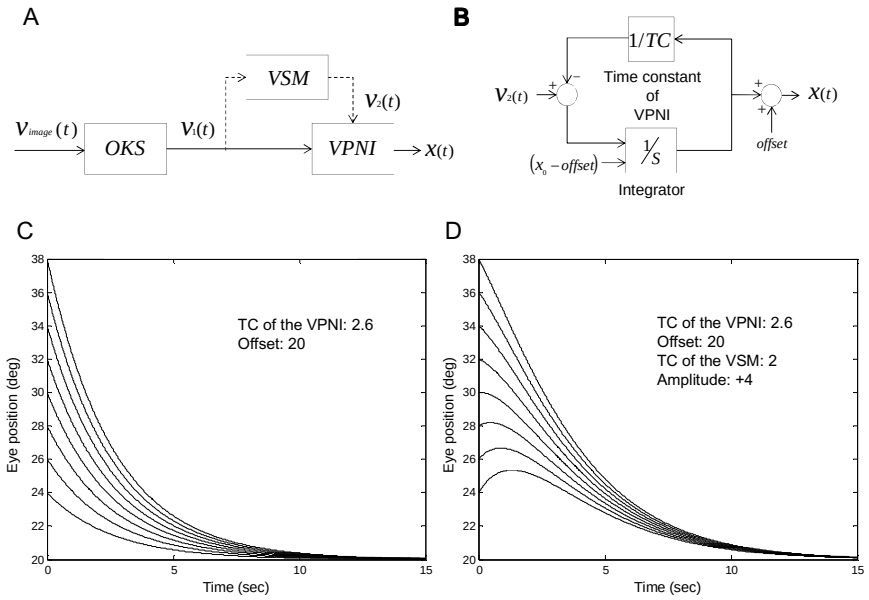

Figure 4.5 Conceptual model of larval ocular motor system, VPNI Simulink model and modeling results. **A,** Conceptual model of larval occult motor system. The optokinetic system (OKS) receives optokinetic signals $v_{image}(t)$ from the visual surround and sends eye velocity signals $v_1(t)$ to the velocity-to-position neural integrator (VPNI). The velocity storage mechanism (VSM) is charged by the velocity signal $v_1(t)$ from the OKS as well and sends velocity commands $v_2(t)$ to the VPNI. The VPNI, then, integrates the velocity commands into position signals *x(t)*. **B,** Schematic plot of the VPNI model. The model receives velocity signals from the VSM and converts these signals into position commands. *TC* denotes the time constant of the VPNI, $v_2(t)$ denotes the velocity signal from the VSM, x_0 denotes initial eye position, *offset* denotes final eye position, and $x(t)$ denotes eye displacement. **C,** Simulated eye drifts without the VSM. **D,** Simulated eye drifts with a stored velocity of an amplitude of 4 deg/s and a time constant of 2 s.

4.4.5 Estimation of VSM time constant

The simulated examples illustrate the difference between post-OKR eye drifts with and without a VSM. In a second step, we used a model including the VSM and the VPNI to compute the time constant of the VSM for every measured post-OKR eye drift. Specifically, in a given zebrafish larva, we selected its post-OKR eye drifts that decayed to a stable centre position without saccadic interruption (e.g. traces in Fig. 4B). The contribution of the VSM is obtained by subtracting the eye position drift, as calculated using the time constant of the VPNI (as determined from spontaneous eye drifts in the dark, Fig. 2D) and the initial and final position of the selected trace, from the measured post-optokinetic eye position trace (Fig. 6A). Then iterative fitting with eqn (4.1), which was obtained by convolution of VSM and VPNI effects, was applied on these selected traces to estimate the time constant of the VSM (see Methods). The mean VSM time constants of the right and the left eye in all zebrafish larvae tested were 2.0 ± 1.0 s and 1.8 ± 0.8 s, respectively. Data points from individual zebrafish are depicted in Fig. 4.6B. As expected, a binomial test result indicated that the VSM time

constant was independent of two eye-movement directions (n = 19, Z = −0.9425, P = 0.8265), which is in contrast to the VPNI time constant that showed a nasal–temporal difference (n = 19, Z = 3.44, P = 0.0003, see Fig. 4.2D).

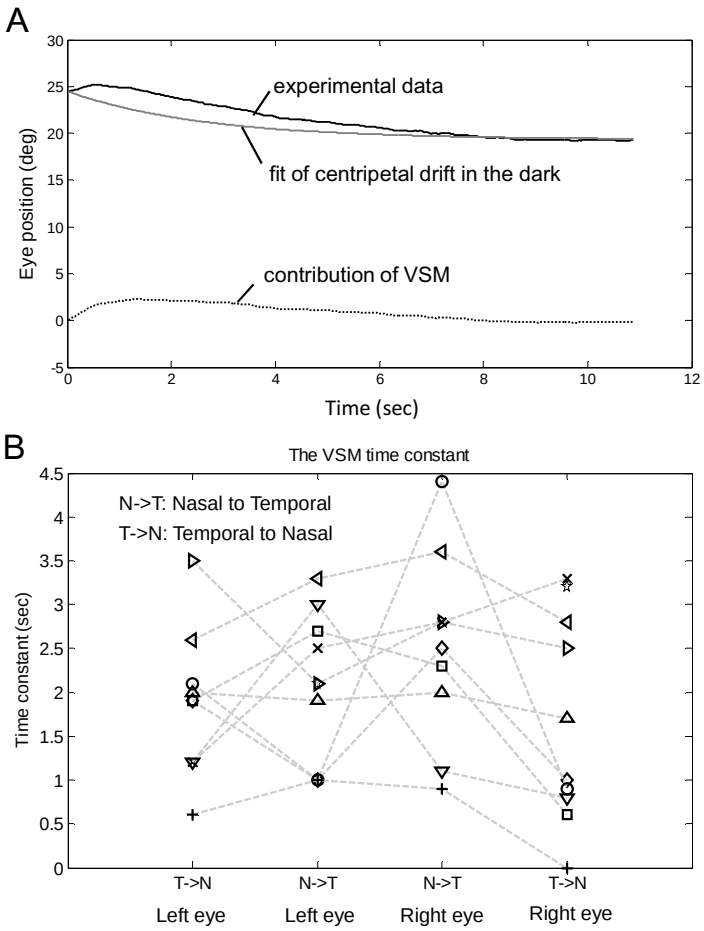

Figure 4.6. Estimation of time constant of the VSM **A,** The black line represents the OKAR obtained from experimental data. The gray line represents predicted eye position from the analysis of drift behavior in the dark. The dotted line represents the contribution of the VSM, used for computing time constant of the VSM by iterative fitting. **B,** The estimated medians of time constant of the VSM of all larvae (n=10). Note that one larva has only two time constants of the VPNI due to absence of eye movements in one direction (see Fig. 4.4D). In this case, time constant of the VSM could not be estimated. Nine larvae had four values indicating the median time constant of two eyes in two directions. Values of each fish, except for the one with only two data points, are connected by a dash line.

4.5 Discussions

4.5.1 VSM in zebrafish larvae

We found the first evidence in zebrafish larvae for the existence of a velocity storage mechanism (VSM) at 5–6 days post-fertilization (dpf). At this early stage, the horizontal angular vestibulo-ocular

response (aVOR) is not yet developed (Beck et al., 2004; Mo et al., 2010) while the optokinetic response (OKR) is already fully functional in 4 dpf larvae (Easter & Nicola, 1997; Huang & Neuhauss, 2008). The display of an optokinetic after-response (OKAR), identifiable through the slower decay of post-optokinetic eye drifts (Fig. 4.6A, black line) compared to that of spontaneous eye drifts in the dark (Fig. 4.6A, grey line), indicates the existence of a VSM (Fig. 4.6A, dotted line).

The very short time constant of the velocity-to-position neural integrator (VPNI) in zebrafish larvae (on average 3–4 seconds), could explain why Beck et al. (2004) did not find evidence for an OKAR of zebrafish larvae in the velocity domain. A simple derivative, as is commonly used to obtain eye velocity, does not, in fact, reproduce the pure VSM signal, but a velocity signal which fades away very quickly, due to the effect of the leaky VPNI. The simulations in Fig. 4.7 show the difference between the output of a VSM model with a time constant of 2 seconds and the derivative of the position signal obtained by processing such output through a VPNI with a time constant of 4 seconds. A single exponential fit to the latter will underestimate the time constant of the VSM to 0.99 s suggesting that no storage function exists.

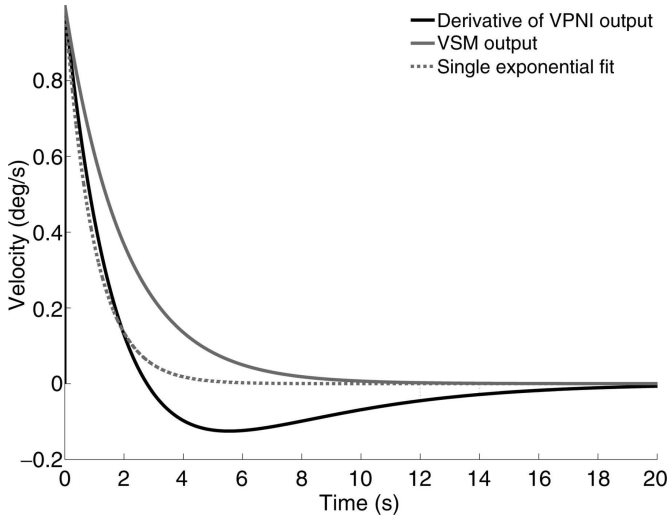

Figure 4.7 Simulations of the effect of VPNI on VSM output The black line shows the derivative of the eye position obtained assuming that a leaky VPNI (time constant = 4 s) processes a negative exponential velocity input similar to the one generated by a VSM with a 2 s time constant during the OKAR (continuous grey line). The grey dotted line shows the best fit of the black line neglecting the role of the VPNI and fitting a single exponential function. The estimated time constant of the VSM is less than half that of the grey continuous line used to generate the black line. Using a lower VPNI time constant, similar to those we found in most of our larvae, would make the difference even more marked.

The function of the VPNI is to convert eye velocity signals (e.g. from saccadic burst neurons) into eye position commands. This is required to keep gaze stable at the new position against the elastic forces of the extra-ocular tissues that pull the eyes toward a central position (Robinson, 1964; Cohen & Komatsuzaki, 1972; Skavenski & Robinson, 1973). In zebrafish larvae, the VPNI is not fully developed (i.e. the integrator is leaky), leading to exponential centripetal drifts after each saccade (Fig.

4.4B). Note that this ocular drift only takes place in darkness. In the presence of a structured visual surround, postsaccadic eye positions are stable (Fig. 4.2A, middle). Thus, it appears that the optokinetic system is able to compensate for the leakiness of the VPNI by minimizing the retinal slip since the smooth pursuit system does not play a role in the afoveated zebrafish. Another consequence of VPNI leakiness is that slow-phase eye velocity during the OKR drops as the beating field of the eyes swiftly moves in the direction of the slow phase after the beginning of optokinetic stimulation. In this situation, the centripetal drift opposes the OKR, which decreases the net velocity (Fig. 4.3B and D).

Overall, zebrafish larvae have a well-developed OKR, an only rudimentarily developed VPNI, a still lacking horizontal aVOR, and – unexpectedly – a VSM. What could be the purpose of this VSM?

We conjecture that the VSM acts mainly to enhance the OKR, which could be beneficial for at least three different ocular motor aspects during optokinetic stimulation.

(1) Maintaining OKR velocity during stimulus interruptions. Maintaining the OKR in a natural environment under water, where illumination changes caused by surface wave reflection are very irregular, is critical for retinal stabilization in zebrafish. Such an irregular visual stimulus can also be induced by swimming behaviour. Thus, the VSM may function as a low-pass filter to smooth brief velocity changes in the visual surround and/or working memory that stores velocity information of the visual surround for subsequent recovery of the OKR after interruptions of the visual stimulus. In other words, the stored velocity signal prevents the OKR from breaking down too quickly in the ever-changing visual surrounding.

(2) Maintaining OKR velocity during fast phases. Similarly, the VSM keeps the slow phase eye velocity relatively stable, although the optokinetic stimulus is repetitively interrupted during fast phases of nystagmus. The time constant for the rise and fall of the OKR is estimated at about 350 ms while fast phases in larval zebrafish last around 500 ms (Fig. 4.3B and D). So without the VSM, OKR velocity would drop close to zero during each fast phase. The VSM thus allows eye velocity to stay close to the stimulus velocity after each saccade, without the need for a substantial ‘build-up' period.

(3) Improving gaze stability before the emergence of a horizontal aVOR. Already at the larval stage (3–4 dpf) when beginning to swim upright, zebrafish display undulatory swimming in the horizontal plane with frequent head/body turns. With no functional horizontal aVOR at this stage, such swimming behaviour could substantially compromise gaze stability. The developmental advantage of a functional VSM at such an early stage could lie in the thus enhanced efficiency of the OKR that may help partially compensate for the absent aVOR and vastly improve gaze stability.

4.5.2 Relation between the VSM and the aVOR

It is generally thought that a functional VSM depends on the aVOR since unilateral labyrinthectomy shortens the VSM time constant and bilateral labyrinthectomy eliminates the VSM (Cohen et al. 1973; Raphan et al. 1979). Since the VSM also drives the OKAR, OKAR duration is shortened after unilateral labyrinthectomy and can no longer be elicited after bilateral labyrinthectomy (Cohen et al., 1973; Uemura & Cohen, 1973; Collewijn, 1976; Zee et al., 1976; Waespe & Wolfensberger, 1985).

Our data suggest that in zebrafish the VSM does not depend on angular vestibular input in early development since zebrafish larvae do not yet have a functional horizontal aVOR (Beck et al., 2004; Lambert et al., 2008). However, bilateral labyrinthectomy and/or section of the VIIIth nerves eliminate the VSM and the horizontal aVOR in adult animals (Cohen et al., 1973, 1983; Uemura & Cohen, 1973; Collewijn, 1976; Zee et al. 1976; Waespe & Wolfensberger, 1985), indicating that aVOR later becomes the dominant and possibly indispensable input to the VSM. Unfortunately, to our best knowledge, no systematic measurements of the OKAR after bilateral labyrinthectomy in fish exist. We hypothesize that, at a later stage when the semicircular canals become functional (horizontal aVOR detectible at 35 dpf; Beck et al., 2004), angular velocity signals from the labyrinths will gain access to the pre-existing VSM. The VSM may also receive angular velocity signals via a utricle-driven mechanism that interacts with visual input (Lauren & Angelaki, 2011; Bianco et al., 2012). The way in which vestibular and optokinetic signals interact to regulate the VSM is complex and needs further study as illustrated by selective abolishment of horizontal aVOR (i.e. horizontal optokinetic after-nystagmus (OKAN) not affected) after canal plugging (Cohen et al., 1983). Taken together, if the early VSM found in the present study did not originate from optokinetic stimulation alone, semicircular canals may contribute to the early VSM either via the lateral semicircular canal nerves or by the canal afferents somehow superimposing rotation signals onto the functional otolith scaffold.

In order to verify the origin of the early development of a VSM without a canal-driven aVOR and the role of the OKR and aVOR in the development of the VSM, follow-up studies need to address the following question: how do early visual deprivation, and conversely, more-than-normal exposure to optokinetic stimulation, shape the VSM development? Moreover, a developmental study of the horizontal aVOR in relation to the development of the OKAR/OKAN is required.

4.5.3 Conclusion

The emergence of the VSM shortly after the manifestation of the OKR when larval zebrafish do not yet display a horizontal aVOR suggests that, at an early larval stage of zebrafish, the VSM may be regulated primarily by the OKR (i.e. the visual signal) to increase the efficacy of ocular motor control.

4.6 Reference

Abadi R & Pantazidou M (1997). Monocular optokinetic nystagmus in humans with age-related maculopathy. Br J Ophthalmol 81, 123–129.

Angelaki DE & Cullen KE (2008). Vestibular system: The many facts of a multimodal sense. Annu Rev Neurosci 31, 125–150.

Baarsma E & Collewijn H (1974). Vestibulo-ocular and optokinetic reactions to rotation and their interaction in the rabbit. J Physiol 238, 603–625.

Beck JC, Gilland E, Tank DW & Baker R (2004). Quantifying the ontogeny of optokinetic and vestibuloocular behaviors in zebrafish, medaka, and goldfish. J Neurophysiol 92, 3546–3561.

Bianco IH, Ma LH, Schoppik D, Robson DN, Orger MB, Beck JC, Li JM, Schier AF, Engert F & Baker R (2012). The tangential nucleus controls a gravito-inertial vestibulo-ocular reflex. Curr Biol 14, 1285–1295.

Cohen B, Henn V, Raphan T & Dennett D (1981). Velocity storage, nystagmus, and visual-vestibular interactions in humans. Ann N Y Acad Sci 374, 421–433.

Cohen B & Komatsuzaki A (1972). Eye movements induced by stimulation of the pontine reticular formation: evidence for integration in oculomotor pathways. Exp Neurol 36, 101–117.

Cohen B, Matsuo V & Raphan T (1977). Quantitative analysis of the velocity characteristics of optokinetic nystagmus and optokinetic after-nystagmus. J Physiol 270, 321–344.

Cohen B, Suzuki JI & Raphan T (1983). Role of the otolith organs in generation of horizontal nystagmus: effects of selective labyrinthine lesions. Brain Res 276, 159–164.

Cohen B, Uemura T & Takemori S (1973). Effects of labyrinthectomy on optokinetic nystagmus (OKN) and optokinetic after-nystagmus (OKAN). Int J Equilib Res 3, 80–93.

Collewijn H (1976). Impairment of optokinetic (after-)nystagmus by labyrinthectomy in the rabbit. Exp Neurol 52, 146–156.

Easter SS Jr & Nicola GN (1997). The development of eye movements in the zebrafish (Danio rerio). Dev Psychobiol 31, 267–276.

Haffter P, Granato M, Brand M, Mullins MC, Hammerschmidt M, Kane DA, Odenthal J, van Eeden FJ, Jiang YJ, Heisenberg CP, Kelsh RN, Furutani-Seiki M, Vogelsang E, Beuchle D, Schach U, Fabian C & Nusslein-Volhard C (1996). The identification of genes with unique and essential functions in the development of the zebrafish, Danio rerio. Development 123, 1–36.

Hess BJM, Prechta W, Reber A & Cazin L (1985). Horizontal optokinetic ocular nystagmus in the pigmented rat. Neuroscience 15, 97–107.

Honrubia V, Downey WL, Mitchell DP & Ward PH (1968). Experimental studies on optokinetic nystagmus II. Normal Humans. Acta Otolaryngol 65, 441–448.

Huang YY & Neuhauss SC (2008). The optokinetic response in zebrafish and its applications. Front Biosci 13, 1899–1916.

Igarashi M, Takahashi M & Homick JL (1977). Optokinetic nystagmus and vestibular stimulation in squirrel monkey model. Arch Otorhinolaryngol 218, 115–121.

Lambert FM, Beck JC, Baker R & Straka H (2008). Semicircular canal size determines the developmental onset of angular vestibuloocular reflexes in larval Xenopus. J Neurosci 32, 8086–8095.

Laurens J & Angelaki DE (2011). The functional significance of velocity storage and its dependence on gravity. Exp Brain Res 210, 407–422.

Miri A, Daie K, Arrenberg AB, Baier H, Aksay E & Tank DW (2011). Spatial gradients and multidimensional dynamics in a neural integrator circuit. Nat Neurosci 14, 1150–1159.

Mo W, Chen F, Nechiporuk A & Nicolson T (2010). Quantification of vestibular-induced eye movements in zebrafish larvae. BMC Neurosci 11, 110.

Mullins MC, Hammerschmidt M, Haffter P & Nusslein-Volhard C (1994). Large-scale mutagenesis in the zebrafish: in search of genes controlling development in a vertebrate. Curr Biol 4, 189–202.

Paige GD (1983). Vestibuloocular reflex and its interactions with visual following mechanisms in the

squirrel monkey. I. Response characteristics in normal animals. J Neurophysiol 49, 134–151.

Ramat S & Bertolini G (2009). Estimating the Time Constants of the rVOR. Ann NY Acad Sci 1164, 140–146.

Raphan T, Cohen B & Matsuo V (1977). A velocity-storage mechanism responsible for optokinetic nystagmus (OKN), optokinetic after-nystagmus (OKAN) and vestibular nystagmus. In Control of Gaze by Brain Stem Neurons, Developments in Neuroscience, vol. 1, ed. Baker R & Berthoz A, pp. 37–47. Elsevier/North-Holland Biomedical Press, Amsterdam.

Raphan T, Matsuo V & Cohen B (1979). Velocity storage in the vestibuloocular reflex arc (VOR). Exp Brain Res 35, 229–248.

Robinson DA (1964). The mechanics of human saccadic eye movement. J Physiol 174, 245–264.

Robinson DA (1977). Linear addition of optokinetic and vestibular signals in the vestibular nucleus. Exp Brain Res 30, 447–450.

Robinson DA (1981). The use of control systems analysis in the neurophysiology of eye movements. Annu Rev Neurosci 4, 463–503.

Schweigart G, Mergner T, Evdokimidis I, Morand S & Becker W (1997). Gaze stabilization by optokinetic reflex (OKR) and vestibulo-ocular reflex (VOR) during active head rotation in man. Vision Res 37, 1643–1652.

Sirkin DW, Hess BJM & Precht W (1985). Optokinetic nystagmus in albino rats depends on stimulus pattern. Exp Brain Res 61, 218–221.

Skavenski AA & Robinson DA (1973). Role of abducens neurons in vestibuloocular reflex. J Neurophysiol 36, 724–738.

Takahashi M & Igarashi M (1977). Comparison of vertical and horizontal optokinetic nystagmus in the squirrel monkey. ORL J Otorhinolaryngol Relat Spec 39, 321–329.

Tan HS, Collewijn H & van der Steen J (1992). Optokinetic nystagmus in the rabbit and its modulation by bilateral microinjection of carbachol in the cerebellar flocculus. Exp Brain Res 90, 456–468.

Tan HS, van der Steen J, Simpson JI & Collewijn H (1993). Three-dimensional organization of optokinetic response in the rabbit. J Neurophysiol 69, 303–317. Abstract/FREE Full Text

Uemura T & Cohen B (1973). Effects of vestibular nuclei lesions on vestibulo-ocular reflexes and posture in monkeys. Acta Otolaryngol Suppl 315, 1–71.

Waespe W & Henn V (1977). Vestibular nuclei activity during optokinetic after-nystagmus (OKAN) in the alert monkey. Exp Brain Res 30, 323–330.

Waespe W & Wolfensberger M (1985). Optokinetic nystagmus (OKN) and optokinetic after-responses after bilateral vestibular neurectomy in the monkey. Exp Brain Res 60, 263–269.

Zee D, Yee RD & Robinson DA (1976). Optokinetic responses in labyrinthine-defective human beings. Brain Res 113, 423–428.

Chapter 5

Outlook

Three studies about the optokinetic nystagmus (OKN) in fish and man are presented in this thesis. In this final chapter, I am going to discuss possible follow-up studies.

5.1 Positive or negative feedback of optokinetic signals: Degree of the misrouted optic flow determines system dynamics of human ocular motor behavior

In a next step, it would be interesting to study the association between the misrouting of optic fibers and the concurrent ocular motor pathology such as an abnormal optokinetic response (OKR) and spontaneous eye oscillations (SEOs) in patients with the misrouting of optic fibers. Functional magnetic resonance imaging (fMRI) could be used to examine how the human visual cortex topographically maps in patients with the misrouting of optic fibers (Hoffmann et al., 2003). The partial visual filed affected by the misrouting can be exposed to a variety of suitable visual stimuli in order to monitor the OKR. Then the relation between the misrouting, the OKR, and gaze stability in human can be analyzed, thus providing more evidences to link the misrouting to the SEOs. In the future, this method is possible to be a way of clinical diagnosis for the causes of infantile nystagmus syndrome (INS).

If the INS is caused by the misrouting, treatment may be difficult since the structural deficit may not be adjusted or cured by drugs or chemical substances. But there is a way to improve the life quality of these INS patients. The INS results in high retinal slip, which severely lowers visual perception. The visual feedback technology applied in this study may be able to lower retinal slip and increase visual acuity even when the eyes are constantly oscillating. The idea is to create a mobile device that can control the real-time image taken from the visual surround to move consistently with the real-time eye movements recorded by a video-oculography (VOG) instrument. In this way, retinal slip is reduced as the image and the eyes oscillate synchronously.

5.2 Afternystagmus in darkness after suppression of optokinetic nystagmus: interaction of a motion aftereffect and retinal afterimages

One promising following-up study would be to investigate the motion aftereffect (MAE)-induced eye movements. It is still unclear why most of the subjects experienced a MAE but only some generated eye movements to pursuit the MAE. Moreover, our pilot study showed that the suppression of the OKN is not the only adaptation process to evoke the MAE-induced eye movements. In our pilot test, we found that long-term smooth-pursuit eye movements and a long lasting OKN were able to evoke

the MAE as well as eye movements to pursue the MAE, suggesting that retinal slip is not the only factor to trigger a MAE; Eye movements play a role as well.

The mechanism responsible for afternystagmus after suppression of OKN (ASOKN) is also possibly linked to the secondary optokinetic afternystagmus (OKAN). It has been known that the primary afternystagmus, in which the slow phases move in the direction of the previous optokinetic stimulus, occurs in the dark after optokinetic stimulation (Cohen et al., 1977; Raphan et al., 1977; Raphan et al., 1979; Robinson, 1977). Interestingly, after the primary OKAN, a secondary OKAN might occur. The secondary OKAN is characterized by its slow phases moving in the opposite direction of the previous optokinetic stimulus (Waespe et al., 1978). As we mentioned in the previous paragraph, we found that the long lasting OKN is able to induce MAE-induced eye movements. Thus, it is possible that the secondary OKAN is produced by the mechanism responsible for ASOKN if retinal afterimages (RAIs) appear after the OKN. Such a correlational study could be accomplished in a way similar to the study reported in Chapter 3.

5.3 Velocity storage mechanism (VSM) in zebrafish larvae

One following-up topic would be to further investigate the ocular motor control in zebrafish larvae. When testing the VSM in zebrafish larvae, we found that, in 5-6 dpf zebrafish larvae, spontaneous eye movements in the dark as well as the OKN were disconjugate. Spontaneous eye movements in zebrafish larvae in the dark usually start with a saccade that brings the eyes from a central position to an eccentric position and followed by a centripetal eye drift that brings the eyes back to the central position. Although the movements of the eyes were yoked, both saccades and eye drifts were disconjugate: the saccadic peak velocity and amplitude were higher in the nasal-to-temporal (N-T) direction than the temporal-to-nasal (T-N) direction while the time constants of eye drift were higher in the T-N direction than the N-T direction. Such disconjugacy may be related to the ocular motor network in zebrafish larvae. More studies are needed to find out the cause.

In the same study, we also found that the beating field shifted in the direction of the slow phase and the slow-phase eye velocity was initially high but dropped during optokinetic stimulation. Both the beating-field shift and the velocity drop presented directional preference: The median eye velocity was lower and the beating field shifted more when the slow phases were in the nasal-to-temporal (N->T) direction. However, the maximum slow-phase eye velocity showed no statistical difference in two-eye movement directions. To our knowledge, the beating-field shift and the eye-velocity drop during optokinetic stimulation have not been reported before. More studies are needed to reveal the mechanism responsible for these phenomena.

5.4 Reference

Cohen B, Matsuo V & Raphan T (1977) Quantitative analysis of the velocity characteristics of optokinetic nystagmus and optokinetic after-nystagmus. J Physiol 270, 321–344.

Hoffmann MB, Tolhurst DJ, Moore AT, et al. (2003) Organization of the visual cortex in human albinism. J Neurosci 23, 8921–8930.

Raphan T, Cohen B & Matsuo V (1977) A velocity-storage mechanism responsible for optokinetic nystagmus (OKN), optokinetic after-nystagmus (OKAN) and vestibular nystagmus. In Control of Gaze by Brain Stem Neurons, Developments in Neuroscience, Vol. I (ed. R. Baker and A. Berthoz). Elsevier/North-Holland Biomedical Press, Amsterdam.

Raphan T, Matsuo V & Cohen B (1979) Velocity storage in the vestibuloocular reflex arc (VOR). Exp Brain Res35, 229-248.

Robinson DA (1977). Linear addition of optokinetic and vestibular signals in the vestibular nucleus. Exp Brain Res 30, 447-450.

Waespe, W., Huber, T., & Henn, V. (1978). Dynamic changes of optokinetic after-nystagmus (OKAN) caused by brief visual fixation periods in monkey and in man. Archiv für Psychiatrie und Nervenkrankheiten, 226(1), 1-10.

Curriculum Vitae

Personal Information

Name:	Chien-Cheng Chen
Present address:	Hegarstrasse 18, 8032 Zurich, Switzerland
Phone:	+41-787296557
E-mail:	cc.chen19820918@gmail.com
Date of birth:	18.09.1982
Place of birth:	Taiwan
Citizenship:	Taiwan

Academic Education

University of Zurich – Zurich, Switzerland

PhD Program in Integrative Molecular Medicine — Jun 2010 – Present

Thesis title: Optokinetic nystagmus in fish and man

Advisor: Dr. Ying-Yu Huang and Prof. Dr. Dominik Straumann

National Taiwan University – Taipei City, Taiwan

Master of Science in Mechanical Engineering — Sep 2004 – Jun 2006

Thesis: Thermo-piezoelectric finite-element modeling for piezoelectric transformers

Advisor: Dr. Yao-Joe Joseph Yang

Bachelor of Science in Mechanical Engineering — Sep 2000 – Jun 2004

Professional Experience

National Taiwan University - Taipei City, Taiwan

Research Assistant in Department of Mechanical Engineering — Aug 2009 –May 2010

Advanced Material Systems Corporation - Taipei City, Taiwan

Engineer in Research and Development Department — Feb 2008 – May 2009

Nano-Electro-Mechanical-System Research Center- Taipei City, Taiwan

Lecturer — Feb 2005 – Feb 2006

National Taiwan University - Taipei City, Taiwan

Teaching Assistant in Department of Mechanical Engineering — Sep 2005 – Feb 2006

Publications

Peer reviewed papers

1. **Chen CC**, Bockisch CJ, Straumann D, Huang MYY (2014). Disconjugacy of spontaneous

eye movements in zebrafish larvae in the dark. (Manuscript in preparation)

2. **Chen CC**, Bockisch CJ, Bertolini G, Straumann D, Huang MYY (2014). Disconjugacy of optokinetic nystagmus in zebrafish larvae. (Manuscript in preparation)
3. **Chen CC**, Huang MYY, Weber KP, Straumann D, Bockisch CJ (2014). Afternystagmus in darkness after suppression of optokinetic nystagmus: an interaction of motion aftereffect-induced eye movements and retinal afterimages. Experimental Brain Research doi.org/10.1007/s00221-014-3971-4.
4. **Chen CC**, Bockisch CJ, Olasagasti I, Weber KP, Straumann D, Huang MYY (2014). Positive or negative feedback of optokinetic signals: Degree of the misrouted optic flow determines system dynamics of human ocular motor behavior. Invest Ophthalmol Vis Sci 55(4):2297-306.
5. **Chen CC**, Bockisch CJ, Bertolini G, Olasagasti I, Neuhauss SCF , Weber KP, Straumann D, Huang MYY (2014). Velocity storage mechanism in zebrafish larvae. The Journal of Physiology 592 (1): 203-214.
6. Huber-Reggi SP, **Chen CC**, Grimm L, Straumann D, Neuhauss SCF, Huang MYY (2012). Severity of Infantile Nystagmus Syndrome-Like Ocular Motor Phenotype Is Linked to the Extent of the Underlying Optic Nerve Projection Defect in Zebrafish *belladonna* Mutant, J Neurosci 32(50): 18079-18086.
7. Traber GL, **Chen CC**, Huang YY, Spoor M, Roos J, Frens MA, Straumann D, Grimm C (2012). Albino Mice as an Animal Model for Infantile Nystagmus Syndrome, Invest Ophthalmol Vis Sci 53(9): 5737-5747.
8. Huang YY, **Chen CC**, Huber-Reggi SP, Neuhauss SCF, Straumann D (2011). Infantile nystagmus syndrome (INS) in achiasmatic zebrafish: comparison to human INS. Ann NY Acad Sci 1233: 285-291.
9. **C.-C. Chen**, C.-W. Kuo, Y.-J. Yang (2011). Generating Passive Compact Models for Piezoelectric Devices. IEEE Transaction on CAD 30(3): 464-467.
10. Y.-J. Yang, **C.-C. Chen**, C.-W. Kuo C.-K. Lee (2008). Thermo-piezoelectric finite-element modeling for piezoelectric transformers. Japanese Journal of Applied Physics 47(4): 2182-2188.
11. Y.-J. Yang, **C.-C. Chen**, Y.-M. Chen, C.-K. Lee (2008). Modeling of piezoelectric transformers using finite-element technique. Journal of the Chinese Institute of Engineers 31(6): 925-932.
12. W.-C. Lin, Y.-J. Yang, G.-W. Hsieh, C.-H. Tsai, **C.-C. Chen**, C.-C. Liang (2006). Selective local synthesis of nanowires on a microreactor chip. Sensor and Actuator A 130(31): 625-632.

International Conferences

1. Huang MYY, **Chen CC**, Bockisch CJ, Straumann D, Visual feedback test in wild-type zebrafish larvae and study of mechanisms behind the INS-like nystagmus, 8th European Zebrafish meeting, Barcelona, Spain, July, 2013.
2. **Chen CC**, Bockisch CJ, Bertolini G, Olasagasti I, Neuhauss SCF , Weber KP, Straumann D, Huang MYY, Velocity storage mechanism in zebrafish larvae, The vestibular system: a clinical and scientific update in SIENA. Siena, Italy, April, 2014.
3. Huang MYY**, Chen CC**, Bockisch CJ, Straumann D, Dancing Eyes: The Positive Optokinetic Feedback Loop, Neuroscience 2012, New Orleans, USA, October, 2012.
4. **Chen CC**, Bockisch CJ, D Straumann, Huang YY, Nystagmus generated by positive visual feedback system in healthy humans, 9th NWG, Göttingen, German, March, 2011.
5. **C.-C. Chen**, C.-W. Kuo, C.-K. Lee and Y.-J. Yang, "Finite-Element Simulation of the Temperature Distribution in a Piezoelectric Transformer", ICAST 2006, Taipei, Taiwan, Oct

16-19, 2006.

6. W.-C. Lin, Y.-J. Yang, G.-W. Hsieh, C.-H. Tsai, **C.-C. Chen** and C.-C. Liang, “Selective Local Synthesis of Nanowires on a Microreactor Chip”, in Proc. 13th International Conference on Solid-State Sensors and Actuators (Transducers' 05), Seoul, Korea, June, 2005.

Acknowledgements

I would like to thank Prof. Dr. Dominik Straumann, Dr. Melody Ying-Yu Huang, and Dr. Christopher J Bockisch for supervising me during these four years of pursuing PhD degree. Thanks for your effort to make these studies solid, concise, and clear, even when the content is abstruse.

I would like to thank Prof. Dr. Stephan D.F. Neuhauss, Prof. Dr. Christian Grimm, and Prof. Dr. Stefan Glasauer for valuable conceptual input, discussions, and critical comments. Their comments push me to improve my presentation skill a lot.

I would like to thank Urs Scheifele and Marco Penner for excellent technical assistance. It is my pleasure to work with you for the fish and human setup.

I would like to thank my colleagues for discussing my research. Well, your names, if you were involved, were on the author list of these studies. This is my way to thank your effort!

I would like to thank my parents and sister to support me to study aboard and be my backup. My nephews are so cute that I miss them so much.

I would like to thanks my friends for visiting me, bringing me a lot of Taiwanese food and cookies, and chatting with me in a way of humor. Nice to have you guys. I had a lot of adventures during these years. These are all life-long memories.

In the end, I would like to thank these patients and subjects who participated in the experiments. Thanks for your time. Because of all of you, these studies are able to be done and may have some contributions in science.